MID-LEVEL VORTICITY IN MESOSCALE CONVECTIVE SYSTEMS

by

Ronnie G. King

Research supported by the National Science Foundation under grant ATM-9313716

Colorado State University

DEPARTMENT OF ATMOSPHERIC SCIENCE

PAPER NO. 606

MID-LEVEL VORTICITY IN MESOSCALE CONVECTIVE SYSTEMS

by

Ronnie G. King

Department of Atmospheric Science
Colorado State University
Fort Collins, CO 80523

Summer 1996

Atmospheric Science Paper No. 606

ABSTRACT

MID-LEVEL VORTICITY IN MESOSCALE CONVECTIVE SYSTEMS

The objective of this study has been to examine and document the development of mid-level Mesoscale Convective Vortices (MCVs) within Mesoscale Convective Systems (MCSs) and Mesoscale Convective Complexes (MCCs) using the Central Plains Wind Profiler Demonstration Network (WPDN). Nine MCSs from the summer of 1993 were picked for this study based on their formation and lifetime spent over the WPDN.

Bartels and Maddox's (1991) climatological study of MCVs for 1981 - 1988 estimated that less than 5% of MCSs exhibit a vortex whose clouds persist long enough after the dissipation of the MCSs' high-level obscuring cirrus cloud to become apparent in visible satellite imagery. This low estimate of MCVs in MCSs leads to the question of how many MCSs produce MCVs. Some researchers state that the MCV is an inherent part of the MCC circulation (Velasco and Fritsch, 1987; Menard and Fritsch, 1989).

The nine MCSs studied here do support the theory that the MCV forms in most, if not all, large MCSs. Each of the nine cases developed to varying degrees a maximum of relative vorticity of $10^{-4}s^{-1}$ or greater in the mid-tropospheric levels near the freezing level. This suggests the importance of latent heat processes enhancing the inflow and horizontal convergence which in turn produces vorticity (Johnson *et al.*, 1995) suggesting that the latent heat release, melting and evaporative cooling in the stratiform region are the primary contributors to the circulation spinup. This finding is consistent with

modeling results (Zhang and Fritsch, 1988) as well as theoretical studies of Hertenstein and Schubert (1991).

This finding is also somewhat supported by the results of comparing the average time rate of change of relative vorticity during the period of maximum increase in the mid-levels to the average stretching (convergence production) term that gives a ratio of 1.16 or 116%. This suggests the stretching term is playing a significant role in the production of vorticity but since the ratio is greater than one the change in vorticity is greater than the stretching term; therefore the tilting term must be contributing also. This result is consistent with other observational studies (Bartels and Maddox, 1991; Johnson and Bartels, 1992) that have found the mid-level convergence production (stretching term) to be the primary producer of mid-level vorticity.

ACKNOWLEDGEMENTS

I would like to express my deepest appreciation to my advisor, Dr. Richard Johnson, for his guidance and dedication to the successful and timely completion of this work. I would also like to thank my other committee members, Dr. Thomas McKee and Dr. Jorge Ramirez.

I would also like to thank Paul Ciesielski, Rick Taft and Steve Finley for their assistance in computer programming and use of the Department of Atmospheric Science computers. Thanks are also extended to Dr. Tom Vonder Haar, Nan McClurg, Kelly Dean and Dave Randal of CIRA for providing the satellite and wind profiler data.

Finally, I would like to thank my wife, Hyang Ku, and my daughter, Sharon, for their support, encouragement and patience.

This research was supported by the National Science Foundation under Grant ATM-9313716. Salary and tuition were paid by the United States Air Force under the Air Force Institute of Technology Graduate Program.

TABLE OF CONTENTS

Chapter 1

INTRODUCTION

Early studies during the past decades brought about the theory that thunderstorms often exist in conglomerates covering meso-α and meso-β scale (terms defined by Orlanski, 1975) regions (Newton, 1950; Fujita, 1955). This theory was confirmed with early weather satellites. The satellite also provided a view of the lifecycles of these systems. These systems have become collectively called mesoscale convective systems (MCS), and are known to account for a large part of the atmospheric vertical heat, moisture and momentum transport (Riehl and Malkus, 1958) as well as a significant portion of the growing season rainfall (Maddox, 1983; Fritsch *et al.*, 1986; Tollerud and Collander, 1993). Within MCSs, individual cumulonimbus cells are often interspersed among large areas of lighter stratiform precipitation (Houze et al., 1990), and are covered by an upper-level cirriform cloud shield that can cover horizontal distances approaching 1000 km.

Maddox (1980) identified a subset of MCSs that are on the higher end of the mesoscale range using the geostationary satellite. He termed these MCSs as Mesoscale Convective Complex's (MCCs), and defined them in terms of their appearance in satellite photographs only. Maddox's definition of an MCC, given in Table 1.1, describes a cirrus cloud shield that covers a land area at least the size of the state of Ohio.

Table 1.1: Mesoscale Convective Complex (MCC)
(based upon analyses of enhanced IR satellite imagery) (from Maddox 1980)

Physical Characteristics	
Size:	A -- Cloud shield with continuously low IR temperature $\leq$ -32°C must have an area $\geq$ 100,000 km^2
	B -- Interior cold cloud region with IR temperatures $\leq$ -52°C must have an area $\geq$ 50,000 km^2
Initiate:	Size definitions A and B are first satisfied
Duration:	Size definitions must be met for a period $\geq$ 6 hours
Maximum extent:	Contiguous cold cloud shield (IR temperature $\leq$ -32°C) reaches maximum size
Shape:	Eccentricity (minor axis/major axis) $\geq$ 0.7 at time of maximum extent
Terminate:	Size definitions are no longer satisfied

Although the MCC has a roughly circular appearance in satellite images, the internal structure and dynamics have not been well defined (Maddox, 1983; Wetzel *et al.*, 1983; Cotton *et al.*, 1989). One of the features found in many MCC case studies is the existence of a mid-level mesoscale convective vortex (MCV) (Johnston, 1982; Verlinde and Cotton, 1990; Bartels and Maddox, 1991; Johnson and Bartels, 1992). Due to the lack of upper air data with a high temporal resolution, the development of an MCV is poorly understood, but with the new Next Generation Doppler Radars (NEXRAD) and Wind Profiler Demonstration Network (WPDN) this may change.

The objective of this study is to use the WPDN to investigate the development of MCVs in relation to satellite cloud fields and determine the evolution of the associated vertical component of relative vorticity (ζ) of MCVs in nine Midwestern MCSs in 1993. Of particular interest is the vertical profile of vorticity within MCVs. Past studies (e.g., Johnson and Bartels, 1992; Zhang, 1992) have indicated maximum vorticity near the 0°C

level suggesting that melting-layer convergence (Johnson *et al.*, 1995) may be an important factor in MCV development.

This study will be unique in the sense that past studies of MCVs using conventional NWS soundings have not been able to adequately resolve their circulation features, while those using data from special high-resolution sounding networks (e.g., the 1985 Oklahoma-Kansas PRE-STORM network) have only been able to examine a limited number of cases. A second objective will be to investigate the dynamics of MCVs, namely, to determine if vorticity stretching due to mid-level convergence is the primary spin-up process on the WPDN or meso-α scale.

Chapter 2

COMMON CHARACTERISTICS OF THE MCC/MCS

Owing to their size and longevity, MCCs and MCC-like MCSs are important producers of precipitation. They account for a significant portion of the growing season rainfall over much of the United States corn and wheat belts (Maddox, 1983; Fritsch *et al.*, 1986). In a study of ten years of warm season precipitation observations over the central United States, Tollerud and Collander (1993) found that although MCCs are relatively rare, they produce a disproportionately large number of the extreme rainfall events. Fritsch *et al.* (1986) found that under slowly evolving synoptic conditions, a series of convective systems can form and travel over the same area producing a rainfall swath similar to an average hurricane. In addition to widespread beneficial rainfall, Maddox (1980) found that many MCCs produce a variety of severe convective phenomena, including tornadoes, hail, wind, flash flooding, and intense electrical storms. Also one of every four MCCs produces injuries or deaths, indicating that these systems are truly significant weather events (Maddox, 1983).

The floods of 1993 can attest to the fact that MCSs are significant rain producers. During 1993 MCSs occurred almost daily over the central plains of the United States, causing 100 rivers to flow out of their banks with 14 at the highest levels ever recorded (Williams, 1994). Rainfall amounts greater than 50 inches were recorded in parts of

Kansas, Missouri and Iowa from April 1 through September 30, 1993 (Southard, 1995). This led to the Mississippi River at Saint Louis, Missouri remaining above flood stage for 144 days during the summer of 1993.

Since Maddox first defined the MCC, much research has been focused on both observational studies and numerical simulations of MCCs and other smaller, yet dynamically similar MCSs. These organized convective systems are seen worldwide, but there do seem to be preferred locations. Recent surveys, based mostly on satellite data, show that large populations of MCCs are favored in the central plains of the United States (Maddox, 1980; Augustine and Howard, 1988), the central plains of South America (Velasco and Fritsch, 1987) and central Africa (Lang and Fritsch, 1993).

From these studies of MCC climatology, a picture of the favored MCC environment has emerged (Maddox, 1983; Olsson, 1994):

-- MCCs tend to develop over land, or near (within about 250 km) a continental land mass.

-- MCCs most frequently develop to the lee (in the sense of the predominant mid-tropospheric flow) of significant mountain ranges. For example, favored locations are to the lee of the Rocky Mountains in North America, east of the Andes Mountains in South America, west of the north African mountains in the Sahel, east of the South African escarpment, and to the east of the Himalayas.

-- MCCs most frequently occur under or along the periphery of a synoptic scale mid-tropospheric ridge.

-- Strong low-level thermodynamic forcing, usually in the form of a poleward flowing low-level jet, is frequently present in the MCC growth region.

-- The favored MCC region seems to migrate poleward during the warm season, often accompanying the poleward migration of the jet stream. Tropical regions do not see a significant migration in the favored location, probably because the seasonal insolation does not vary significantly.

-- The ripe MCC environment generally has large values of Convective Available Potential Energy (CAPE) in excess of 10^3 J/kg.

-- The favored MCC environment is one that has, climatologically, a low albedo, e.g., a relatively cloud free region.

-- MCCs tend to occur in a precursor region of mesoscale convergence and upward motion (slow moving or stationary boundaries).

The climatological and composite studies have also led to a common picture of the behavior of the MCC as a storm system. The following features are noted (Olsson, 1994):

-- The storm duration tends to be between 9 and 12 hours. MCCs in central South America tend to be somewhat larger and longer lived than in other midlatitude locations.

-- The first thunderstorms that may be attributed to the development of the MCC occur in the late afternoon, near the end of the diurnal heating cycle. Thus, the MCC itself tends to be predominantly, though certainly not exclusively, a nocturnal phenomenon.

-- In favored MCC regions a significant percentage of warm season precipitation derives from nocturnal MCCs.

-- The storm tracks of MCCs tend to have an anticyclonic curvature, most likely due to their favored location on the periphery of a broad ridge.

-- MCCs tend to have some component of motion along the low-level temperature gradient and often have strong low-level warm advection.

A significant point to note is several geographical regions that tend to experience very frequent deep convection are not necessarily likely spots for MCC generation (Olsson, 1994). For example, the rain forests of the Amazon Basin and the Gulf of Thailand have widespread convection and yet experience small populations of MCCs (Velasco and Fritsch, 1987; Lang and Fritsch, 1993). This would indicate that the MCC is not just the chance occurrence of clustered convection, but more a distinct and organized mesoscale system (Olsson, 1994).

The MCC has been defined by its physical size, shape and longevity in satellite images (Maddox, 1980). Although the appearance of the MCC by satellite is roughly circular, the internal structure has not been well defined. MCCs are probably dynamically and thermodynamically similar in many respects to squall lines with a trailing region of stratiform precipitation. Many MCCs result from the merger of cells, and in effect are the approximate equivalents to broken areal squall lines. Some systems may evolve from broken lines and broken areal squall lines while others may evolve from backbuilding squall lines (Bluestein, 1993).

Houze *et al.* (1990) identified two 'classifiable' types and a third 'unclassifiable' type of precipitation organization in the study of 63 MCSs (including both squall lines and MCCs). They found that most systems that produce large amounts of precipitation (minimum of 25 mm of rain in 24 hours over an area exceeding 12,500 km^2) had both a convective echo region and a stratiform echo region. The two classes of the precipitation patterns are termed symmetric and asymmetric. Both the symmetric and asymmetric

cases are characterized by a leading line of convective cells followed by a trailing area of stratiform precipitation. In the symmetric case, the most intense cells may be found at any location along the convective line, while in the asymmetric case new cell growth and the most intense cells are located on the southwestern end of the convective line. Nearly one third of the cases studied by Houze *et al.* (1990) fit neither the symmetric nor the asymmetric pattern but had both convective and stratiform regions.

An understanding of the airflow patterns in and around the MCS has provided information regarding the formation of these systems, their internal structure, associated pressure fields and their influence on the surrounding environment. Figure 2.1 depicts the symmetric and asymmetric precipitation patterns with associated surface pressure fields (Loehrer and Johnson, 1995), while Figure 2.2 shows a conceptual model of a convective line with a trailing stratiform region (Houze *et al.*, 1989). A mesoscale region of stratiform precipitation, organized mesoscale ascent aloft, a mesoscale downdraft at low levels, and a warm core high (anticyclonic outflow) near the tropopause resulting from latent heat release are all common characteristics. Motions within an MCS with a leading convective region and a trailing stratiform region are generally characterized by low-level convergence usually associated with some form of a weak surface boundary and a low-level jet near the leading edge and, low-level divergence in the stratiform region and divergence at the upper levels (Ogura and Liou, 1980).

One of the more striking features found in many MCC case studies is the existence of a mesoscale convective vortex (MCV) found in the mid-levels of the MCS. By using visible satellite data, some researchers have found that several MCCs develop a mid-level MCV (Johnston, 1982; Verlinde and Cotton, 1990; Bartels and Maddox, 1991;

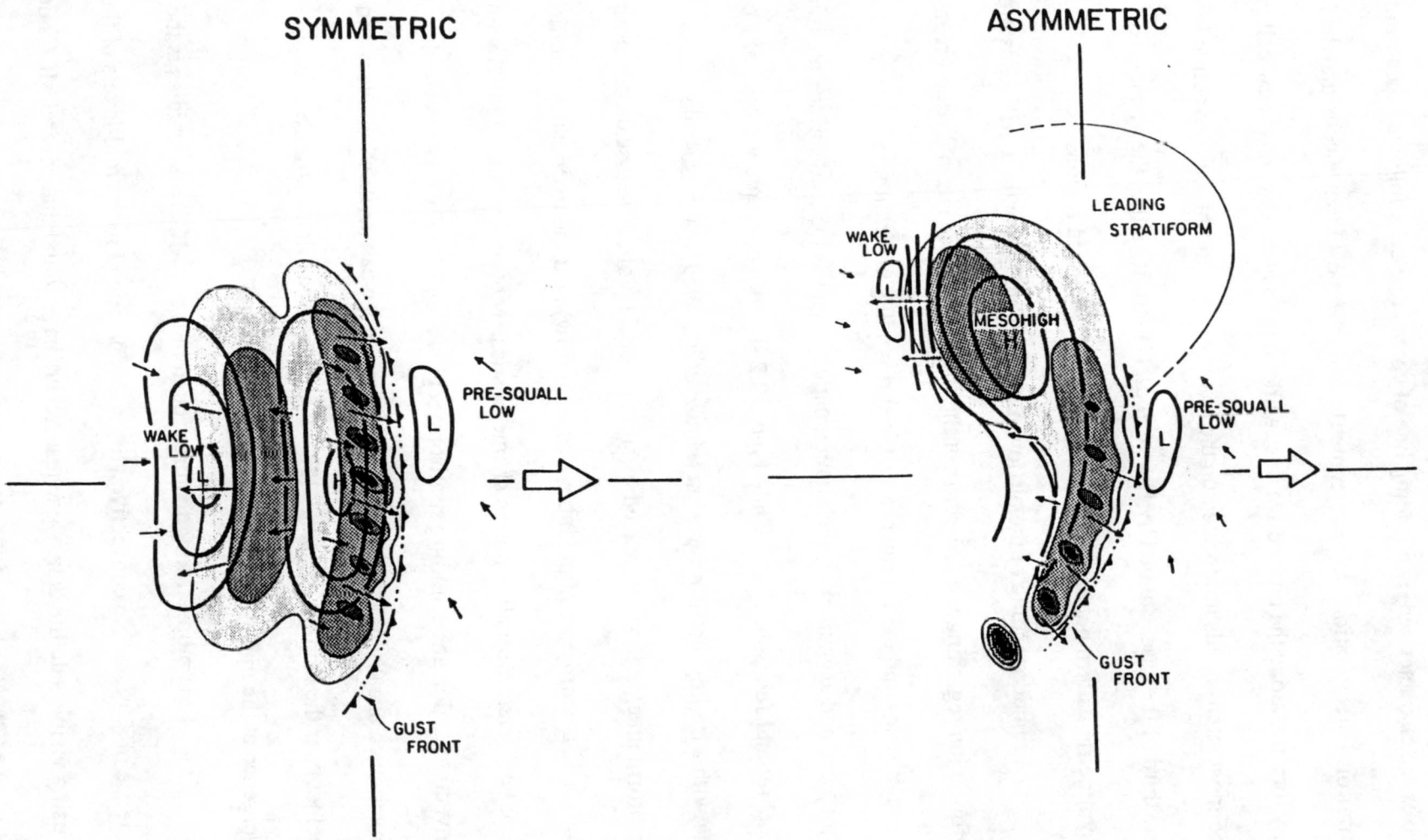

Figure 2.1: Schematics depicting symmetric and asymmetric precipitation patterns with the surface pressure fields overlaid (Loehrer and Johnson 1995).

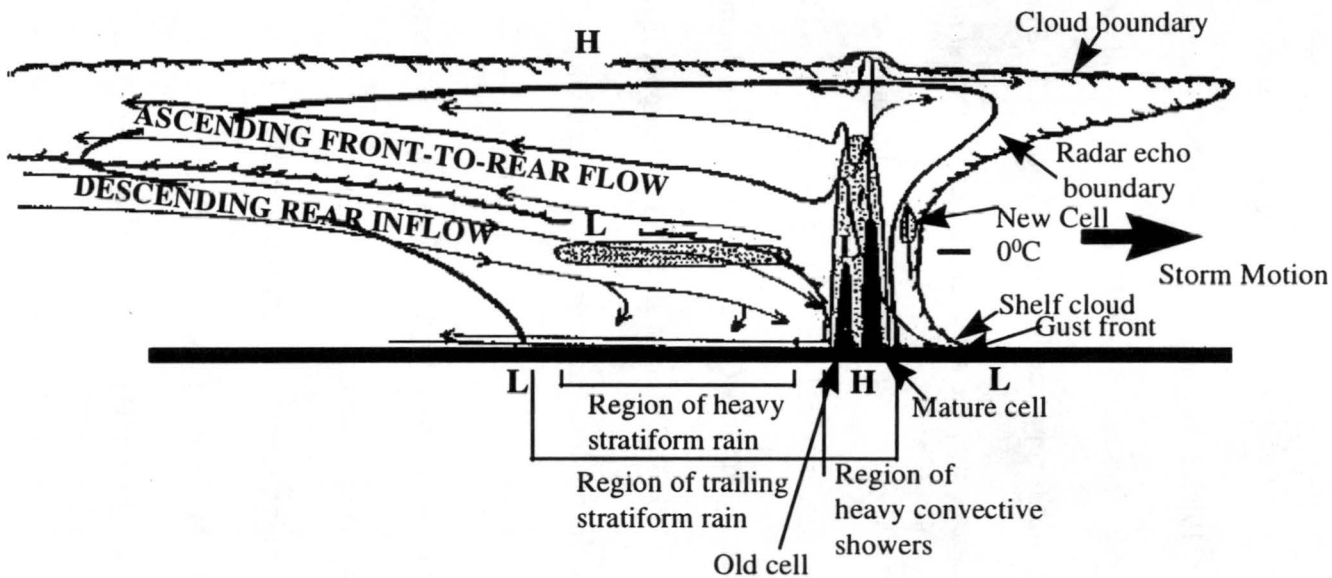

Figure 2.2: Conceptual model of a MCS with a trailing stratiform region viewed perpendicular to the convective line (from Houze *et al.*, 1989).

Johnson and Bartels, 1992). The first direct observational evidence of residual cyclonic circulation was provided by Johnston (1982), who identified a number of circulations in film loops of visible satellite imagery. The MCVs were only apparent after overlying anvil debris had dissipated or advected away. Since then, observational studies (Smull and Houze, 1985; Leary and Rappaport, 1987; Zhang and Fritsch, 1989; Johnson and Bartels, 1992; Fritsch *et al.*, 1994) have shown that the cyclonic circulation develops within the stratiform precipitation region of MCS. The MCV can last for hours and sometimes days after the MCS dissipates (Fritsch *et al.*, 1994). Fritsch *et al.* (1994) tracked an MCV that was instrumental in initiating and organizing five MCSs.

The process that leads to the formation of an MCV is poorly understood, but the synoptic setting for an MCC has been fairly well documented (e.g., Maddox, 1983; Wetzel *et al.* 1983; Cotton *et al.* 1989). The upper level charts usually show a long wave ridge to be the predominant feature associated with the formation of MCCs and MCVs (Bartels and Maddox, 1991). A weak short wave trough is often present in the mid-levels, but upward vertical motion appears to be forced more by low-level moisture and thermal advection associated with the low-level jet. Therefore, MCV generation occurs in regions where large scale relative vorticity is much less than the Coriolis parameter (Bartels and Maddox, 1991). The implication of this is that, to a first approximation, the development of a MCV might be explained by the simple quasi-geostrophic vorticity equation (i.e., convergence acting on the Coriolis parameter). The simple vorticity equation is appropriate as only a first approximation since the observations are not consistent with quasi-geostrophic dynamics (e.g. divergence is greater than relative vorticity) (Bartels and Maddox, 1991).

Bartels and Maddox (1991) estimated the relative values for the terms of the quasi-geostrophic vorticity equation based on what they considered representative MCV conditions as $\zeta(\nabla \bullet \mathbf{V}) = 10^{-8}s^{-2}$, $f(\nabla \bullet \mathbf{V}) = 10^{-7}s^{-2}$ and $(\partial \mathbf{V}/\partial z \times \nabla w) = 5 \times 10^{-8}s^{-2}$ where ζ is the relative vorticity, f is the Coriolis parameter, $\mathbf{V}$ is the horizontal wind vector and w is the vertical wind component. This implies the tilting and advection terms can probably be ignored compared to the stretching term owing to weak winds, weak vertical wind shear, negative background relative vorticity and weak vorticity gradients for the large-scale environment of the MCV. With a mesoscale convergence value of $10^{-3}s^{-1}$ the stretching term would cause an exponential increase in relative vorticity in less than two hours (Bartels and Maddox, 1991). This is consistent with observations of the development of MCVs following short-lived convective systems.

Bartels and Maddox's (1991) climatology of MCV events for 1981 - 1988 estimated that less than 5% of MCSs exhibit a vortex whose clouds persist long enough after the dissipation of the MCSs' high-level obscuring cirrus cloud to become apparent in visible satellite imagery. This suggests there may be specific atmospheric conditions that interact to produce visually documentable long-lived mesoscale vortices. A preexisting vortex may explain the fact that small and/or short-lived systems can generate MCVs. An alternative explanation is that both the scale and duration of latent heating and the character of the background synoptic or mesoscale settings in which the convective system develops are critical factors controlling whether an MCV is generated (Bartels and Maddox, 1991). Recent modeling results (Zhang and Fritsch, 1988) suggest the latent heat release and evaporative cooling in the stratiform region are the primary contributors to the circulation spinup. This is expected for situations where the horizontal

scale of the heating is comparable to or larger than the Rossby radius of deformation (Schubert *et al.*. 1980; Zhang and Fritsch 1988; Cotton *et al.*, 1989), so that much of the energy from the heating goes into quasi-balanced flow. This theory is also supported by the theoretical studies of Hertenstein and Schubert (1991) concerning potential-vorticity anomalies associated with squall lines. They found that a heating profile resembling that associated with a squall line containing a trailing stratiform region leads to a strong positive potential-vorticity anomaly in the mid-levels.

Studies have shown the maximum vorticity associated with the MCV is found near the freezing level, which is usually around 600 mb in the summer time. Johnson and Bartels (1992) found positive relative vorticity in a layer from 900 mb to 350 mb with a maximum of $1.1 \times 10^{-4} s^{-1}$ at approximately 550 mb in their study of a 23-24 June 1985 MCV. Zhang (1992) found similar results in his study of a 10-11 June 1985 MCV. He found a layer of positive relative vorticity from 900 mb to 300 mb with a maximum of $2.6 \times 10^{-4} s^{-1}$ at 550 mb. These findings are significant in that they show the approximate magnitude of the vorticity associated with MCVs and the MCVs' proximity to the freezing level

Even if all MCSs generate a MCV, factors favorable for visual identification may not exist, i.e. a lack of persisting mid-level clouds after the dissipation of the upper-level cirrus clouds. Fortunately MCVs can be observed through other means, e.g., Doppler radar and conventional rawinsonde soundings (Johnson and Bartels, 1992). Radar has the greatest ability to observe the mesoscale internal structure of MCSs, but an individual radar has a range limit that does not allow it to observe the system for the entire lifetime of the MCS. Radar composites can overcome the range limits of an individual radar and

with the new NEXRAD system this method will probably be explored in the near future. Other observational studies of MCVs have, for the most part, relied on the conventional NWS sounding network that is characterized by widely spaced (~ 400 km) and twice per day upper-air observations. The new WPDN, however, with higher spatial and much higher temporal (one hour or less) resolution provides the opportunity for much more detailed documentation of MCVs than has heretofore been possible.

Chapter 3

WIND PROFILERS

Upper-air winds were first measured more than 100 years ago, when Schreiber (1886) followed the flight of a balloon with two theodolites. For many decades pilot-balloons and, since the 1930s, radiosondes have been the only way to measure winds in the atmosphere. The recent development of modern remote sensing techniques like Doppler radar now offer an alternative (Monna, 1994). The first wind measurements with Doppler radar were made at the end of the 1960s (Dobson, 1970). Wind profilers, which are vertically pointing Doppler radars, have now evolved towards highly sophisticated systems with high temporal and vertical resolution (Monna, 1994).

Height coverage and resolution of wind profilers are fundamentally determined by the physics of the scattering mechanism, which depends on the radar frequency and the refractive index fluctuations of the atmosphere (Frisch and Weber, 1992). Wind profilers can operate between 40 and 1400 MHz (Monna, 1994). In practice, systems are built for three frequency bands, i.e. around 50 MHz, 400 MHz and 1 GHz. Characteristic values for height coverage are 20, 10 and 3 km respectively, and for resolution of 1, 0.3 and 0.1 km respectively (Monna, 1994).

Traditionally, wind is measured simultaneously twice each day by a vast global radiosonde network. Radiosonde data are essentially slantwise point measurements. A

fundamental reason to prefer a wind profiler for these measurements is that it produces a vertical profile of volume and time averaged wind data, which is more representative for the actual state of the atmosphere (Monna, 1994). Moreover, wind profilers can measure wind profiles with a high temporal resolution (up to every six minutes but more typically every hour) (Schlatter and Zbar, 1994).

Numerical models typically need hourly wind information up to at least 12 km, with a vertical resolution of about 200 m. For this purpose, the 400 MHz profiler is a good choice to provide wind data, because its performance shows the best compromise between the necessary height coverage and vertical resolution. To resolve atmospheric mesoscale systems, one needs a sufficiently dense network of systems. Experiments with wind profilers showed an improvement in the short term forecast (Kuo and Guo, 1989; Schlatter and Zbar, 1994). These results have led to the establishment of the Wind Profiler Demonstration Network (WPDN) in the central part of the United States (Serafin and Dabberdt, 1989).

Installation of the WPDN began in early 1991 and was completed in May 1992. One of the goals was to assess the extent to which a network of wind profilers could support and enhance routine field operations and numerical weather predictions as well as provide high temporal resolution data for research needs. This led to the critical element of siting the profiling radars in designing the WPDN. Since profiler data had a wide variety of uses, no single siting strategy would be ideal for all applications (Schlatter and Zbar, 1994). The final result was a dual network, as seen in Figure 3.1, of profilers with 22 profilers constituting the outer network and seven more, in the shape of a hexagon with the center at Lamont, Oklahoma, constituting the inner network.

The WPDN uses the 404 MHz profiler with about 300 km spacing between the stations in the outer network and about 200 km spacing between the stations in the inner network. The WPDN has a temporal resolution of six minutes and height resolution of 250 m from 500 m about ground level (AGL) to 16 km AGL. The six minute data are also averaged hourly. Hourly averaged winds measured by ground based profilers are generally very accurate; studies have shown that more than 97% of the measurements

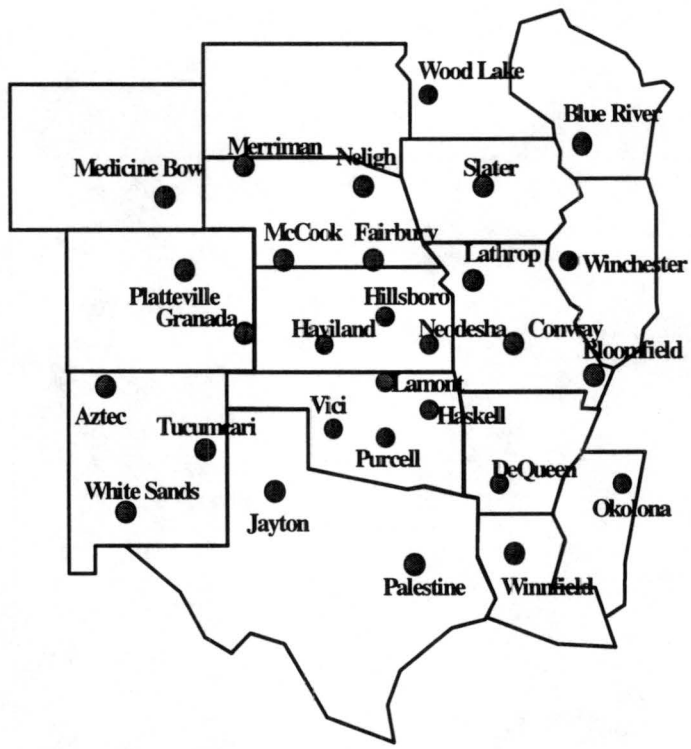

Figure 3.1: Location of WPDN sites on the central plains of the United States.

accurately represent the tropospheric winds (Schlatter and Zbar, 1994). Occasionally, however, measurement errors can occur because of spurious radar targets (e.g., aircraft or migrating birds), radio frequency interference, non-uniform precipitation, receiver recovery noise, or other phenomena.

Chapter 4

DATA AND ANALYSIS PROCEDURES

Data from the summer of 1993 were used for this study. The summer of 1993 was picked because of the high number of MCSs that occurred over the central part of the United States causing extensive flooding in the Midwestern states. Infra-red satellite data from the Geostationary Operational Environmental Satellite (GOES) Seven were used to identify MCCs and MCC-like MCSs over the Midwestern United States. MCCs that spent their lifetime over the WPDN were then picked for a more in-depth study using wind data from the WPDN. Because of the low number of MCCs (4) that actually spent their entire lifetime other the WPDN, five additional MCSs that had strong MCC characteristics but did not meet Maddox's (1980) time or size requirements were also picked for study to increase the sample size. For example case #1, the smallest of the five, only reached a maximum areal coverage of 60,000 km^2 but otherwise had all the characteristics of a MCC (i.e. circular cloud pattern, cold cloud tops, time, etc.).

The WPDN data will only allow for analysis at the lower limit of the meso-α scale (200 - 2000 km) (Orlanski, 1975) due to the spacing of the profilers over the central plains. The spacing of the WPDN outer profilers is approximately 300 km while the inner network centered over Oklahoma has a spacing of approximately 200 km. At the same time, on a temporal scale the WPDN hourly data allows an analysis on the meso-β

scale (1 hour to 1 day).

Once the nine systems were picked, hourly averaged horizontal wind data from the WPDN were gathered at 50 mb vertical increments from 800 mb up to 400 mb using heights for a U.S. Standard Atmosphere to determine the height levels in pressure coordinates. Only data between 800 mb and 400 mb were used because 1) the main focus of this study is the mid-level cyclonic vortex, 2) wind data below 800 mb in and around convective systems are greatly effected by individual thunderstorms, downbursts and outflow boundaries disturbing the meso-α scale flow, 3) wind data above 400 mb were usually very sparse. The wind data were then visually inspected for both time and height consistency, and compared with available rawinsonde data for bad data. Bad data were corrected when possible but most of the time they were deleted. One of the most frequent problems with the WPDN wind data was a sudden change in direction accompanied by a dramatic speed increase often greater than 50 ms^{-1} at one or two levels. This is usually associated with a folding problem in the Doppler radar (Doviak and Zrnic, 1984). There was also a systematic problem of some stations reporting the same identical wind data for an extended period of time, sometimes up to 24 hours. An estimated 5% of the data were deleted.

After the data were determined to be good they were analyzed using the General Meteorological Package (GEMPAK) software. GEMPAK is part of the National Centers Advanced Weather Interactive Processing System (N-AWIPS) software developed within the National Weather Service (NWS) by the National Center for Environmental Prediction (NCEP). GEMPAK was used to perform a Barnes (1964) objective analysis for the vertical component of relative vorticity and horizontal divergence with 0.5 degree

(approximately 55 km) grid spacing. The hourly 600 mb relative vorticity charts derived from the Barnes objective analysis were used to determine the center of maximum vorticity associated with the MCS (from now on the use of the term vorticity, unless otherwise stated, will refer to the vertical component of vorticity only). The 600 mb level was selected because of its proximity to the 0°C level in the summer time environment of convective systems. The freezing level is significant because melting has been shown to induce horizontal wind perturbations (mid-level convergence) in precipitation systems (Atlas *et al.*, 1969; Lin and Stewart, 1986: Szeto *et al.*, 1988; Nicholls *et al.*, 1991) and observational studies have shown the MCV is strongest near the freezing level (Zhang and Fritsch, 1988; Johnson and Bartels, 1992; Zhang, 1992). After the center of maximum relative vorticity was determined, the point of the maximum center was then used to get a vertical profile of the relative vorticity and horizontal divergence.

The hourly vertical profiles were then used to determine an average vertical profile of relative vorticity during the first three hours that the system appears to be organized in the satellite photos and during the period of maximum mid-level vorticity (from here on referred to as the maximum stage) averaged over three hours centered around the hour of maximum mid-level relative vorticity. Averages over a three hour period were used to help eliminate noise in the data as well as show that the mid-level increase in relative vorticity is a persistent feature lasting more than an hour.

Lastly, steps were taken to understand the horizontal location of the vorticity center in relation to the satellite cloud shield and the theorized main cause of the increase in the mid-level vorticity and the formation of the MCV. The time rate of change in the

relative vorticity is given by the vorticity equation (Eqn. 4.1) using a coordinate system moving with the system (C is the movement of the MCS) where (1) is the time rate of

$$\underset{(1)}{\frac{d(\zeta+f)}{dt}} = \underset{(2)}{\frac{\delta\zeta}{\delta t}} + \underset{(3)}{(V-C)\bullet\nabla(\zeta+f)} + \underset{(4)}{\omega\frac{\partial\zeta}{\partial p}} = \underset{(5)}{-\nabla\bullet V(f+\zeta)} + \underset{(6)}{k\bullet(\frac{\partial V}{\partial p}\times\nabla\omega)} \qquad (4.1)$$

change in the vorticity center, (2) is the local variation at a coinciding point in the moving system (Petterssen, 1956), (3) is the horizontal advection term in a moving coordinate system, (4) is vertical advection term, (5) is the stretching term, (6) is the tilting term, ζ is the relative vorticity, t is time, f is the Coriolis parameter and p is pressure. In Equation 4.1, effects of friction are neglected.

As discussed earlier in Chapter 3, Bartels and Maddox (1991) estimated the stretching term to be approximately double the tilting term and therefore the primary factor in the formation of the MCV. In their study of the 23-24 June 1985 MCS, Johnson and Bartels (1992) computed a vorticity budget based on sounding data and came to the conclusion that the convergence production (stretching term) of vorticity in the stratiform precipitation was the critical factor in intensifying the circulation while tilting played only a minor role due to relatively weak environmental wind shear. On the other hand other researchers (Biggerstaff and Houze, 1991; Brandes, 1990) have found tilting of horizontal vorticity into vertical vorticity to be the primary production of mid-level vorticity. Biggerstaff and Houze (1991) found the tilting term to be 2-10 times greater than the stretching term in their study of the 10-11 June 1985 squall line system, but on scales much smaller than can be identified by the WPDN. If tilting effects are important on the storm scale, it is not expected that they can be detected with the WPDN.

The time rate of change of vorticity [$d(\zeta+f)/dt \cong \delta\zeta/\delta t + (V-C)\bullet\nabla\zeta$] was determined for the mid-levels (650 mb to 550 mb) during the period of maximum increase of relative vorticity leading to the maximum stage of mid-level vorticity in the storm. The term $\delta\zeta/\delta t$ was computed by assuming a linear increase during the two hour period of maximum increase in ζ while the advection and stretching terms were computed central time point of the same two hour period. The vertical advection of vorticity was neglected because the vertical gradient of the vorticity is relatively small making the vertical advection term small compared to the other terms (approximately two orders of magnitude smaller on this scale of computation). This small vertical gradient can be seen in the vertical profiles at the beginning stage of each system (i.e., Figure 4.10). This change was then compared to the expected change due to the mid-level convergence or stretching term ($-[\zeta+f]\nabla\bullet V$, where V is the horizontal wind vector). From now on this will be referred to as the stretching term.

The tilting term cannot be accurately computed from this data set because accurate fields of ω are not known. Therefore only assumptions can be made about the tilting term (plus other remaining neglected terms: vertical advection and friction) based on the ratio of the time rate of change of vorticity to the stretching term (or the difference between these two terms).

Table 4.1 provides a quick summary of all nine cases studied. The column labeled TYPE indicates if the system meets Maddox's (1980) requirements for a MCC or not. The column labeled CIR refers to whether or not a circulation can be seen when the hourly satellite images are looped on a computer screen (from now this will be referred to as a satellite loop). None means a circulation in the system could not be seen and cyc

means a cyclonic circulation while anti means an anticyclonic circulation was noticeable. Note that one system (case # 6) indicated a anticyclonic circulation. This is probably due to the anticyclone in the upper-tropospheric levels above the MCS. Five of the systems indicated cyclonic circulation in the satellite data to some degree. (All nine had a mesovortex based on WPDN data.) This satellite detection percentage is higher than the finding of Bartels and Maddox (1991). This is probably because of their strict requirements in identifying MCVs.

Table 4.1: Summary of the nine systems studied.

CASE #	TYPE	CIR.	MAX SIZE (10^3 km$^{2)}$	BEGIN ζ ($10^{-5}s^{-1}$)	MAX ζ / LEVEL ($10^{-5}s^{-1}$)	FZ LEVEL (mb)	SHEAR ($10^{-3}s^{-1}$)	TIME TO MAX (hr.)	RATIO
1	MCS	none	60	4.5 / 550	10.5/600	570	2.8	5	0.90
2	MCC	none	200	3.9 / 600	22.0/650	580	3.1	8	0.95
3	MCC	cyc.	125	3.3 / 800	14.0/550	580	3.1	8	1.51
4	MCS	cyc.	160	8.2 / 450	30.0/550	570	1.6	6	1.26
5	MCC	cyc.	260	8.4 / 600	17.8/550	575	4.8	7	0.99
6	MCS	anti.	95	1.3 / 700	21.3/550	560	3.0	8	1.62
7	MCS	cyc.	385	11.9/750	14.9/600	590	4.0	7	0.80
8	MCC	none	280	1.0 / 500	13.4/600	570	3.1	9	1.05
9	MCS	cyc.	175	8.8 / 650	12.0/600	570	2.4	6	1.34
avg.			193	5.7 / 622	17.3/583	574	3.1	7.1	1.16
std. dev.			101	3.8 / 115	6.2 / 35	8.6	0.9	1.3	0.29

MAX SIZE refers to maximum size the system reached during its lifetime. BEGIN ζ / LEVEL refers to the maximum relative vorticity averaged over the first three hours after the system appears organized in the satellite images and the level of the maximum. MAX ζ / LEVEL refers to the maximum relative vorticity and the level it is found at averaged over three hours centered on the hour of maximum mid-level vorticity. FZ LEVEL refers to the height of the freezing level and SHEAR refers to the 300-850 mb wind shear. TIME TO MAX refers to the time from when the system first appears organized until the time when the mid-level relative vorticity reaches a maximum.

Lastly, RATIO refers to ratio of the time rate of change of vorticity to the stretching production term. The last two rows are the average and standard deviation for each column.

There are a few things to note about Table 4.1. First note that all nine of the systems develop mid-level vorticity to a value equal to or greater than the Coriolis parameter ($10^{-4}s^{-1}$). This consistent increase in all the systems would suggest that the processes, whatever they may be, that lead to a MCV are occurring in all MCSs. A second thing to notice is that the two systems with the highest shear are two of the larger systems studied and both systems indicated to some extent a cyclonic circulation in the satellite loop. This suggests that the higher shear that might destroy the MCV is overcome by the larger scale of horizontal latent heat processes. This is expected for situations where the horizontal scale of the heating is comparable to or larger than the Rossby radius of deformation (Schubert *et al.*, 1980; Zhang and Fritsch, 1988; Cotton *et al.*, 1989), so that much of the energy from the heating goes into quasi-balanced flow. Finally, notice the close proximity of the maximum vorticity level to the freezing level. This result is consistent with other studies showing enhanced inflow into MCSs near the melting level (e.g., Johnson *et al.*, 1995).

The results for each individual case, including satellite photos with an MB enhancement (Carlson, 1981), NWS radar summaries, the synoptic setting, freezing level and the vertical wind shear (from rawinsonde data), are shown in sections 4.1 through 4.9. Due to the unstable orbit of GOES7 during 1993 there are some griding problems with the satellite images. This is sometimes evident when the satellite images are compared to the radar summaries. The freezing level is included to show that it generally

coincides with the maximum vorticity level. This feature is hypothesized to be due to the enhanced inflow into MCSs near the melting level that increases the mid-level convergence and therefore produces vorticity (Johnson *et al.*, 1995). The vertical shear is also included because some researchers think that weak vertical shear is needed to produce and maintain a MCV (Bartels and Maddox, 1991; Johnson and Bartels, 1992). For readers not familiar with shear in the form presented here, a 300 - 850 mb shear of $1.0 \times 10^{-3} s^{-1}$ means an increase of approximately 10 m s^{-1} between 850 and 300 mb while a shear of $4.0 \times 10^{-3} s^{-1}$ means an increase of approximately 30 m s^{-1}.

4.1 CASE # 1

Case #1 occurred on June 8, 1993, and is a MCC-like MCS (Figure 4.2 and 4.3) that does not meet the size requirement to be an MCC (Maddox, 1980). The system starts in Oklahoma and moves northeast at approximately 20 m s^{-1} parallel to a cold front (Figure 4.1) growing to cover a maximum area of approximately 60,000 km^2 by 1000 UTC. Figures 4.2 through 4.3 show the hourly infrared satellite photos and NWS radar summaries for this system. Looping of the hourly images on a computer screen does not indicate a circulation in this system. The system starts between 0300 UTC and 0400 UTC as a large thunderstorm in Oklahoma just ahead of the north - south oriented cold front (Figure 4.1) that is slowly moving east and behind a dying squall line. The MCS develops in an area of low-level convergence and is fed warm moist air from the south by the 40 knot low-level jet (Figure 4.1) which is consistent with the typical MCC environment found by Maddox (1983).

The system grows and develops a stratiform region on the north side, which is suggested in the 0635 UTC radar summary (Figure 4.2), as it moves to the northeast. Figures 4.4 through 4.9 show the 600 mb level relative charts for this system (note: in order to conserve space, horizontal vorticity charts will not be shown for the other eight cases). The + symbols on the satellite photos (Figure 4.2 and 4.3) show the relative position of the 600 mb relative vorticity maximum as the system develops. The vorticity maximum starts on the south side where the most intense convection is occurring, but by 0900 UTC the vorticity maximum appears to move into the stratiform region.

Figure 4.10 shows the beginning (0500 UTC to 0700 UTC) and maximum stage (0900 UTC to 1100 UTC) vertical profiles of relative vorticity between 800 mb and 400 mb. The profiles show the system starts with a positive vorticity maximum of 4.5×10^{-5} s^{-1} at 550 mb that is probably associated with a weak shortwave trough (Figure 4.1). The vorticity then increases up to $10.5 \times 10^{-5} s^{-1}$ at 600 mb. This maximum is slightly below the freezing level at 570 mb (Figure 4.10) suggesting the significance of latent heat processes enhancing the horizontal convergence in this area. This is consistent with other MCV studies that found the maximum vorticity near the freezing level (Zhang and Fritsch, 1988; Johnson and Bartels, 1992; Zhang, 1992).

The time rate of change of the relative vorticity during the period of maximum increase (0800 UTC to 1000 UTC) is 9.6×10^{-9} s^{-2} while the stretching term at 0900 UTC is $1.07 \times 10^{-8} s^{-2}$. The ratio of the time rate of change to the stretching term is .90 or 90%. Since this ratio is close to one it suggests the increase in vorticity is primarily due to the stretching production term, suggesting production by the tilting term is small on this scale of computation.

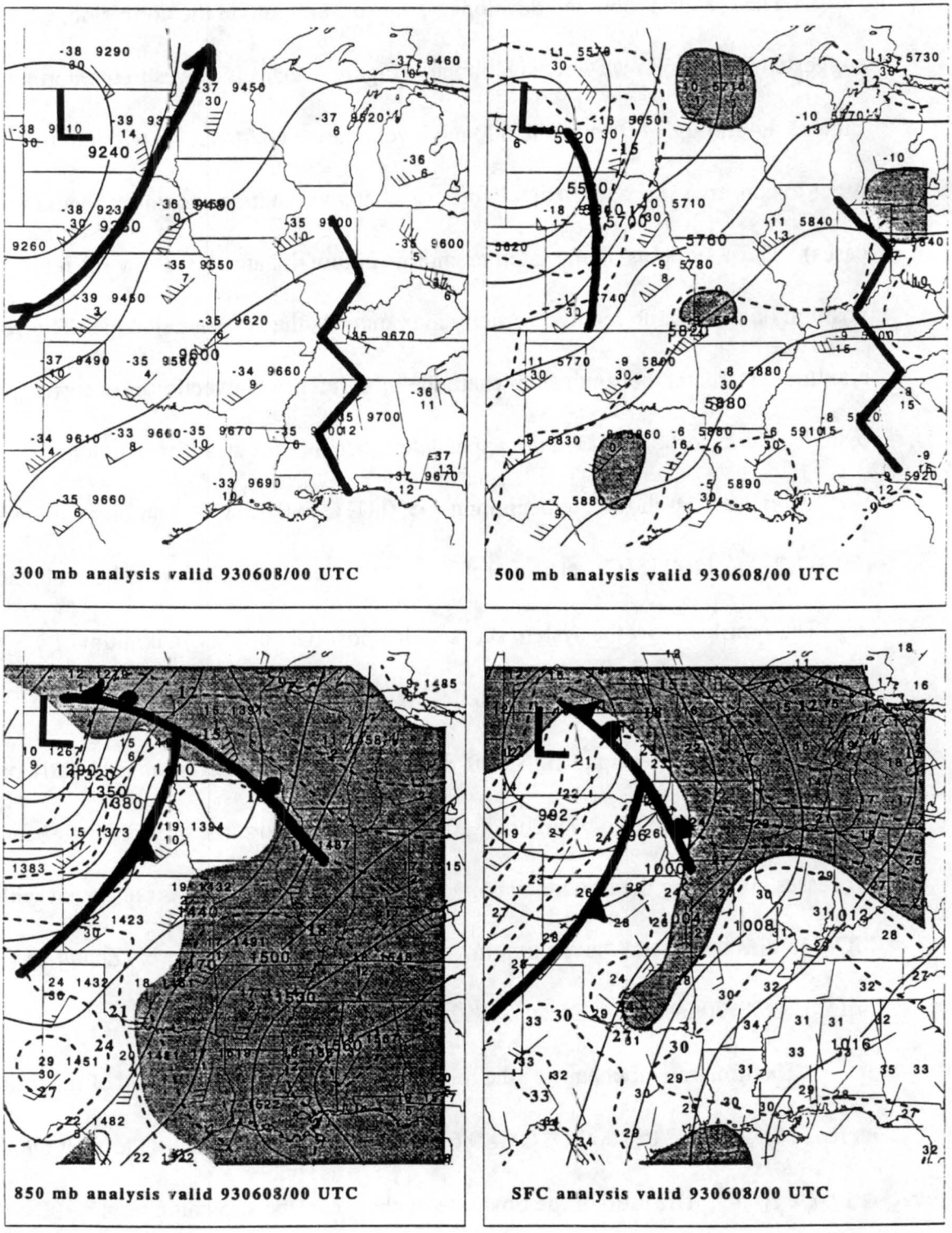

Figure 4.1: Analysis for the 300 mb, 500 mb, 850 mb and surface levels for 00 UTC on 8 June 1993. The gray shaded regions are areas of dewpoint depressions of 5°C or less.

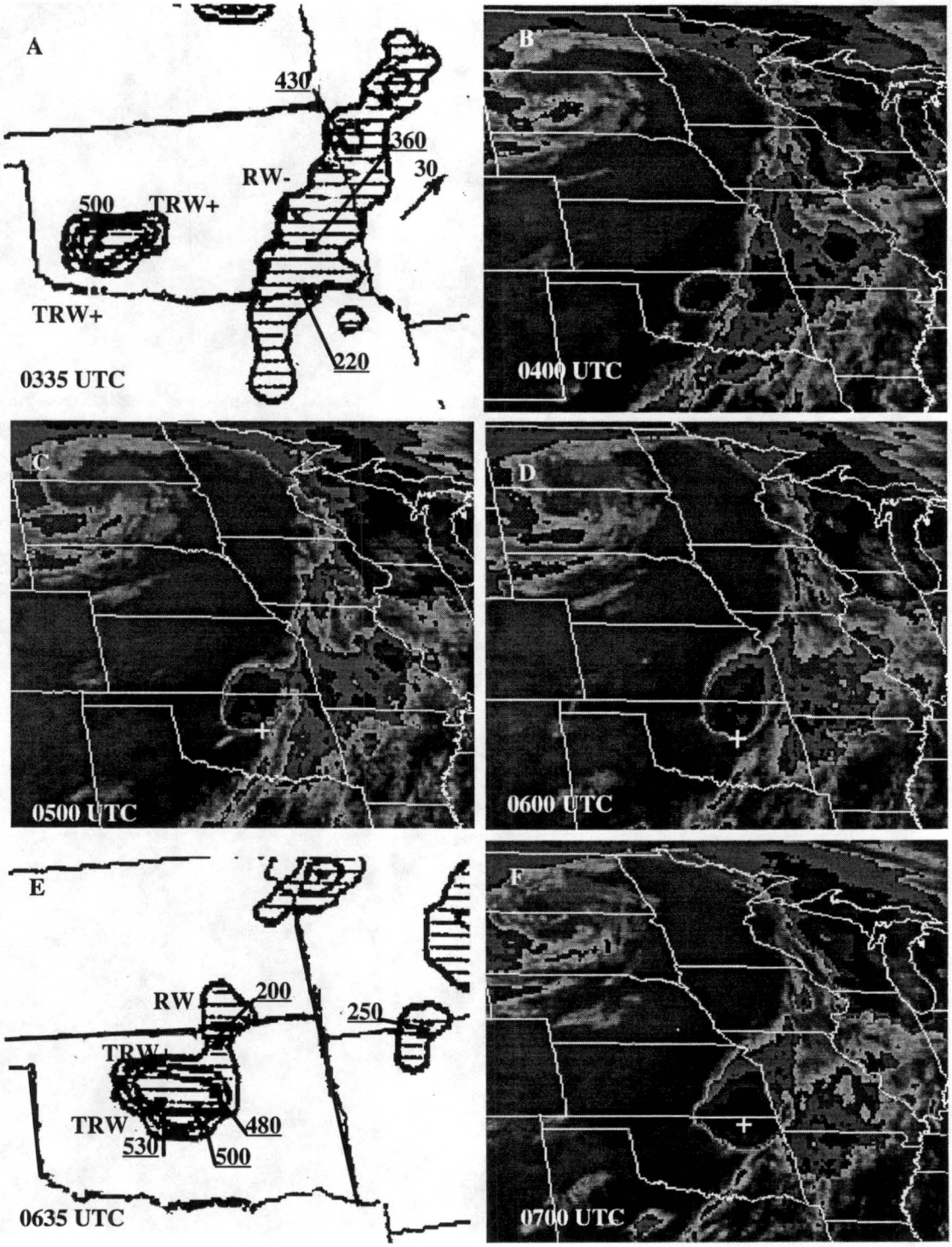

Figure 4.2: NWS radar summaries for (A) 0335 UTC and (E) 0635 UTC and infrared satellite images for (B) 0400 UTC, (C) 0500 UTC, (D) 0600 UTC and (F) 0700 UTC on 8 June, 1993.

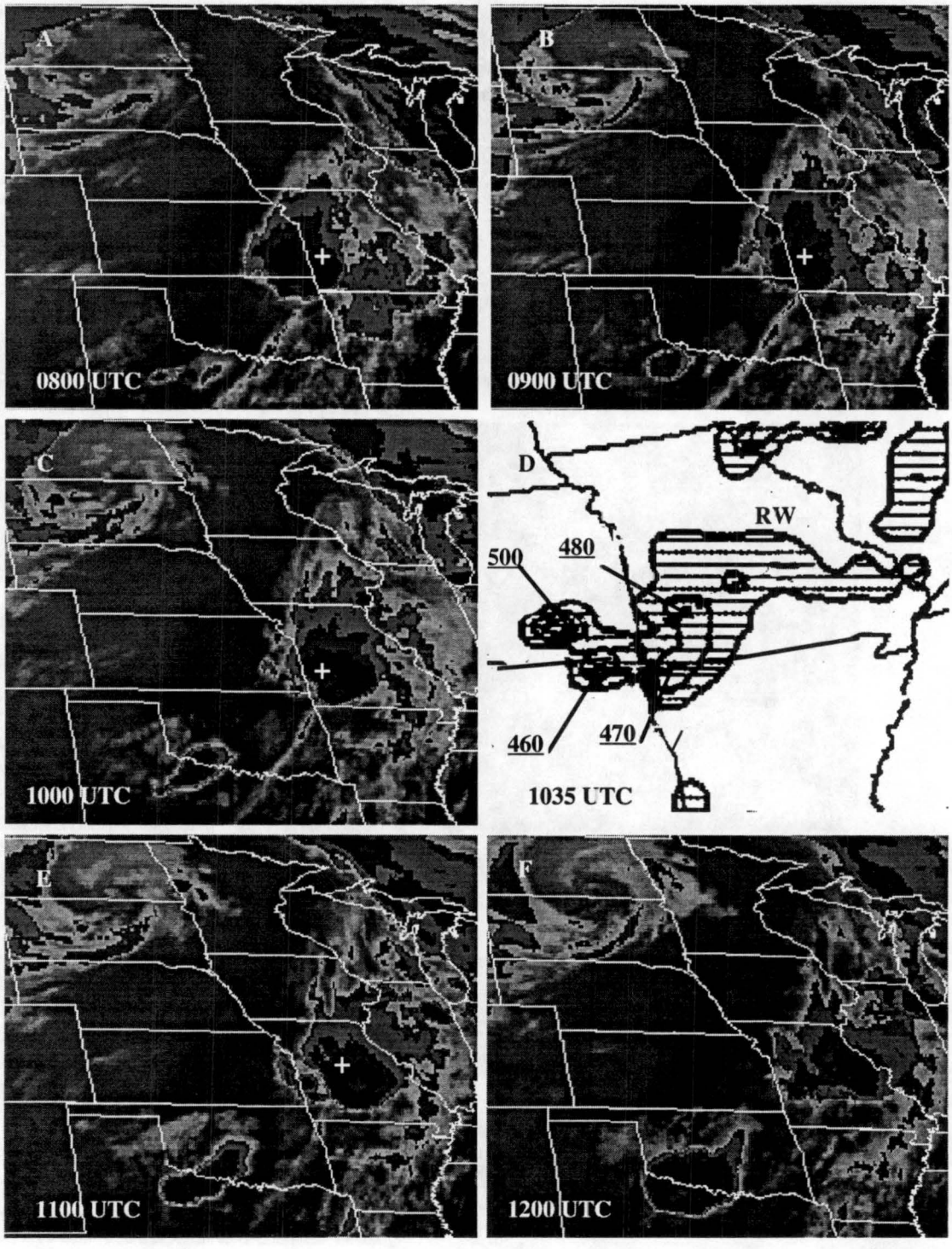

Figure 4.3: NWS radar summary for (D) 1035 UTC and infrared satellite images for (A) 0800 UTC, (B) 0900 UTC, (C) 1000 UTC, (E) 1100 UTC and (F) 1200 UTC on 8 June, 1993.

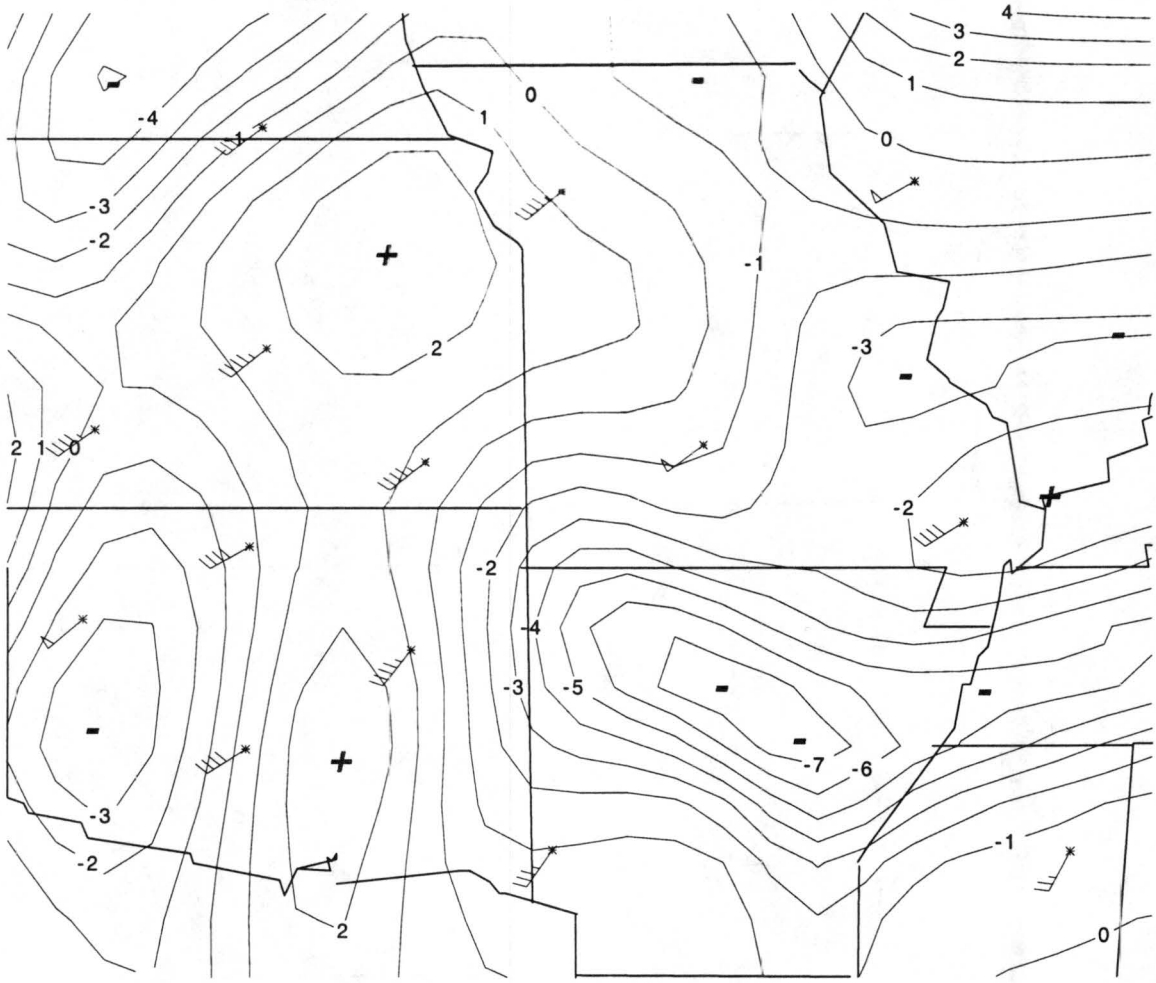

Figure 4.4: 600 mb vorticity ($10^{-5}s^{-1}$) chart for 0500 UTC 8 June 1993.

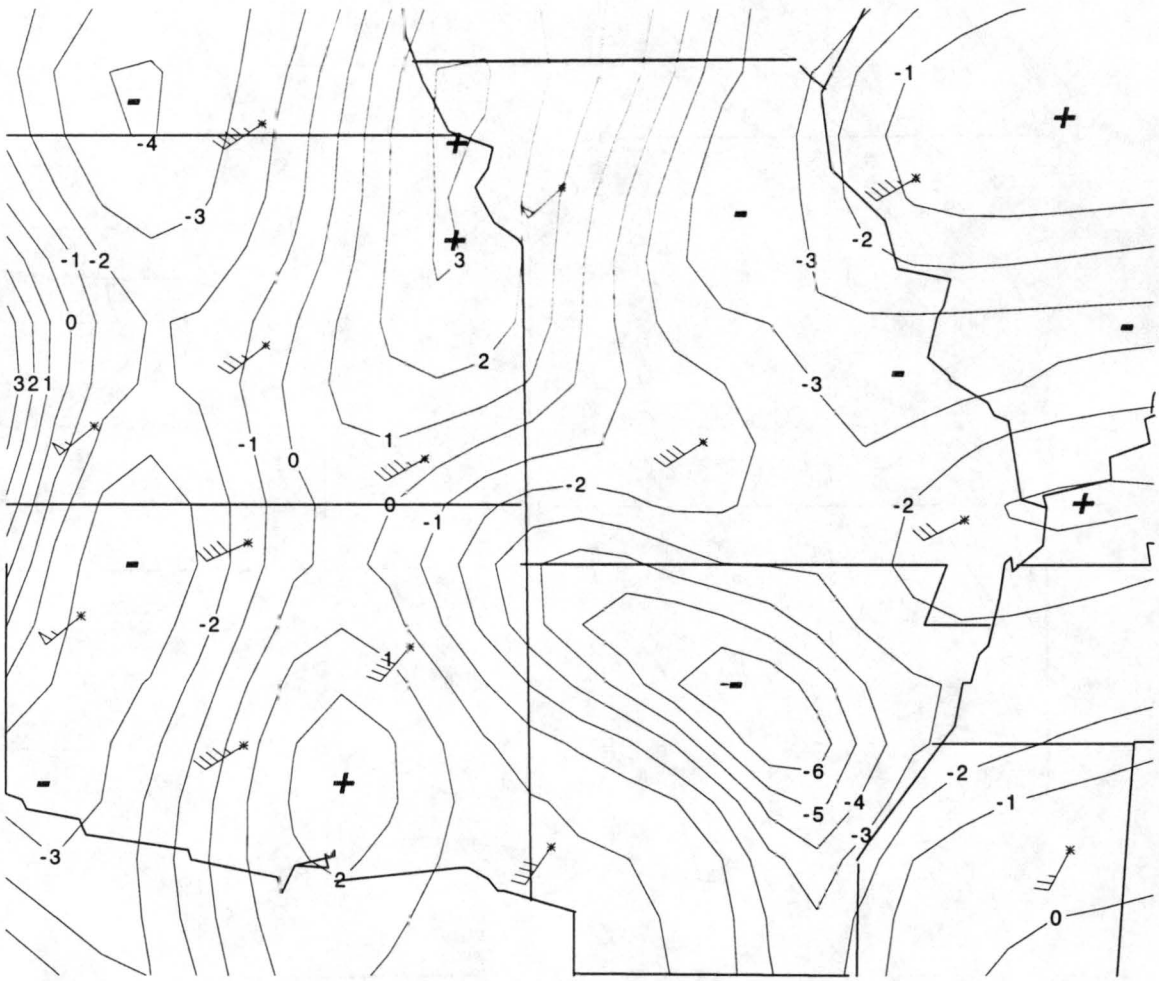

Figure 4.5: 600 mb vorticity ($10^{-5}s^{-1}$) chart for 0600 UTC 8 June 1993.

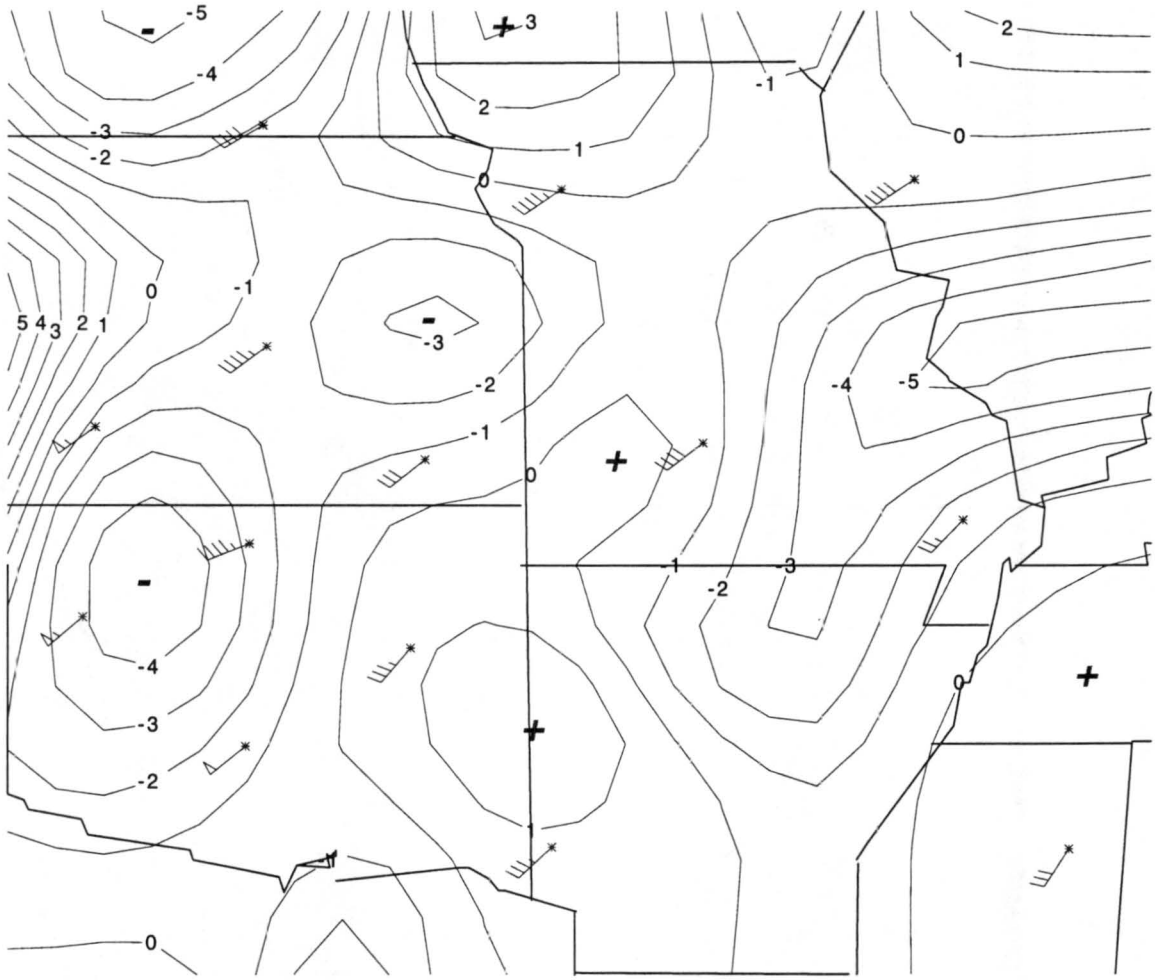

Figure 4.6: 600 mb vorticity ($10^{-5}s^{-1}$) chart for 0700 UTC 8 June 1993.

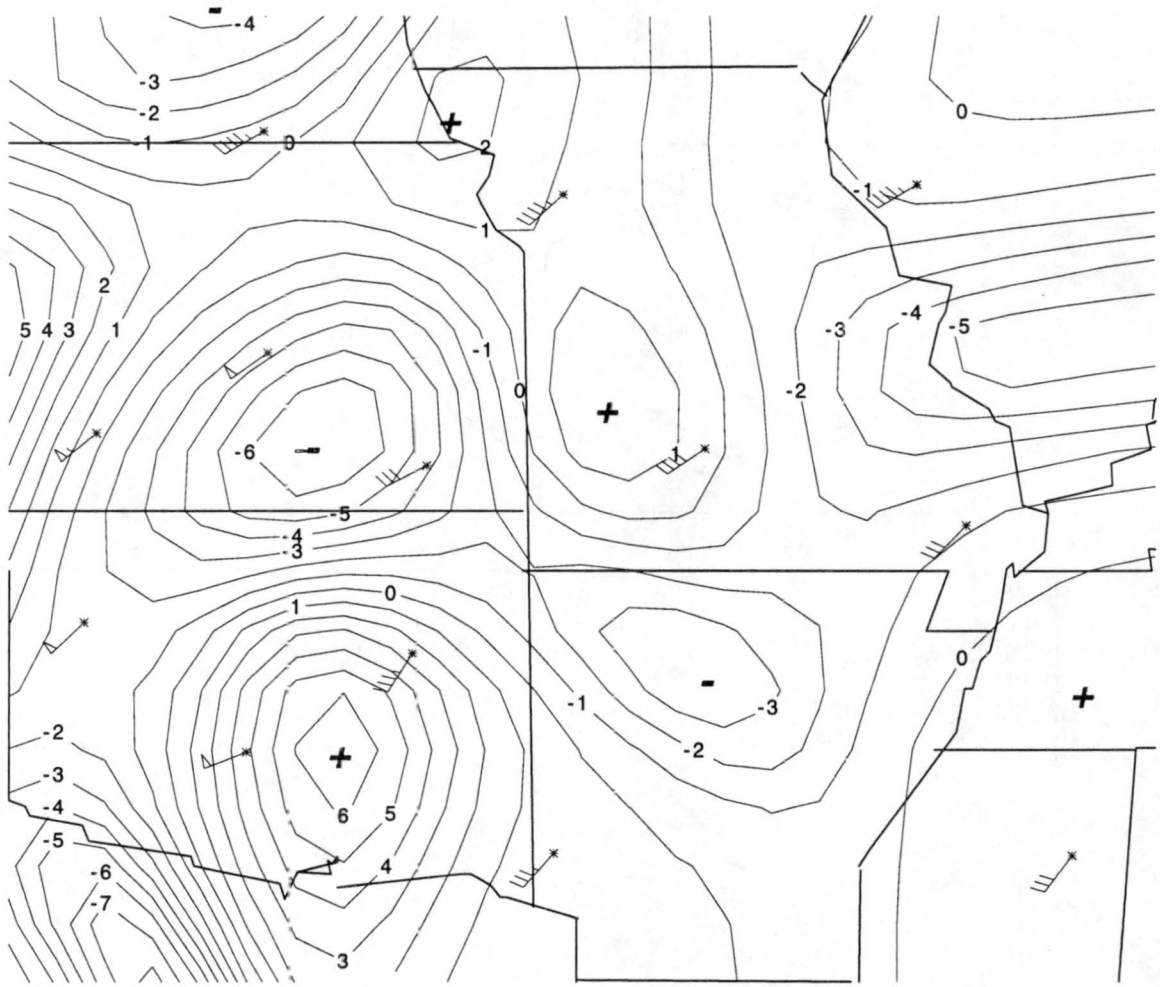

Figure 4.7: 600 mb vorticity ($10^{-5}s^{-1}$) chart for 0800 UTC 8 June 1993.

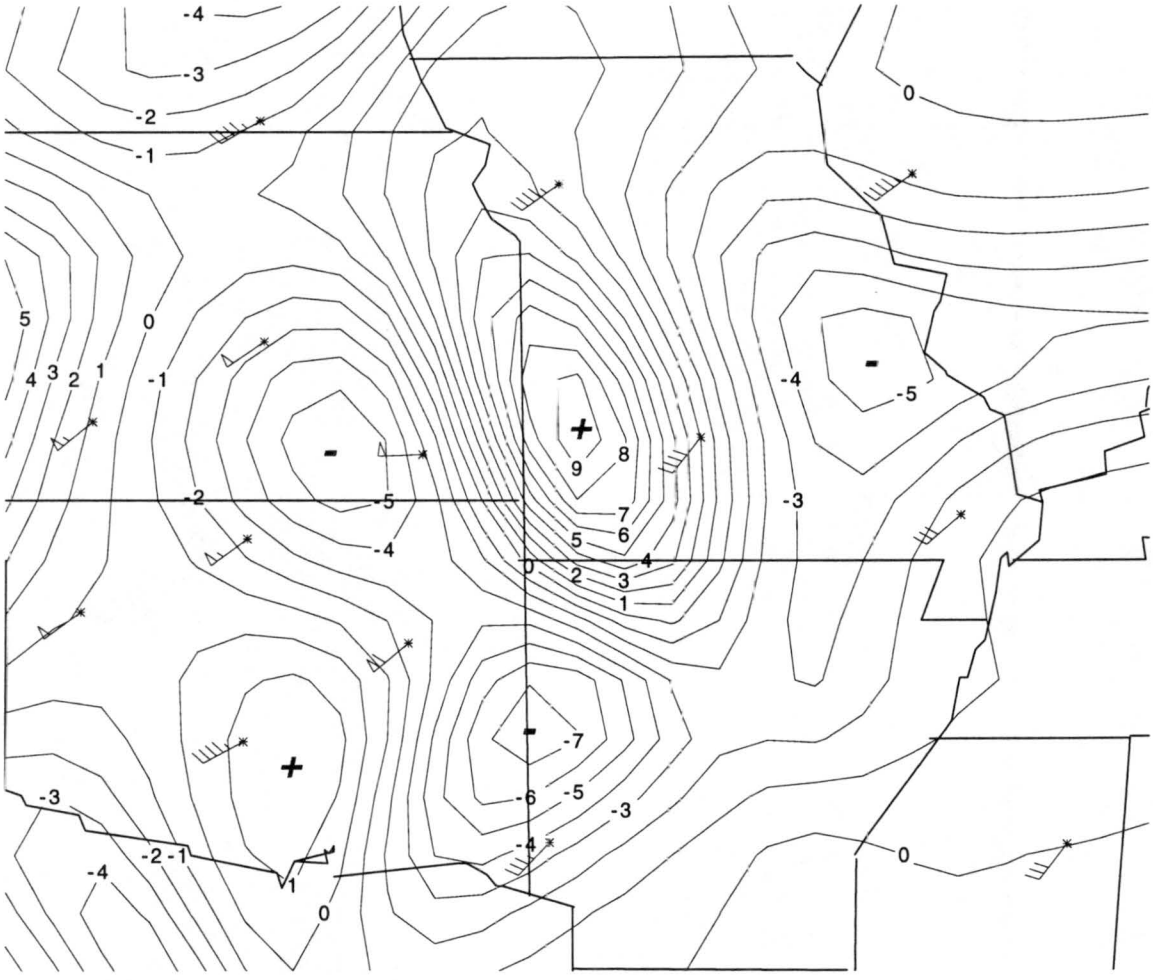

Figure 4.8: 600 mb vorticity ($10^{-5}s^{-1}$) chart for 0900 UTC 8 June 1993.

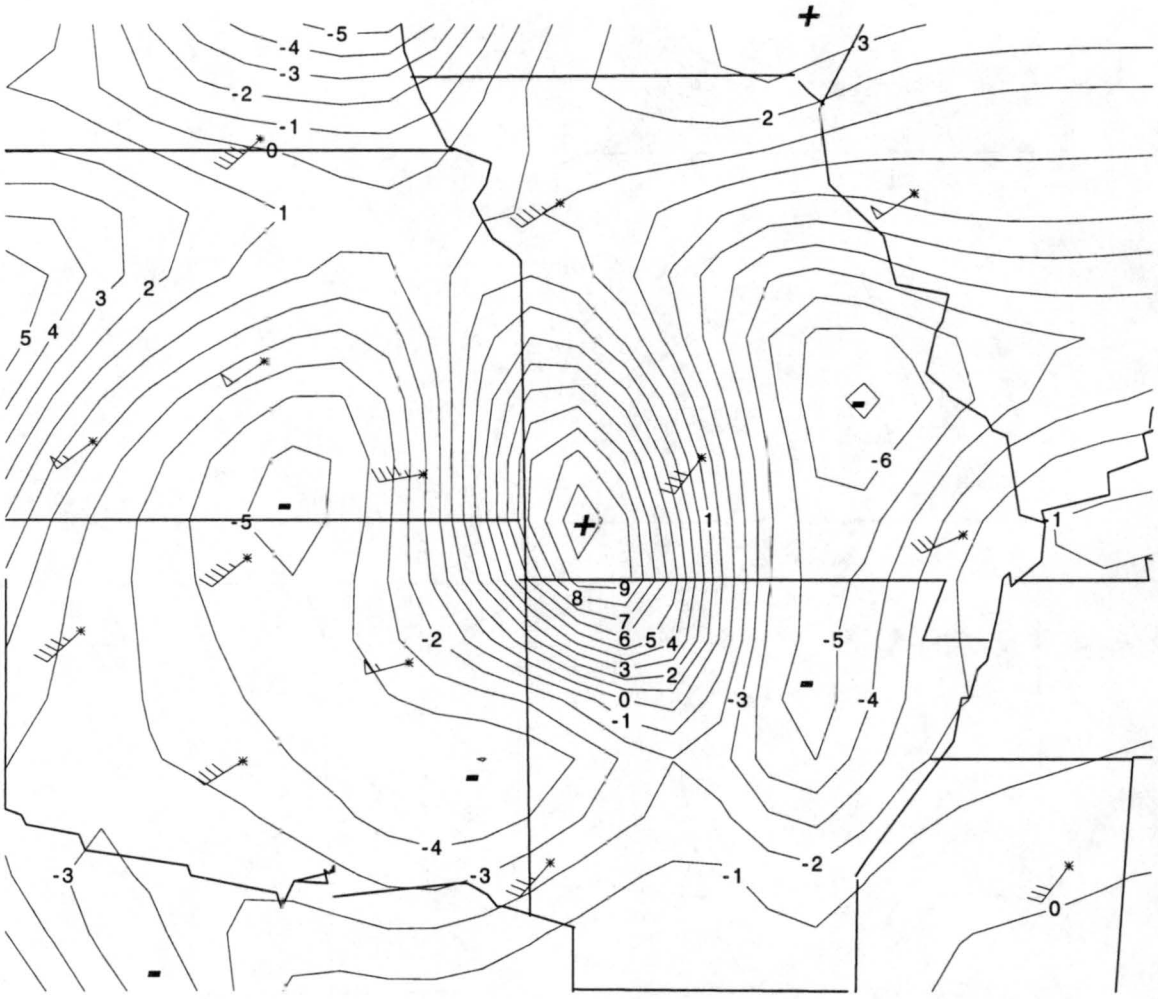

Figure 4.9: 600 mb vorticity ($10^{-5}s^{-1}$) chart for 1000 UTC 8 June 1993.

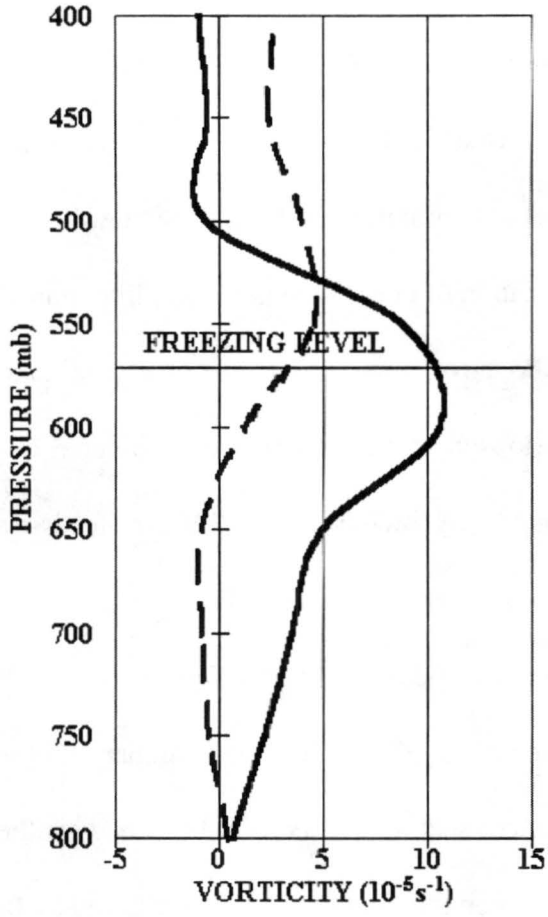

Figure 4.10: Average vertical profiles of relative vorticity for the 8 June 1993 MCS. The dashed line is for the beginning stage of the MCS and the solid line is for the maximum stage.

4.2 CASE # 2

Case #2 occurred on June 13, 1993 and is a MCC (Figures 4.12 through 4.14) that formed in western Nebraska ahead of a NNE - SSW oriented frontal system (Figure 4.11). The system moves east at approximately 12 m s^{-1} with a slight anticyclonic curvature and does not show an indication of circulation in the satellite loop. The system begins around 0000 UTC and grows to cover a maximum area of approximately 200,000 km^2 by 0700 UTC. The MCC develops in an area of low-level upslope flow just to the north of a surface Low (Figure 4.11). A low-level jet of 30 knots feeds warm air from the south and aids in the low-level convergence (Figure 4.11).

The system grows and develops a stratiform region on the west and northwest side, which is suggested in the 0335 UTC radar summary (Figure 4.12), as it moves to the east. The most intense convection occurs on the east and southeast side of the MCC. The vorticity maximum starts on the west side of the MCC and by 0300 UTC the vorticity maximum appears to be in the stratiform region (Figure 4.12).

Figure 4.15 shows the beginning (0100 UTC to 0300 UTC) and maximum (0800 UTC to 1000 UTC) stage vertical profiles of relative vorticity between 800 mb and 400 mb. The profiles show the system starts with a positive relative vorticity maximum of 3.9 x $10^{-5}s^{-1}$ at 600 mb. The mid-level vorticity reaches a maximum of 2.2 x $10^{-4}s^{-1}$ at 650 mb, which is 70 mb below the freezing level, by 0900 UTC. The time rate of change of the mid-level vorticity for the period from 0700 UTC to 0900 UTC is 1.8 x $10^{-8}s^{-2}$ while the stretching term is 1.9 x $10^{-8}s^{-2}$. The ratio of the time rate of change to the stretching term is .95 or 95%, suggesting the stretching term is the primary production term.

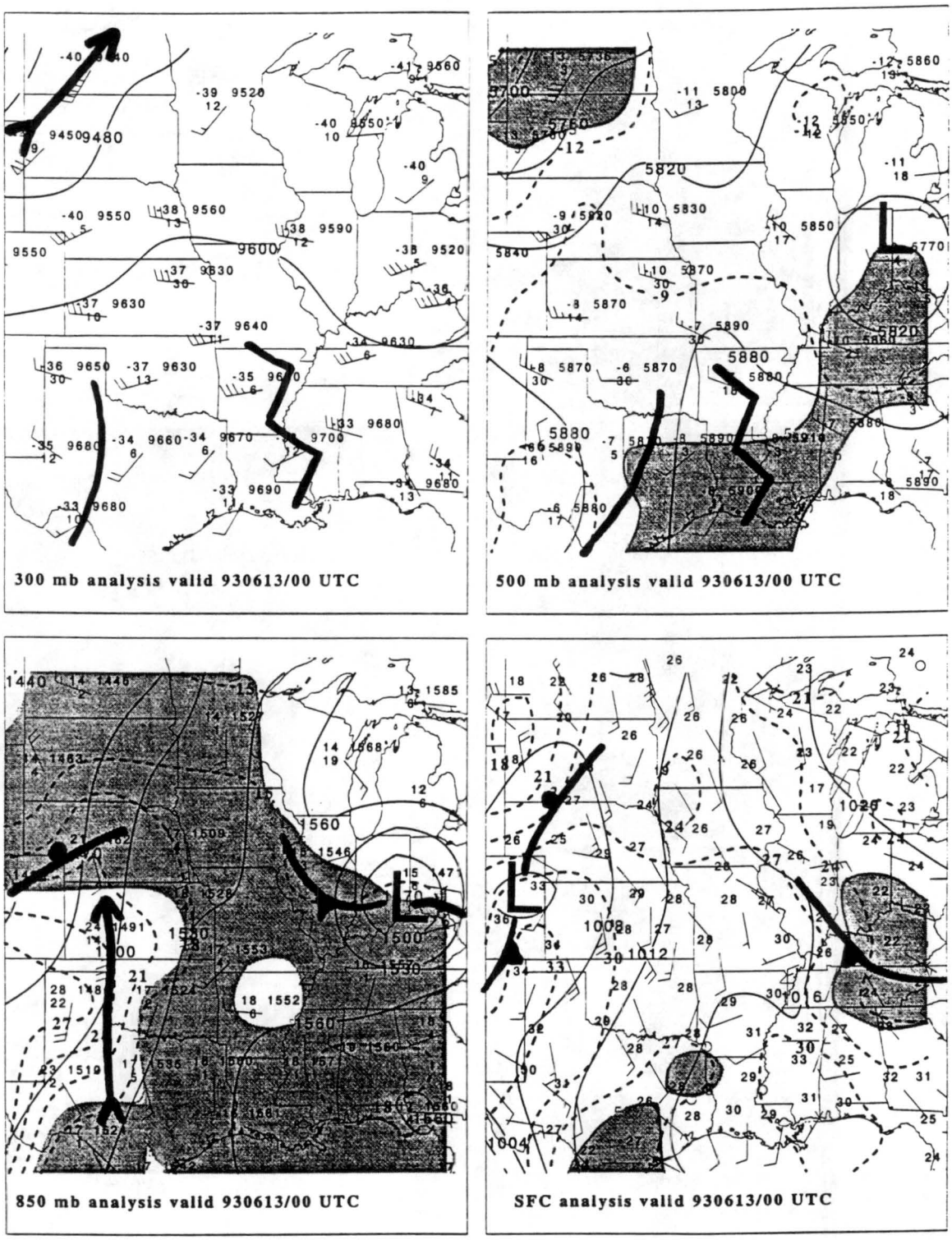

Figure 4.11: Analysis for the 300 mb, 500 mb, 850 mb and surface levels for 00 UTC on 13 June 1993. The gray regions are areas of dewpoint depressions of 5°C or less.

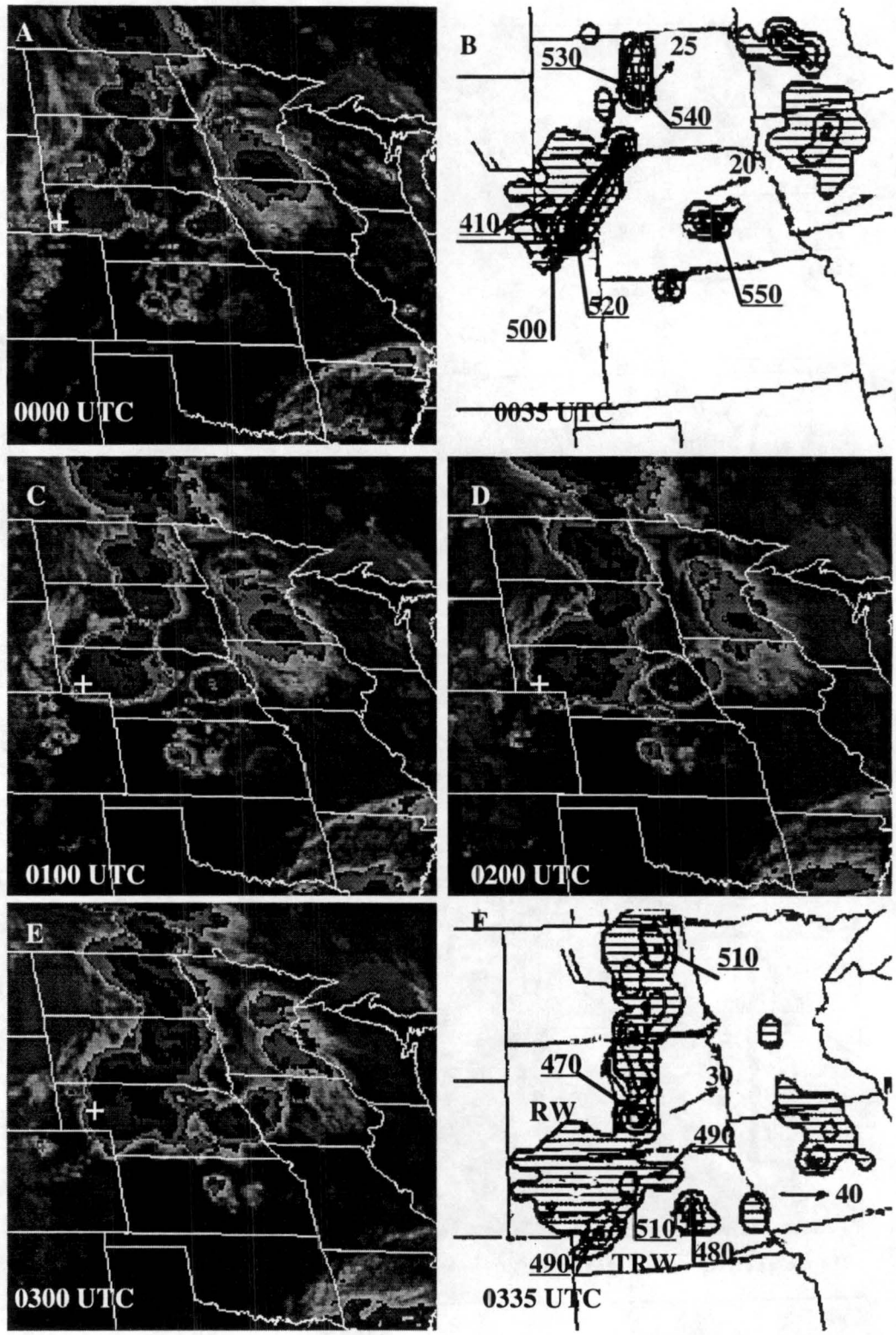

Figure 4.12: Infrared satellite images for (A) 0000 UTC, (C) 0100 UTC, (D) 0200 UTC, (E) 0300 UTC and NWS radar summaries for (B) 0035 UTC and (F) 0335 UTC on 13 June, 1993.

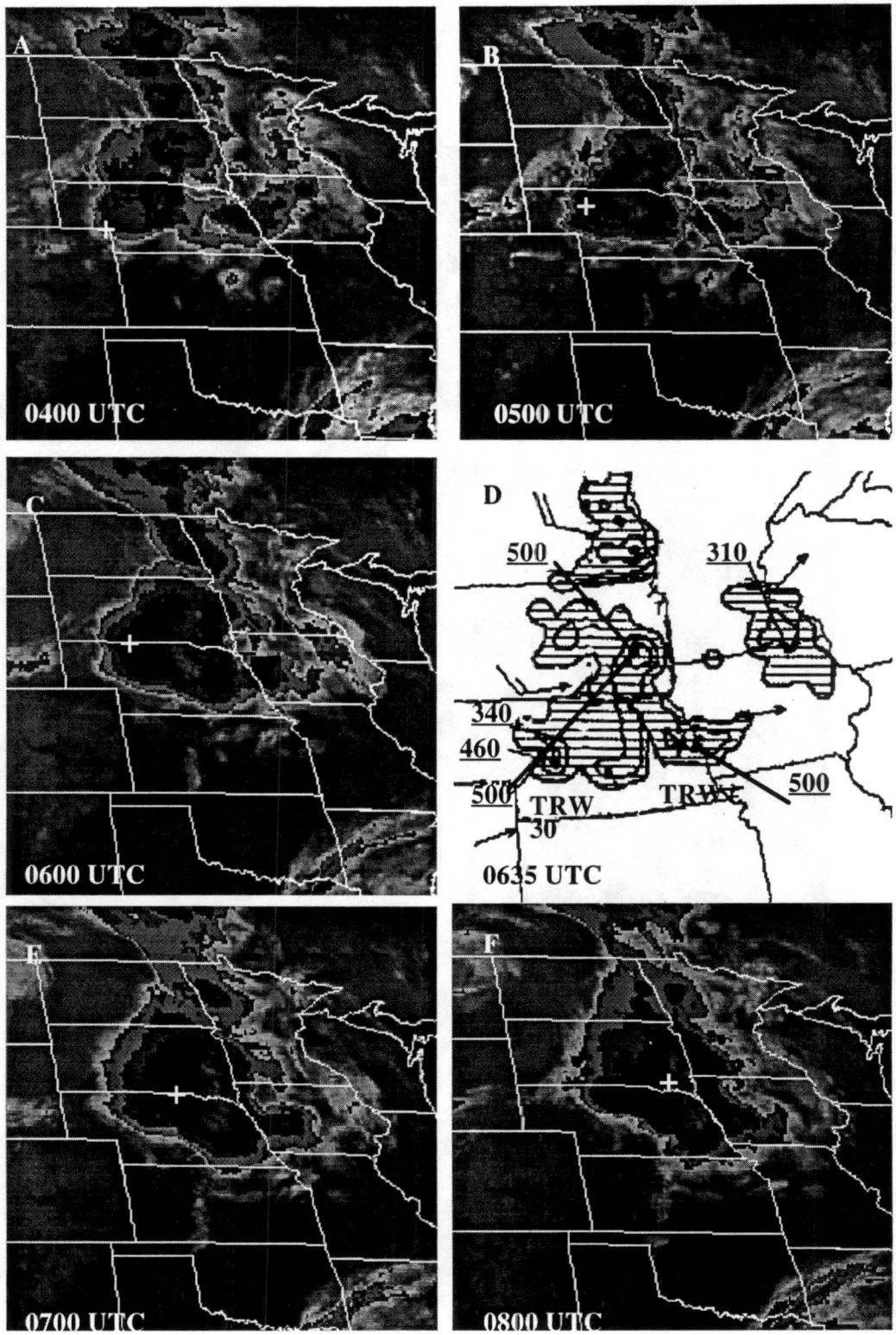

Figure 4.13: Infrared satellite images for (A) 0400 UTC, (B) 0500 UTC, (C) 0600 UTC, (E) 0700 UTC, (F) 0800 UTC 13 June, 1993 and NWS radar summary for (D) 0635 UTC 13 June, 1993.

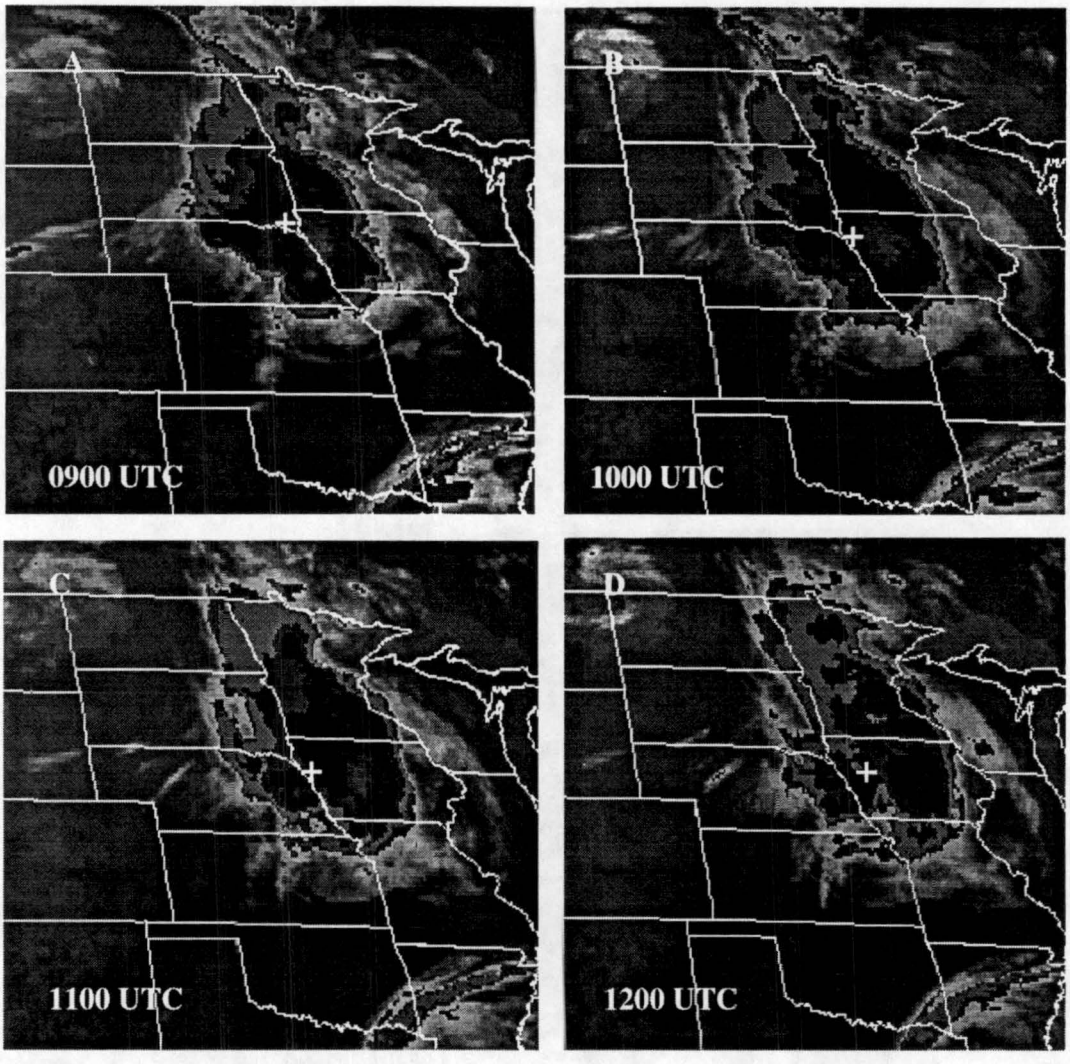

Figure 4.14: Infrared satellite images for (A) 0900 UTC, (B) 1000 UTC, (C) 1100 UTC and (D) 1200 UTC 13 June, 1993.

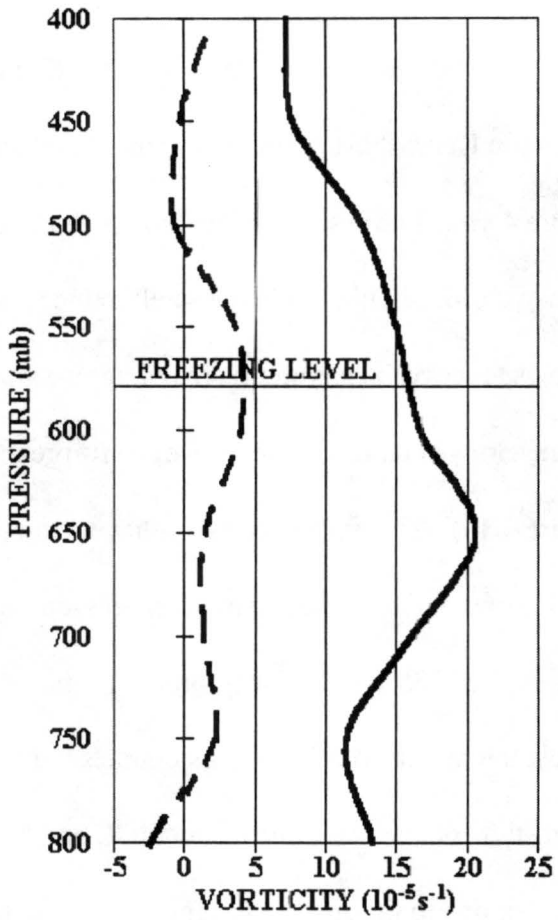

Figure 4.15: Average vertical profiles of relative vorticity for the 13 June 1993 MCC. The dashed line is for the beginning stage of the MCC and the solid line is for the maximum stage.

4.3 CASE # 3

Case #3 occurred on June 14, 1993 and is an MCC (Figure 4.17 through 4.19) that formed in southwestern Kansas just north of an upper-level anticyclone and a weak surface front (Figure 4.16). The system moves slowly to the southeast at 5 m s^{-1} and develops a definite cyclonic circulation in the satellite loop. The system begins around 1000 UTC and grows to cover a maximum area of approximately 125,000 km^2 by 0700 UTC. The MCC develops in an area of low-level convergence associated with the surface front (Figure 4.16). This system does not have a low-level jet associated with it.

The system grows and develops a stratiform region on the east northeast side, which is suggested in the 1235 UTC radar summary (Figure 4.17), as it moves to the southeast. The most intense convection occurs on the southwest side of the MCC. The vorticity maximum starts on the west side of the MCC and by 1400 UTC the vorticity maximum appears to move to the stratiform region.

Figure 4.20 shows the beginning (1200 UTC to 1400 UTC) and maximum (1900 UTC to 2100 UTC) stage vertical profiles of relative vorticity between 800 mb and 400 mb. The profiles show the system starts with a vorticity maximum of $0.6 \times 10^{-5} s^{-1}$ at 600 mb. The vorticity does not significantly change until 1800 UTC but then start increasing to reach a maximum $1.4 \times 10^{-4} s^{-1}$ at 550 mb, which is 30 mb above the freezing level, by 2000 UTC. The time rate of change of the mid-level vorticity for the period between 1800 UTC and 2000 UTC is $1.4 \times 10^{-8} s^{-2}$ while the stretching term is $9.3 \times 10^{-9} s^{-2}$. The ratio of the time rate of change to the stretching term is 1.51 or 151%. This would suggest the stretching term is only producing about two thirds of the vorticity increase and therefore the tilting term may be significant in this system.

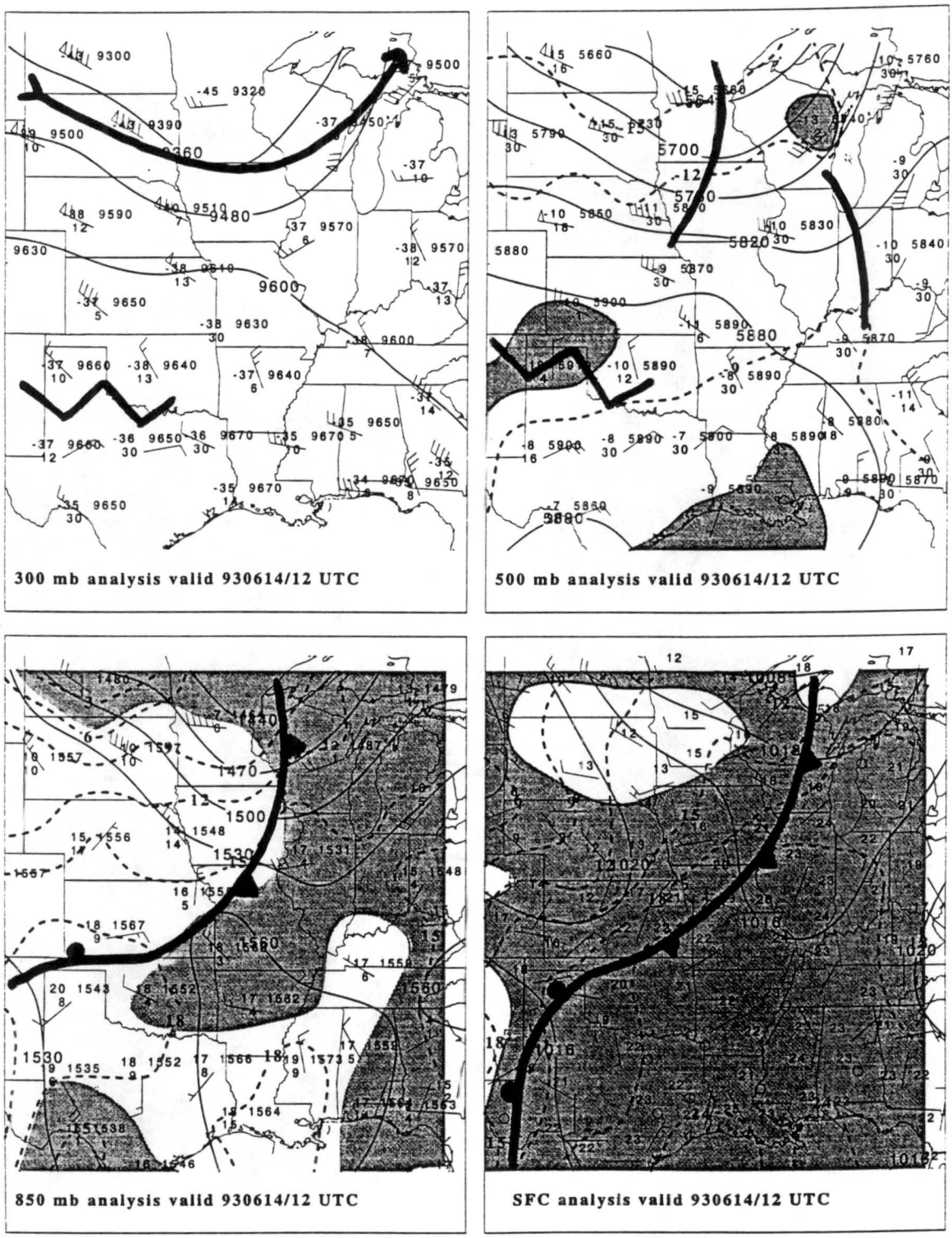

Figure 4.16: Analysis for the 300 mb, 500 mb, 850 mb and surface levels for 1200 UTC 14 June 1993. The gray shaded regions are areas of dewpoint depressions of 5°C or less.

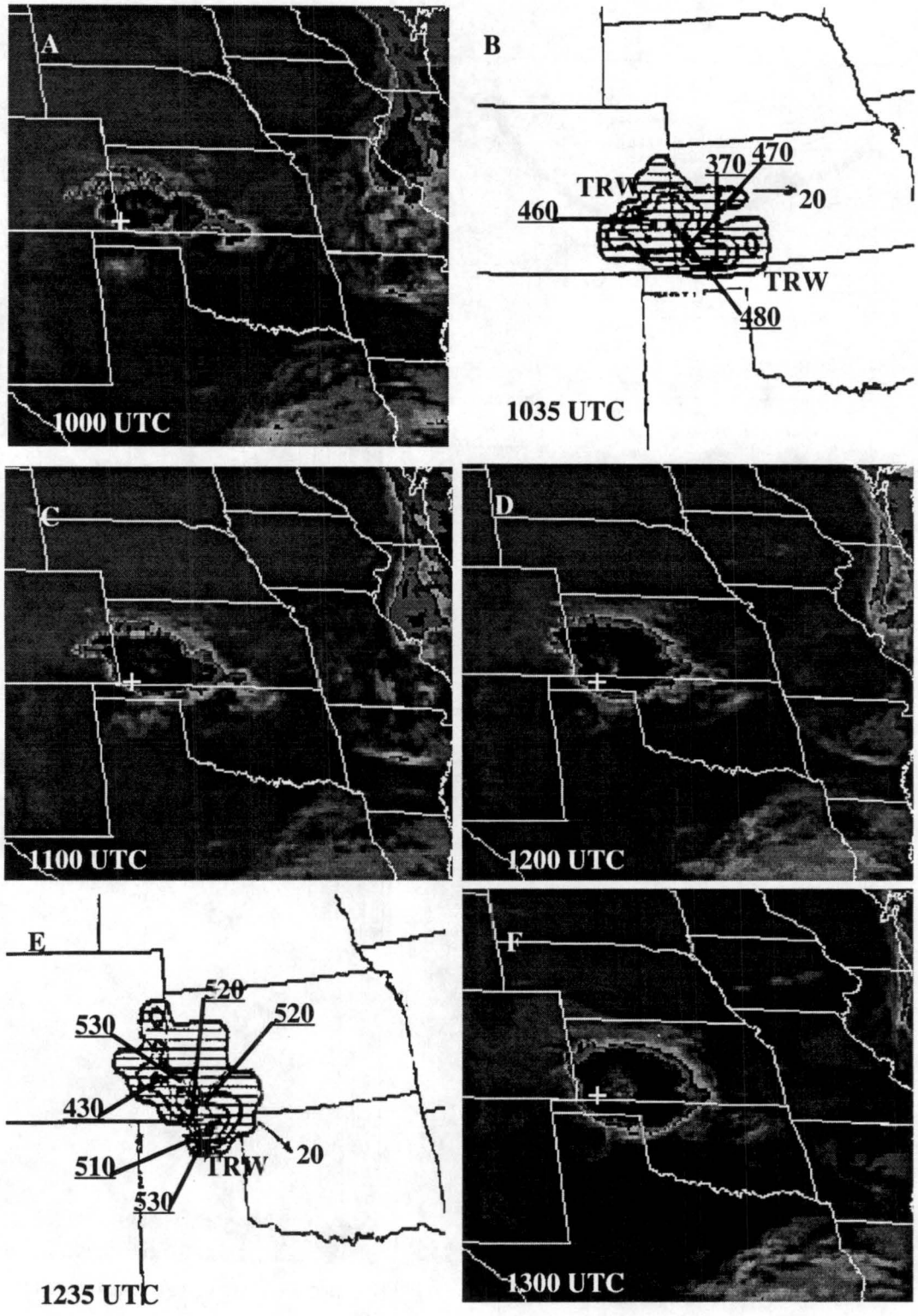

Figure 4.17: Infrared satellite images for (A) 1000 UTC, (C) 1100 UTC, (D) 1200 UTC, (F) 1300 UTC 14 June 1993 and NWS radar summaries for (B) 1035 UTC and (E) 1235 UTC 14 June 1993.

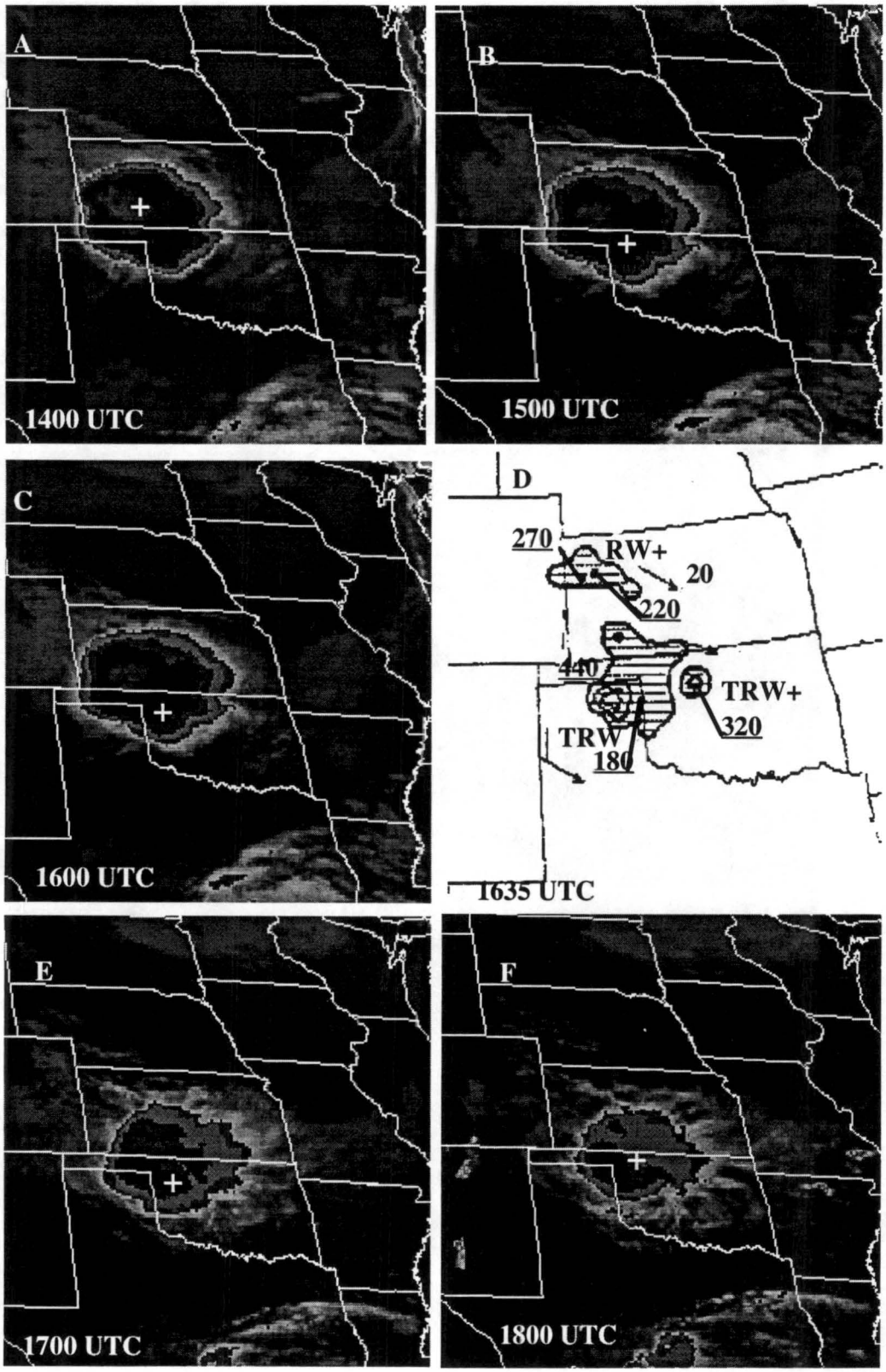

Figure 4.18: Infrared satellite images for (A) 1400 UTC, (B) 1500 UTC, (C) 1600 UTC, (E) 1700 UTC, (F) 1800 UTC 14 June 1993 and NWS radar summary for (D) 1635 UTC 14 June 1993.

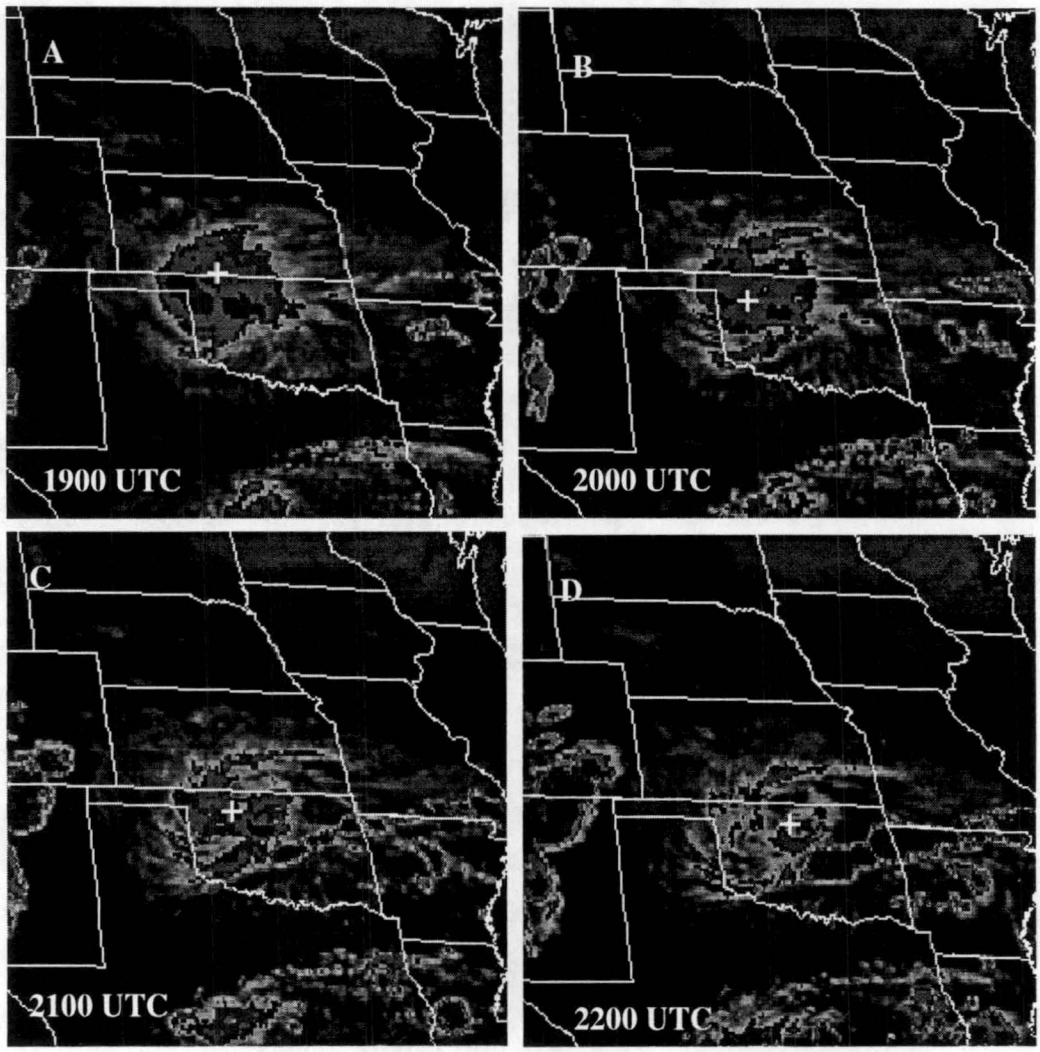

Figure 4.19: Infrared satellite images for (A) 1900 UTC, (B) 2000 UTC, (C) 2100 UTC and (D) 2200 UTC 14 June 1993.

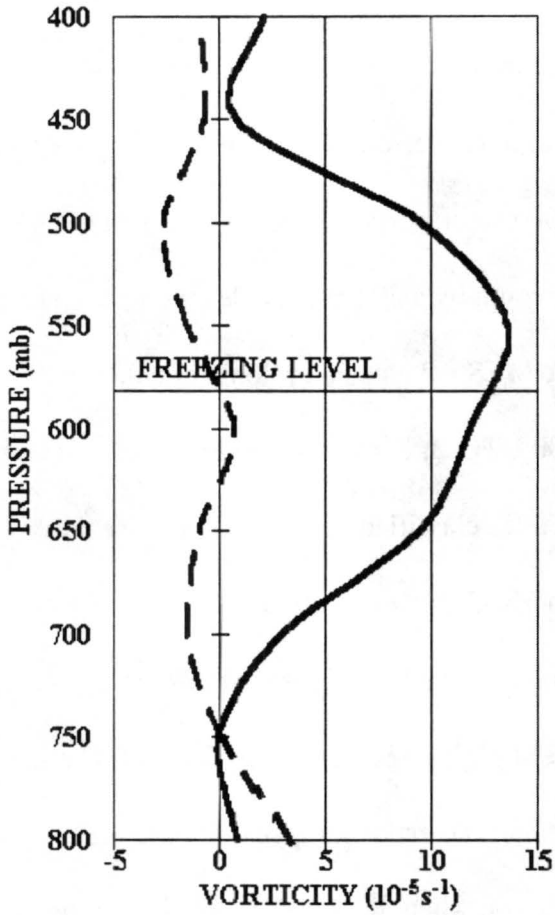

Figure 4.20: Average vertical profiles of relative vorticity for the 14 June 1993 MCC. The dashed line is for the beginning stage of the MCC and the solid line is for the maximum stage.

4.4 CASE # 4

Case #4 occurred on June 27, 1993 and is an MCC-like MCS (Figures 4.22 and 4.23) that formed in northwestern Kansas under an upper-level (300 mb) shortwave trough and south of a weak surface front (Figure 4.21). This system is fed low-level warm air from the south by a 30 knot low-level jet as it moves to the southeast at 19 ms^{-1} (Figure 4.21). The MCS develops a cyclonic circulation in the satellite loop. The system begins around 0000 UTC and grows to cover a maximum area of approximately 160,000 km^2 by 0500 UTC. It's classified as an MCS because it does not meet the time requirement for an MCC (Maddox, 1980).

The system grows and develops a stratiform region on the north side. The stratiform region is slightly suggested in the 0335 UTC radar summary and strongly suggested in the 0635 UTC radar summary (Figure 4.22). The most intense convection occurs on the south side where the low-level jet is feeding the system (Figure 4.21). The vorticity maximum starts on the south side of the MCS in the convective region and by 0500 UTC the vorticity maximum appears to move to the stratiform region.

Figure 4.24 shows the beginning (0400 UTC to 0600 UTC) and maximum (0900 UTC to 1100 UTC) stage vertical profiles of relative vorticity between 800 mb and 400 mb. The profiles show the system starts with a mid-level positive relative vorticity maximum of $8.2 \times 10^{-5} s^{-1}$ at 450 mb then increases to a maximum of $3.0 \times 10^{-4} s^{-1}$ at 550 mb, which is 20 mb above the freezing level (Figure 4.24). The time rate of change of the mid-level vorticity for the period from 0800 UTC to 1000 UTC is $2.4 \times 10^{-8} s^{-2}$ while the stretching term is $1.9 \times 10^{-8} s^{-2}$. The ratio of the time rate of change to the stretching term is 1.26 or 126%, suggesting the tilting term is contributing also.

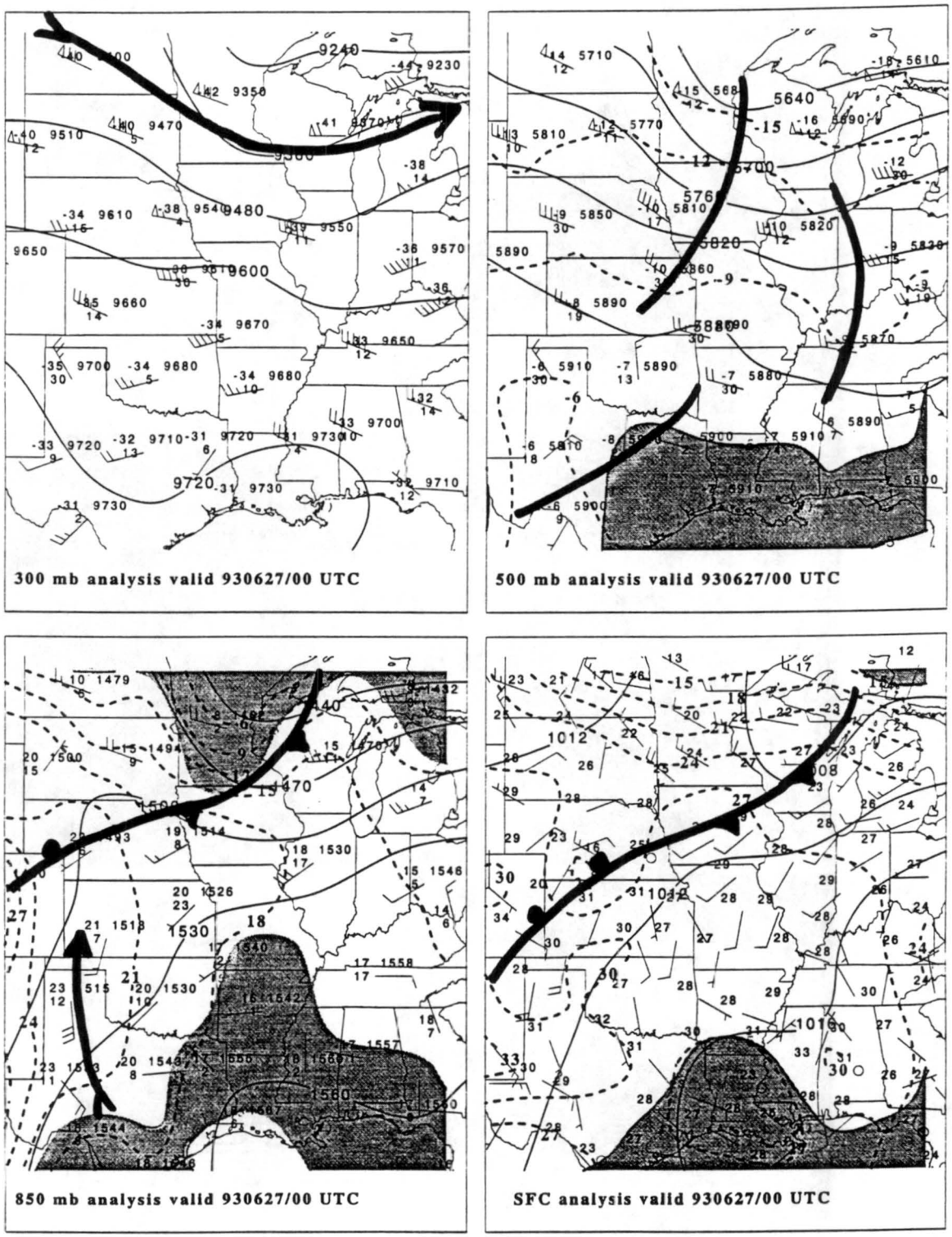

Figure 4.21: Analysis for 300 mb, 500 mb, 850 mb and surface levels for 0000 UTC 27 June 1993. The gray shaded regions are areas of dewpoint depressions of 5°C or less.

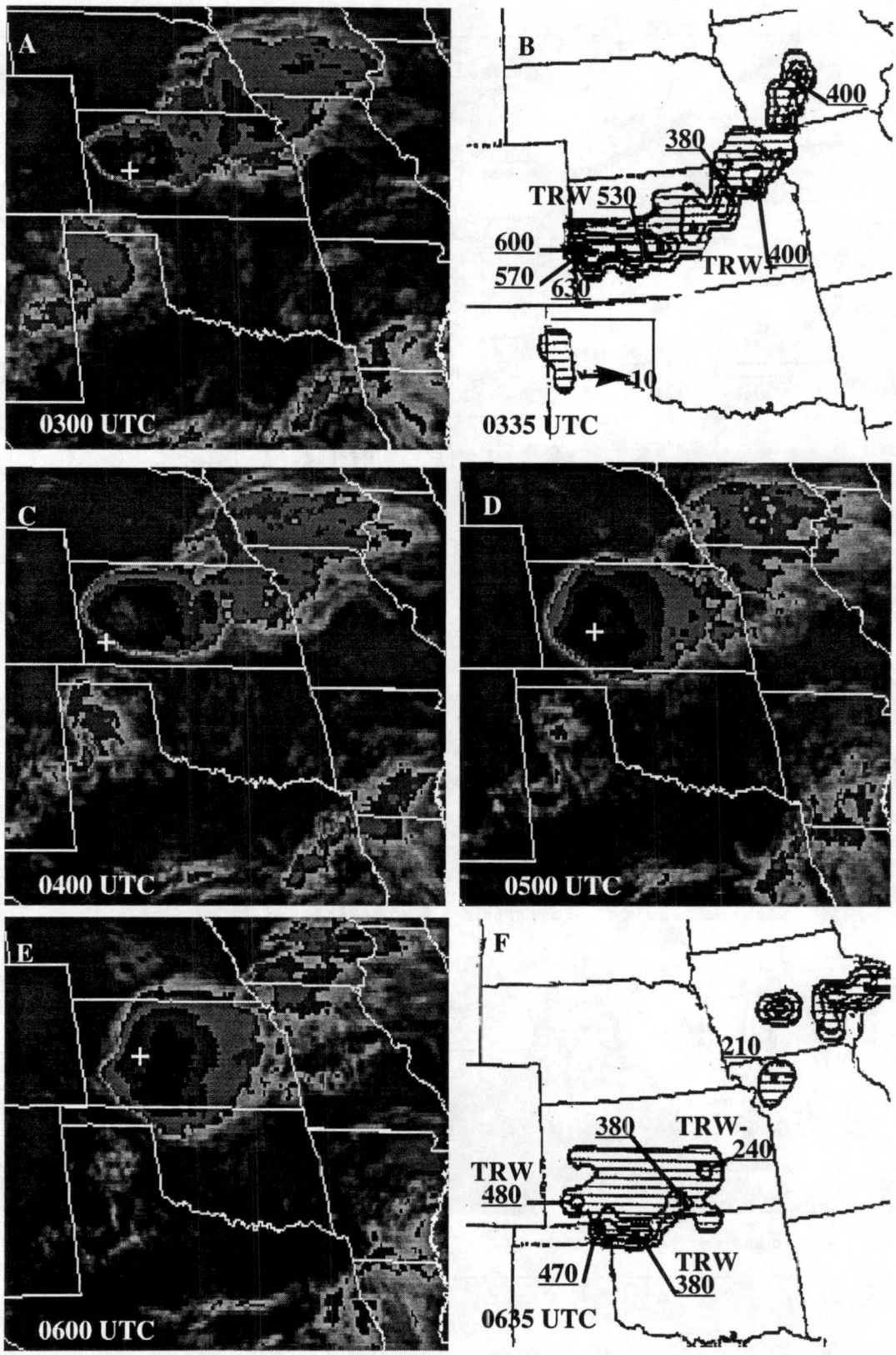

Figure 4.22: Infrared satellite images for (A) 0300 UTC, (C) 0400 UTC, (D) 0500 UTC, (E) 0600 UTC 27 June 1993 and NWS radar summaries for (B) 0335 UTC and (F) 0635 UTC 27 June 1993.

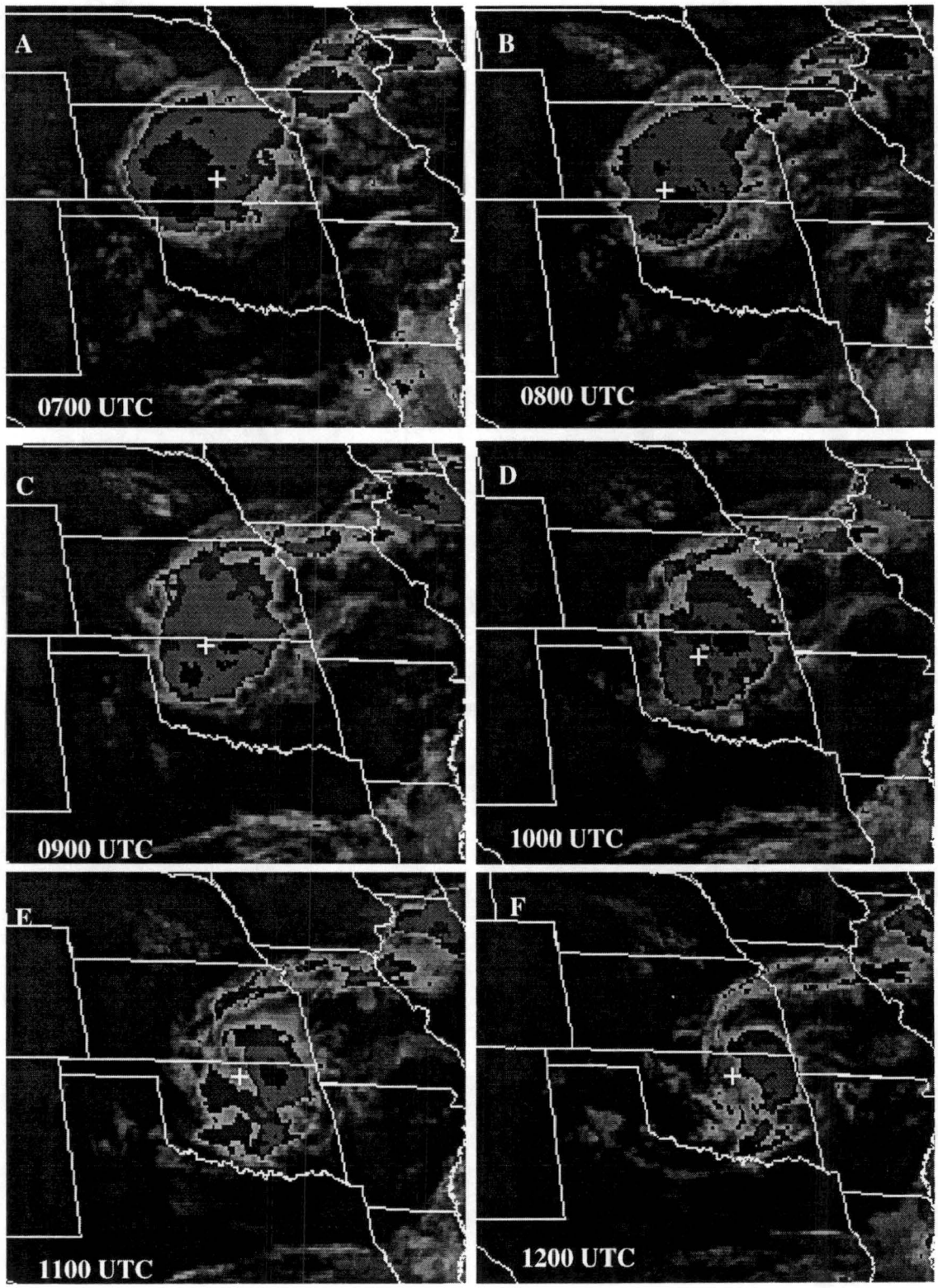

Figure 4.23: Infrared satellite images for (A) 0700 UTC, (B) 0800 UTC, (C) 0900 UTC, (D) 1000 UTC, (E) 1100 UTC and (F) 1200 UTC 27 June 1993.

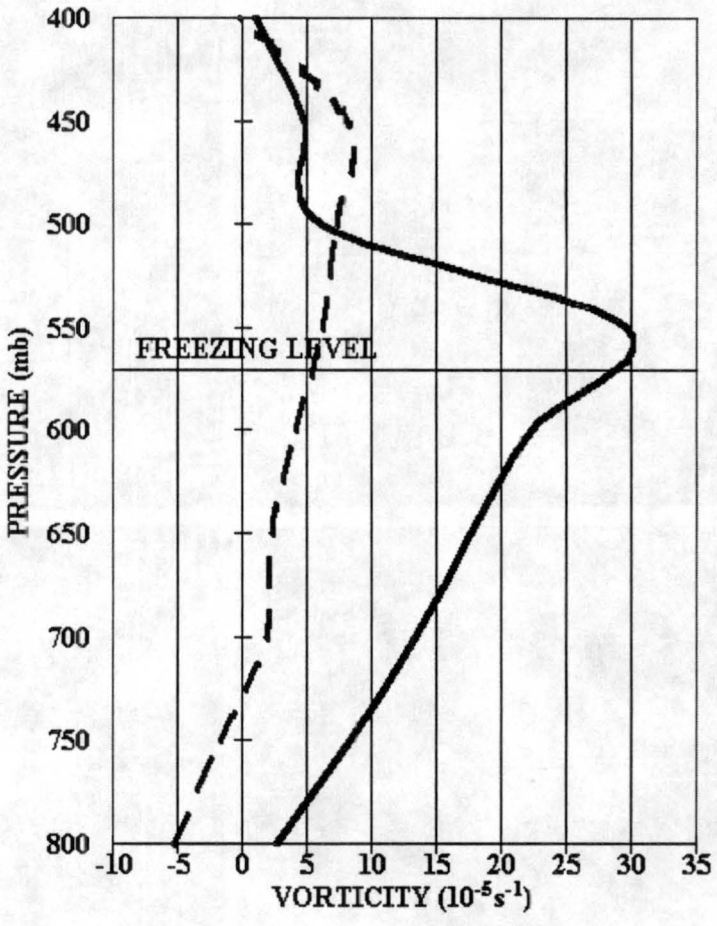

Figure 4.24: Average vertical profiles of relative vorticity for the 27 June 1993 MCS. The dashed line is for the beginning stage of the MCS and the solid line is for the maximum stage.

4.5 CASE #5

Case #5 occurred on July 13, 1993 and is an MCC that formed in central Nebraska and South Dakota from the merger of two MCSs (Figures 4.26 and 4.27). This system is associated with a 500 mb trough aloft and low-level warm air advection and convergence caused by a 30 knot low-level jet (Figure 4.25). The MCC moves to the east - southeast at approximately 14 m s^{-1} and does not show an indication of circulation in the satellite loop. The two MCSs merge at approximately 0700 UTC with the northern most MCS being the dominant one. It then grows to cover a maximum area of approximately 260,000 km^2 by 0900 UTC.

The system grows and develops a stratiform region on the north side. The stratiform region is suggested in the 0635 UTC radar summary (Figure 4.26). The most intense convection occurs on the east and southeast side where it is being fed by the low level jet. The vorticity maximum starts on the west side of the MCSs and is associated with the 500 mb trough (Figure 4.25). The vorticity maximum appears to move to the stratiform region by 0800 UTC.

Figure 4.28 shows the beginning (0500 to 0700 UTC) and maximum (1100 to 1300 UTC) vertical profiles of relative vorticity between 800 mb and 400 mb. The mid-level relative vorticity starts with a maximum of $8.4 \times 10^{-5} s^{-1}$ at 600 mb and increases up to a maximum of $17.8 \times 10^{-5} s^{-1}$, which is 25 mb below the freezing level (Figure 4.28). The time rate of change of the mid-level vorticity for the period from 1000 to 1200 UTC is $9.8 \times 10^{-9} s^{-2}$ while the stretching term is $9.9 \times 10^{-9} s^{-2}$. The ratio of the time rate of change of the vorticity to the stretching term is .99 or 99%, which suggest the tilting term is small compared to the stretching term in this case.

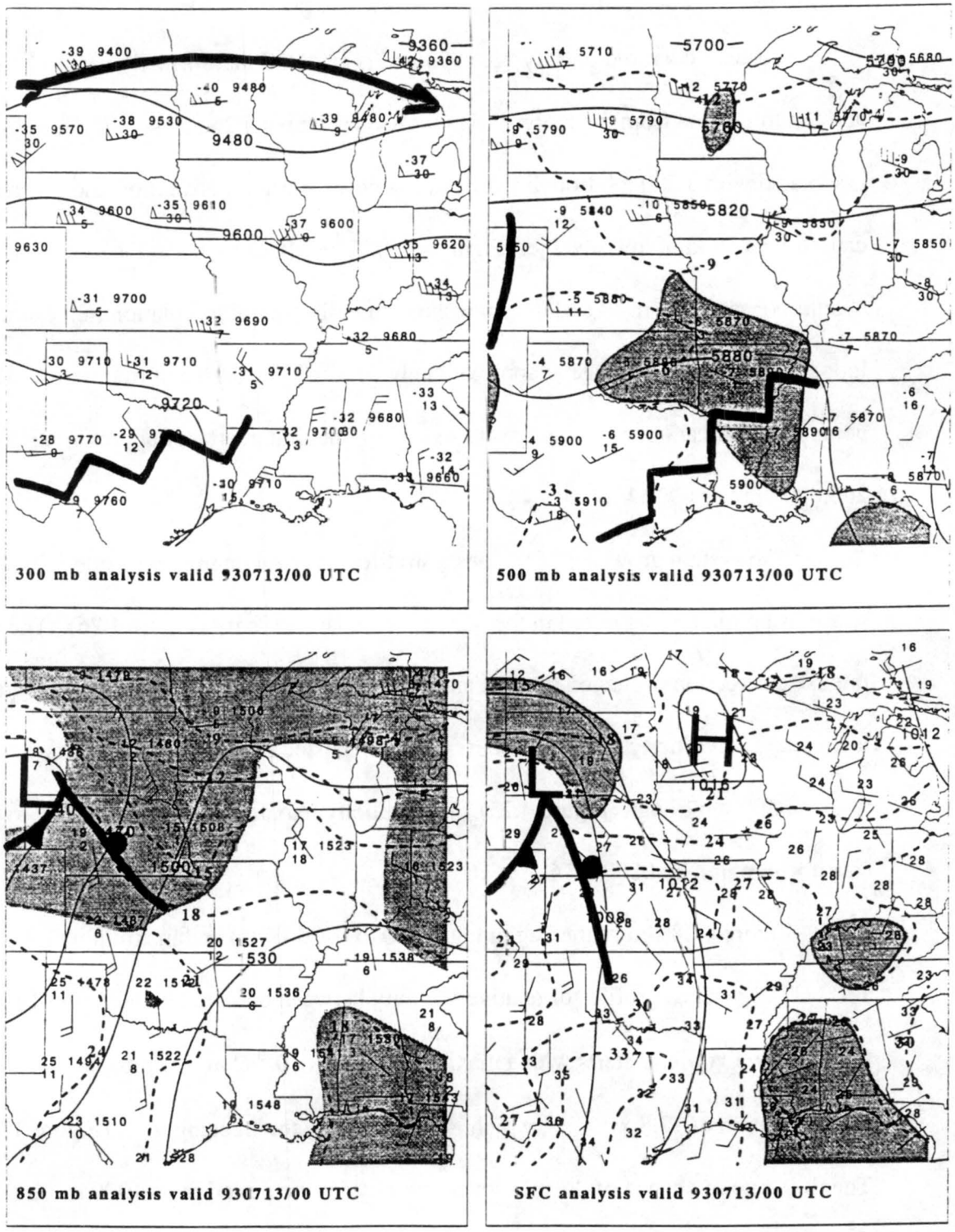

Figure 4.25: Analysis for 300 mb, 500 mb, 850 mb and surface levels at 0000 UTC 13 July 1993. The gray shaded regions are areas of dewpoint depressions of 5°C or less.

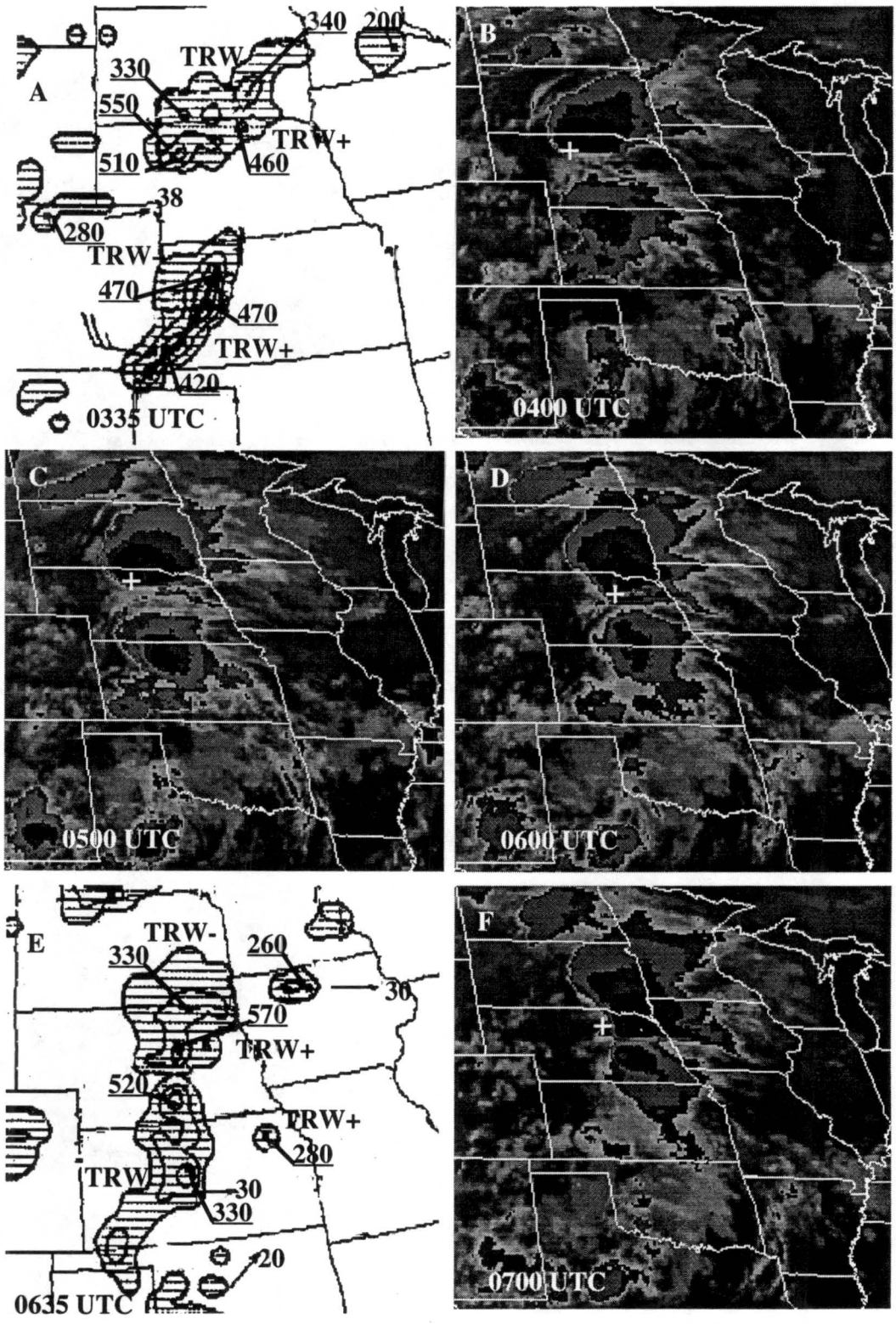

Figure 4.26: Infrared satellite images for (B) 0400 UTC, (C) 0500 UTC, (D) 0600 UTC, (F) 0700 UTC 13 July 1993 and NWS radar summaries for (A) 0335 UTC and (E) 0635 UTC 13 July 1993.

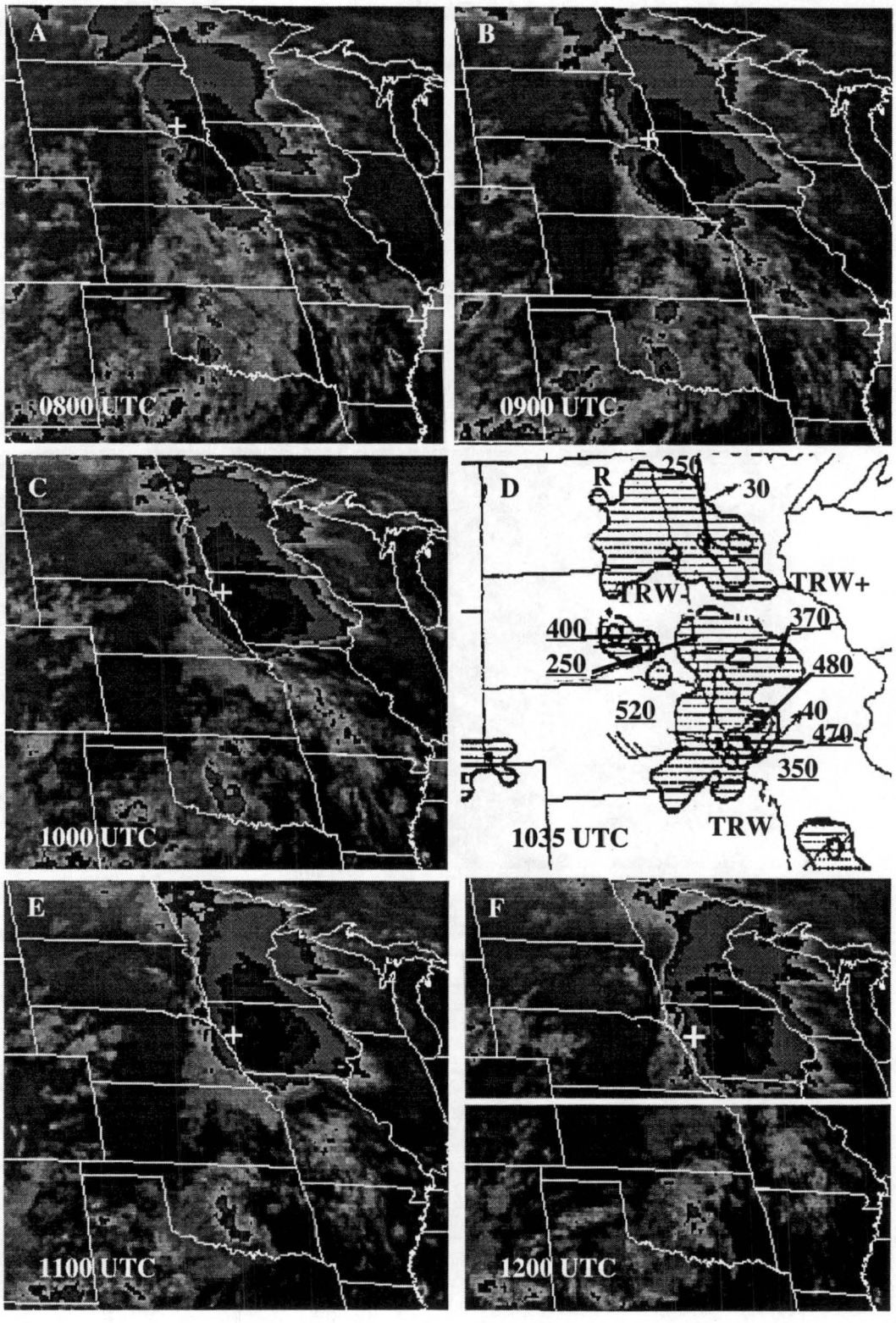

Figure 4.27: Infrared satellite images for (A) 0800 UTC, (B) 0900 UTC, (C) 1000 UTC, (E) 1100 UTC, (F) 1200 UTC 13 July 1993 and NWS radar summary for (D) 1035 UTC 13 July 1993.

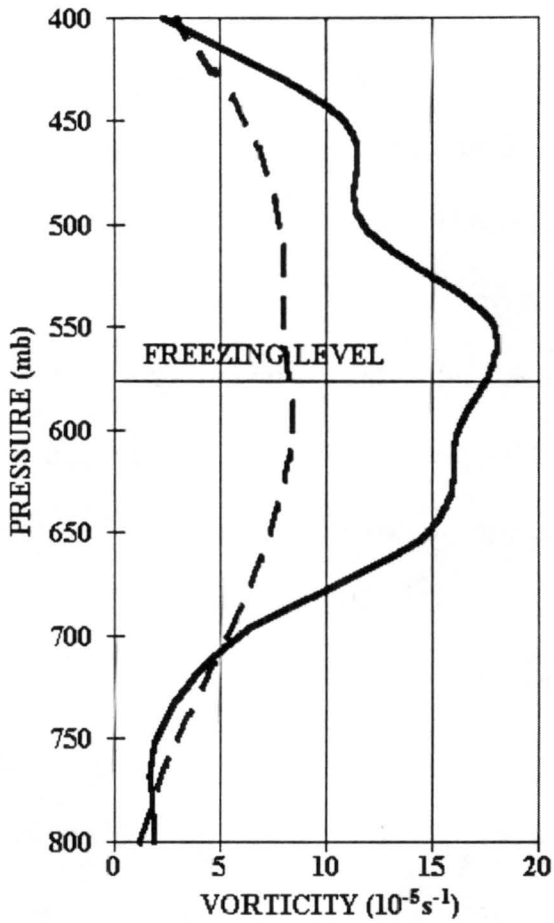

Figure 4.28: Average vertical profiles of relative vorticity for the 13 July 1993 MCC. The dashed line is for the beginning stage of the MCC and the solid line is for the maximum stage.

4.6 CASE #6

Case #6 occurred on July 19, 1993 and is an MCS that formed in north central Kansas (Figures 4.30 through 4.32). This is the only system studied that displayed anticyclonic circulation in the satellite loop. The MCS moves east at approximately 19 m s^{-1} with a slight anticyclonic curvature associated with a ridge of high pressure in the upper-levels (Figure 4.29). This system forms ahead of the tail end of a 500 mb trough and a surface front (Figure 4.29). The system begins around 0600 UTC as an area of thunderstorms that grow to cover a maximum area of approximately 95,000 km^2 by 1100 UTC which does not meet Maddox's (1980) size requirement.

The system grows and develops a stratiform region, which is weakly suggested in the 1035 UTC radar summary (Figure 4.30), on the west-southwest side. The most intense convection occurs on the east side with a second area in the southwest corner. The vorticity maximum appears to move to the stratiform region by 1300 UTC.

Figure 4.33 shows the beginning (0700 to 0900 UTC) and maximum (1400 to 1600 UTC) stage vertical profiles of relative vorticity between 800 mb and 400 mb. The mid-level relative vorticity starts with a maximum of $1.3 \times 10^{-5} s^{-1}$ at 700 mb and reaches a maximum of $21.3 \times 10^{-5} s^{-1}$ at 550 mb, which is 10 mb above the freezing level (Figure 4.33). The time rate of change of the mid-level vorticity for the period from 1300 to 1500 UTC is $1.5 \times 10^{-8} s^{-2}$ while the stretching term is $9.3 \times 10^{-9} s^{-2}$. The ratio of the time rate of change of vorticity to the stretching term is 1.62 or 162%, which suggest the stretching is only contributing to about two thirds of the vorticity increase and therefore the tilting effects could be significant in this system.

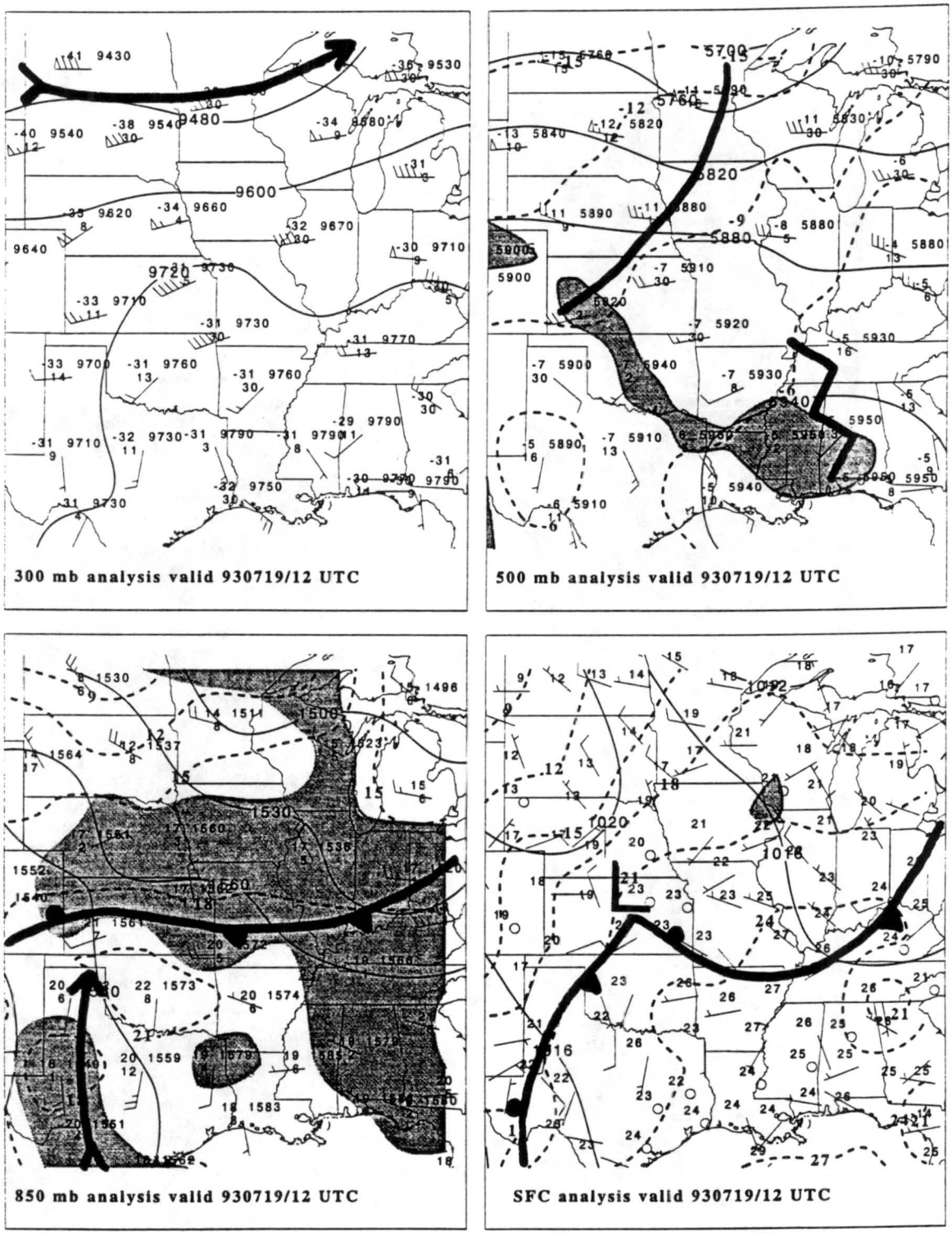

Figure 4.29: Analysis for 300 mb, 500 mb, 850 mb and surface levels at 1200 UTC 19 July 1993. The gray shaded regions are areas of dewpoint depressions of 5°C or less.

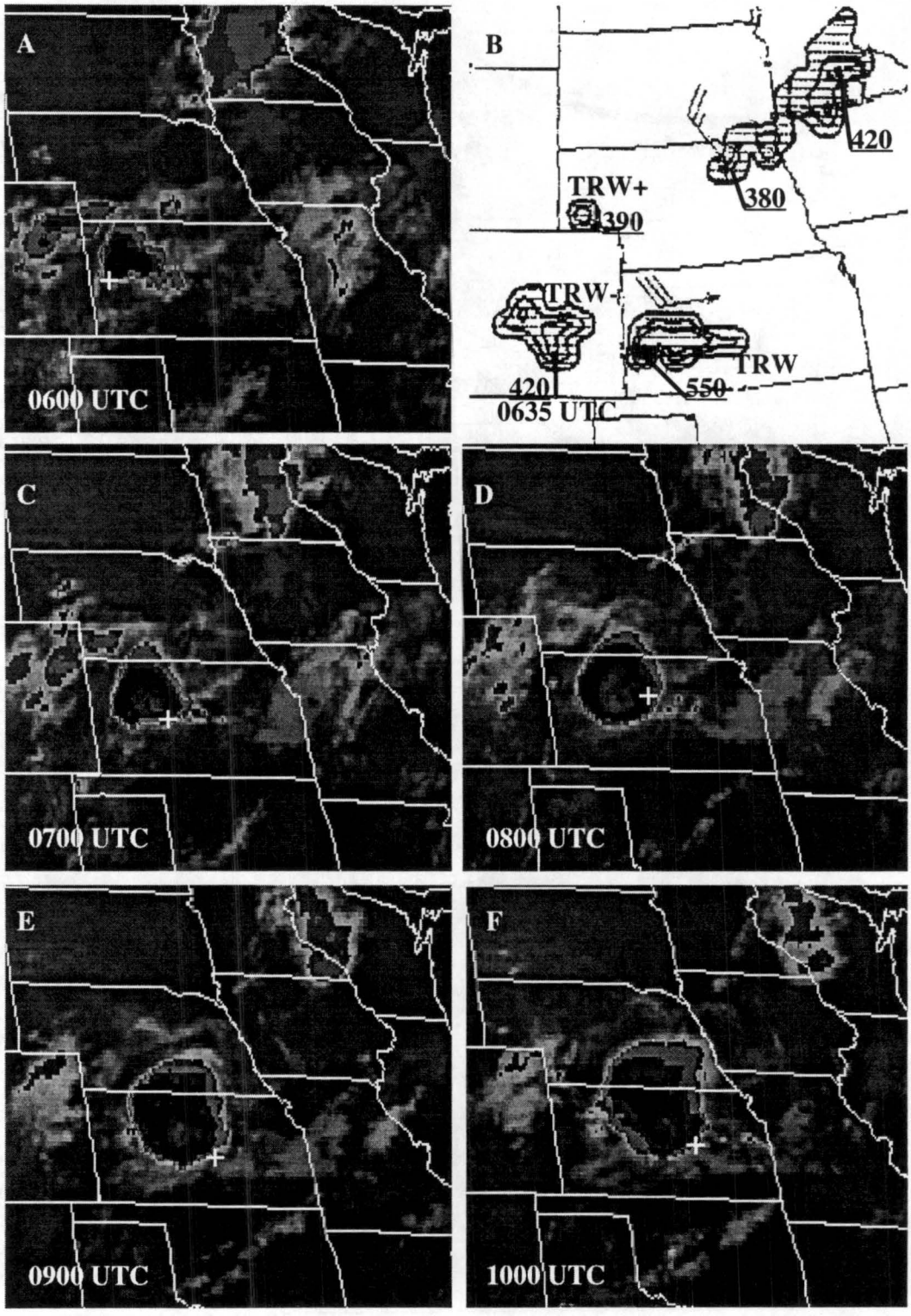

Figure 4.30: Infrared satellite images for (A) 0600 UTC, (C) 0700 UTC, (D) 0800 UTC, (E) 0900 UTC, (F) 1000 UTC 19 July 1993 and NWS radar summary for 0635 UTC 19 July 1993.

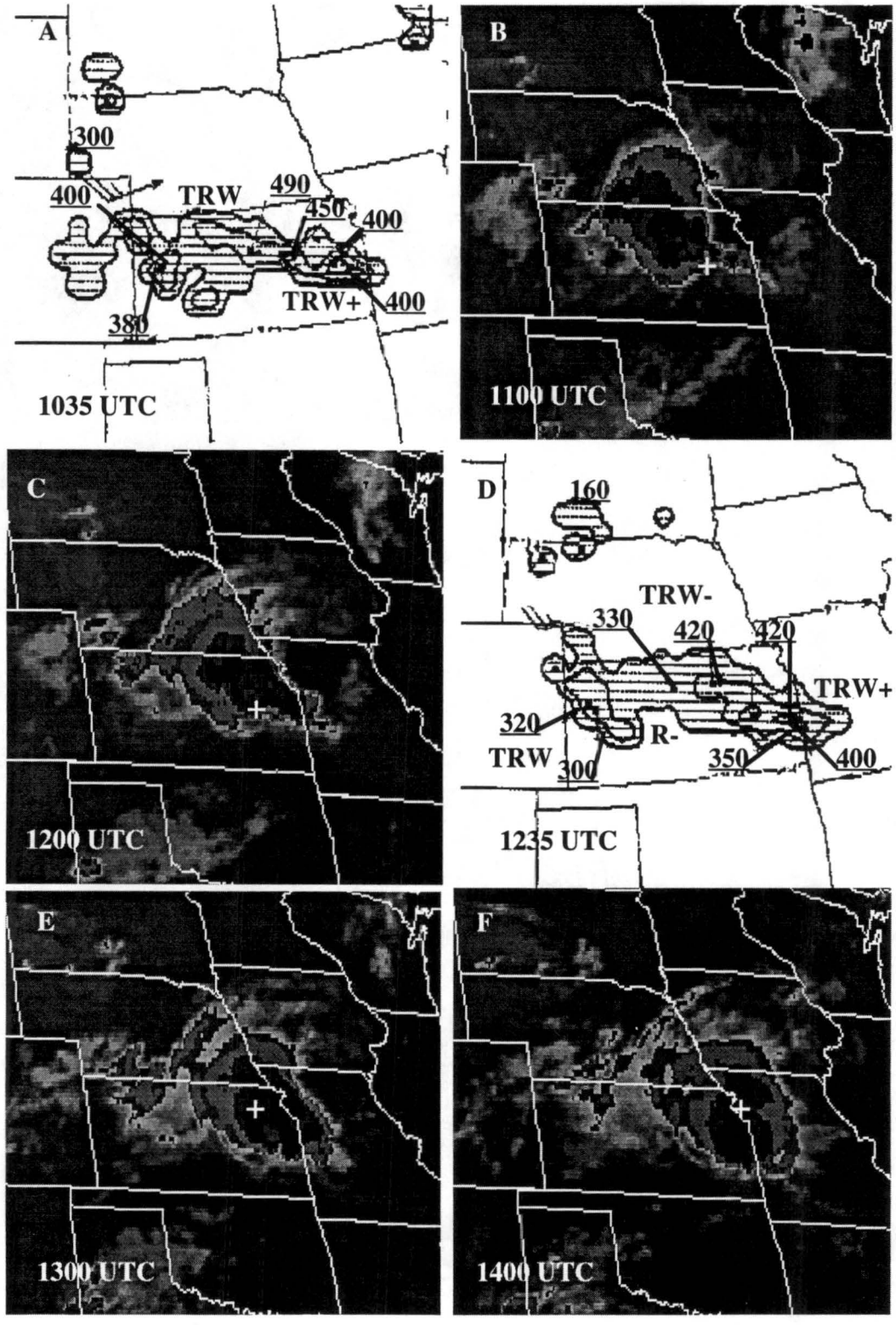

Figure 4.31: Infrared satellite images for (B) 1100 UTC, (C) 1200 UTC, (E) 1300 UTC, (F) 1400 UTC 19 July 1993 and NWS radar summaries for 1035 UTC and 1235 UTC 19 July 1993.

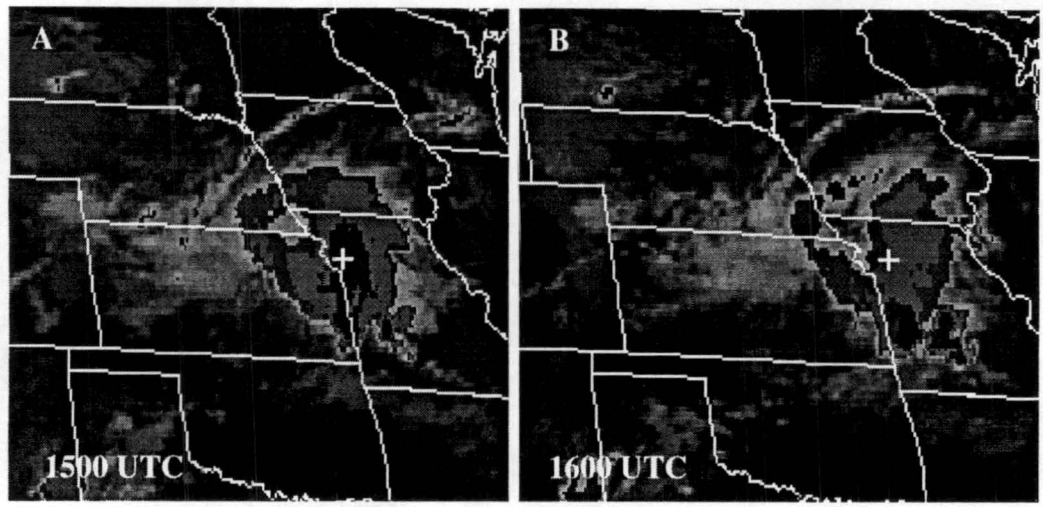

Figure 4.32: Infrared satellite images for (A) 1500 UTC and (B) 1600 UTC 19 July 1993.

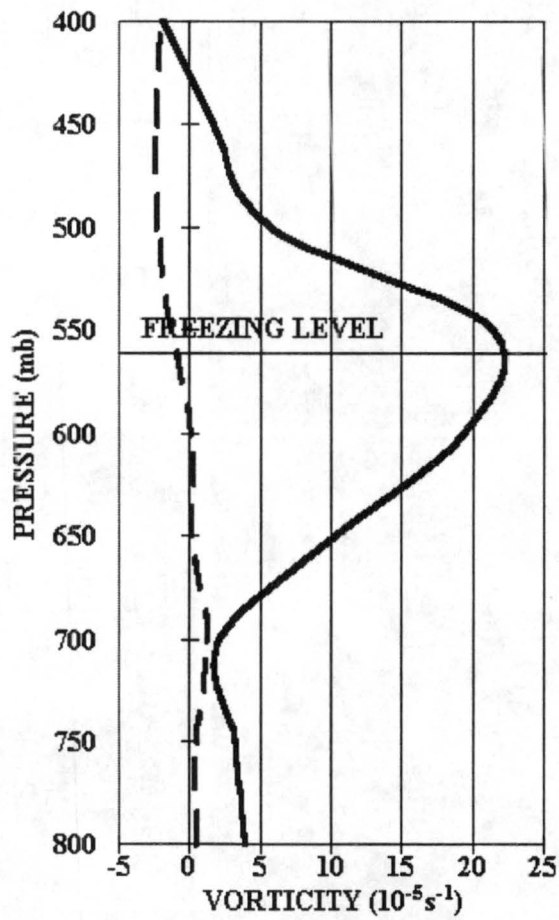

Figure 4.33: Average vertical profiles of relative vorticity for the 19 July 1993 MCS. The dashed line is for the beginning stage and the solid line is for the maximum stage.

4.7 CASE #7

Case #7 occurred on August 5, 1993 and is an MCS that formed in central Kansas and Oklahoma (Figures 4.35 through 4.37). This system is associated with a weak 500 mb trough aloft to the northwest and low-level warm air advection and convergence caused by a weak front being enhanced by a 40 knot low-level jet (Figure 4.34). The MCS moves to the east at approximately 22 m s^{-1} and develops a cyclonic circulation in the satellite loop. The system begins between 0900 UTC and 1000 UTC as two areas of thunderstorms along the warm front that merge into a large MCS. It grows to cover a maximum area of approximately 385,000 km^2 by 2000 UTC. This system is not an MCC because it does not meet the cold cloud top requirements (Maddox, 1980).

The system grows and develops a stratiform region on the north side. The stratiform region is weakly suggested in the 1235 UTC radar summary (Figure 4.35) and strongly suggested in the 1635 UTC radar summary (Figure 4.36). The most intense convection occurs on the east and southeast side where it is being fed by the low level jet (Figure 4.34). The vorticity maximum starts on the southwest side of the MCS and appears to move to the stratiform region by 1800 UTC.

Figure 4.38 shows the beginning (1200 to 1400 UTC) and maximum (1800 to 2000 UTC) vertical profiles of relative vorticity. The mid-level relative vorticity starts with a maximum of 11.9 x $10^{-5}s^{-1}$ at 750 mb and increases up to 14.6 x $10^{-5}s^{-1}$ at 600 mb, 10 mb below the freezing level (Figure 4.38). The time rate of change of the mid-level vorticity for the period from 1700 to 1900 UTC is 1.2 x $10^{-8}s^{-2}$ while the stretching term is 1.5 x $10^{-8}s^{-2}$. The ratio of the time rate of change of the vorticity to the stretching term is .80 or 80%, which suggest the tilting term is small in this case.

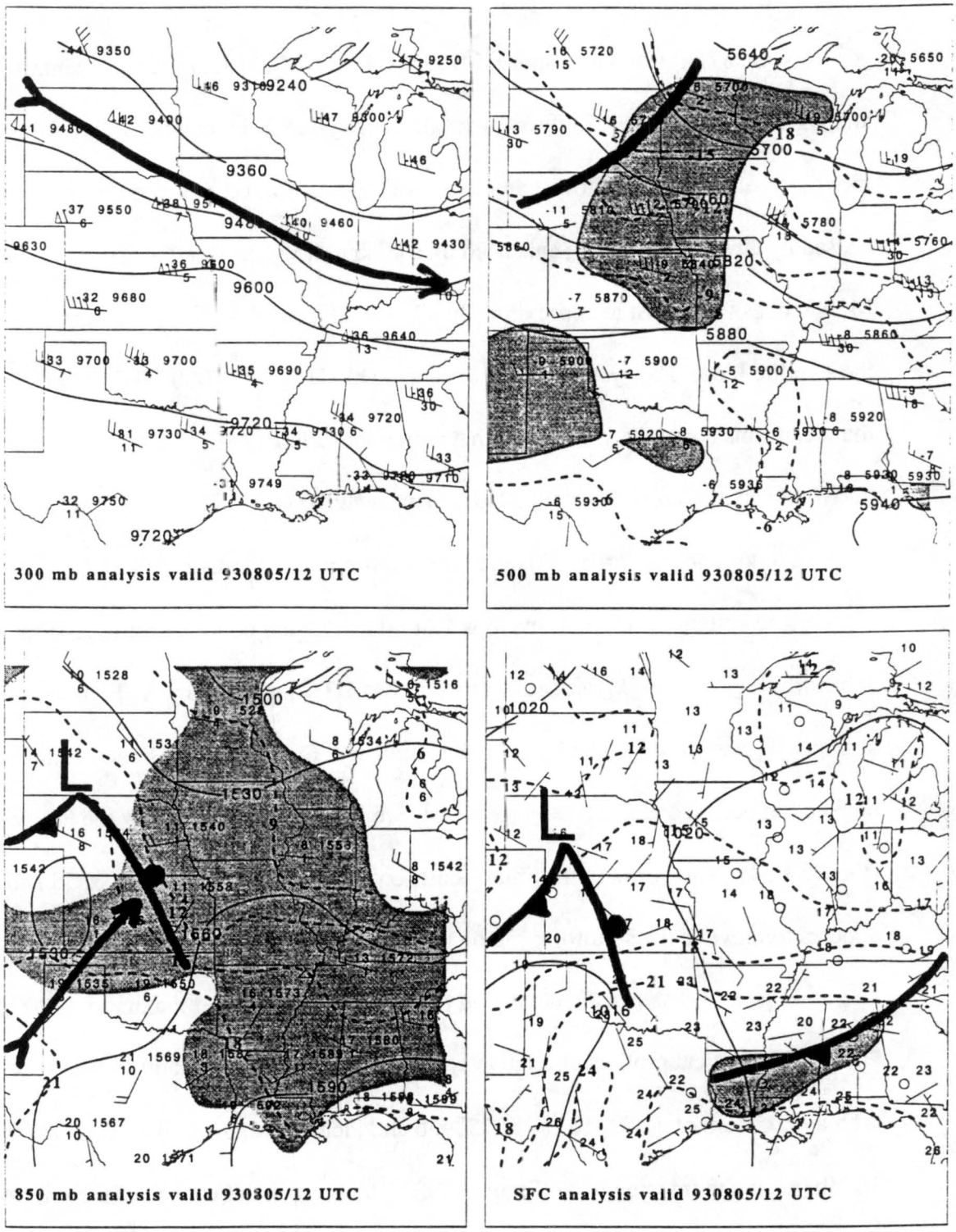

Figure 4.34: Analysis for 300 mb, 500 mb, 850 mb and surface levels at 1200 UTC 5 August 1993. The gray shaded regions are areas of dewpoint depressions of 5°C or less.

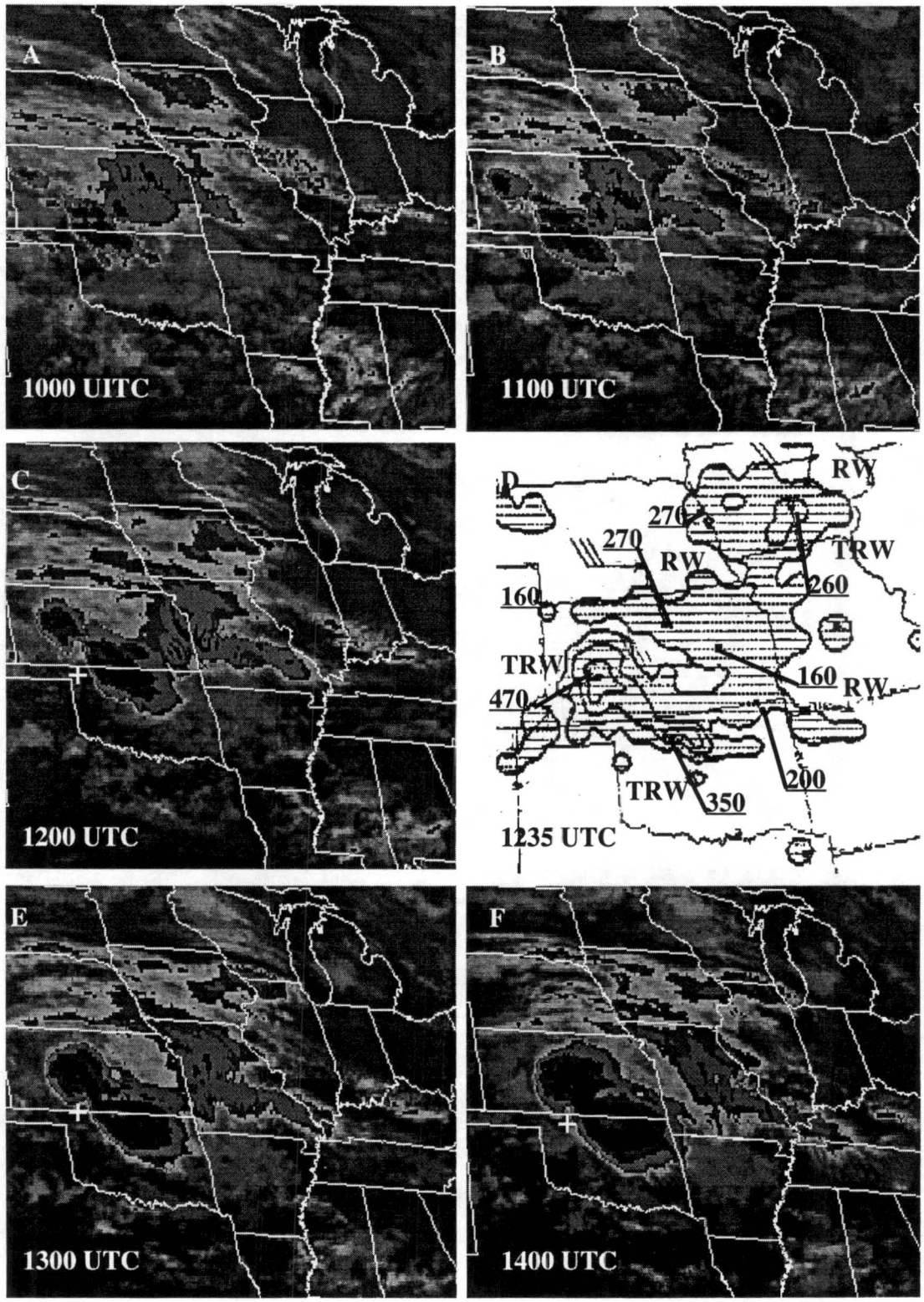

Figure 4.35: Infrared satellite images for (A) 1000 UTC, (B) 1100 UTC, (C) 1200 UTC, (E) 1300 UTC, (F) 1400 UTC 5 August 1993 and NWS radar summary for (D) 1235 UTC 5 August 1993.

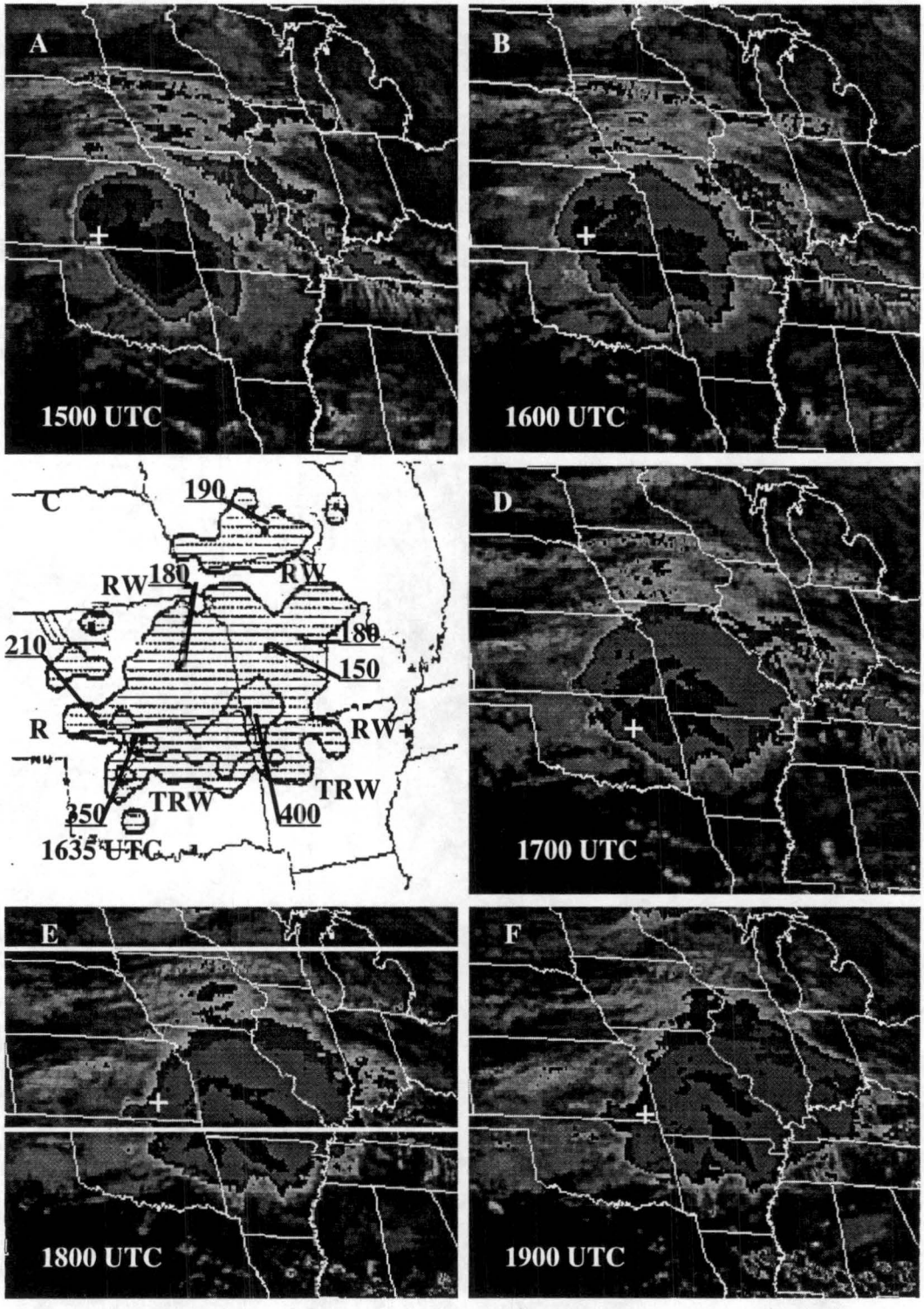

Figure 4.36: Infrared satellite images for (A) 1500 UTC, (B) 1600 UTC, (D) 1700 UTC, (E) 1800 UTC, (F) 1900 UTC 5 August 1993 and NWS radar summary for (C) 1635 UTC 5 August 1993.

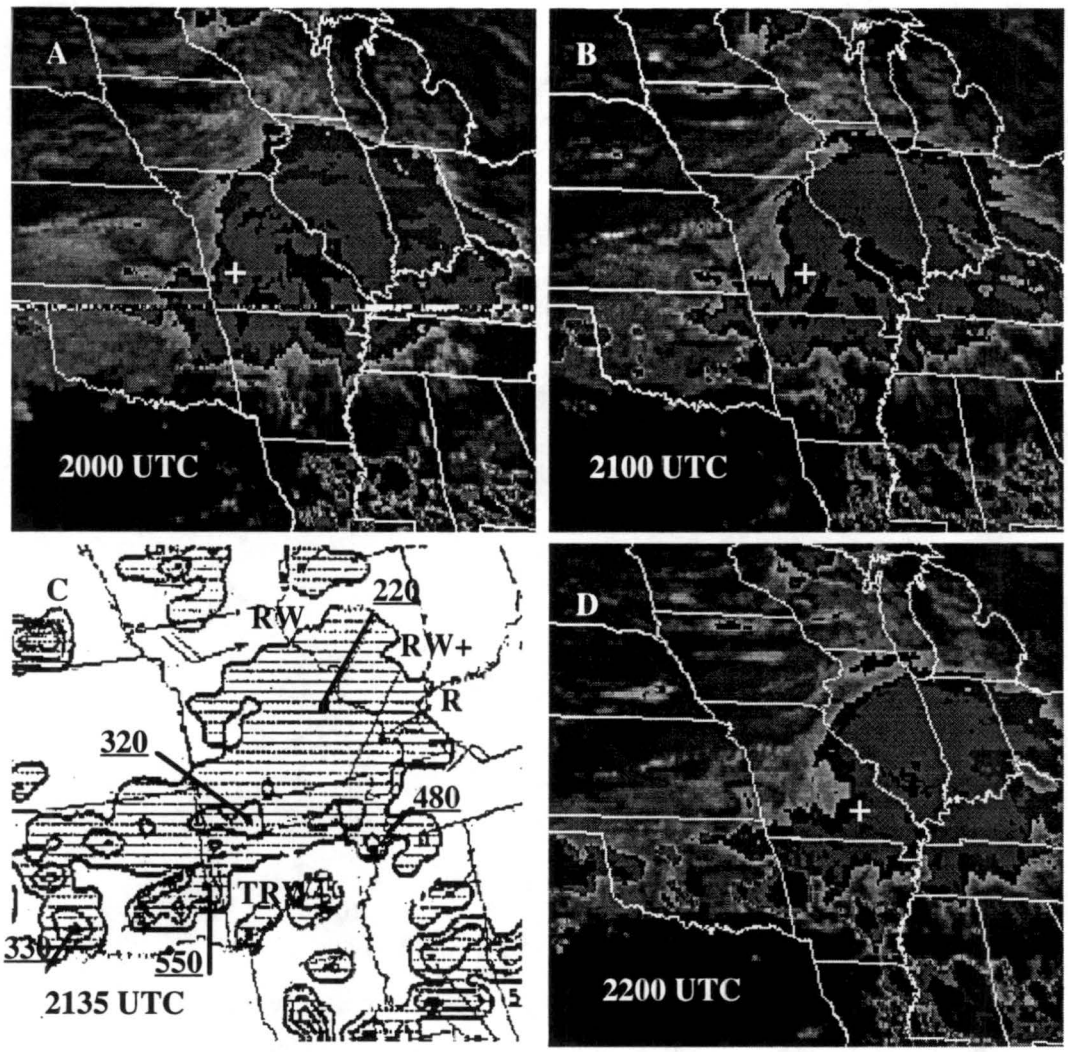

Figure 4.37: Infrared satellite images for (A) 2000 UTC, (B) 2100 UTC, (C) 2200 UTC 5 August 1993 and NWS radar summary for 2135 UTC 5 August 1993.

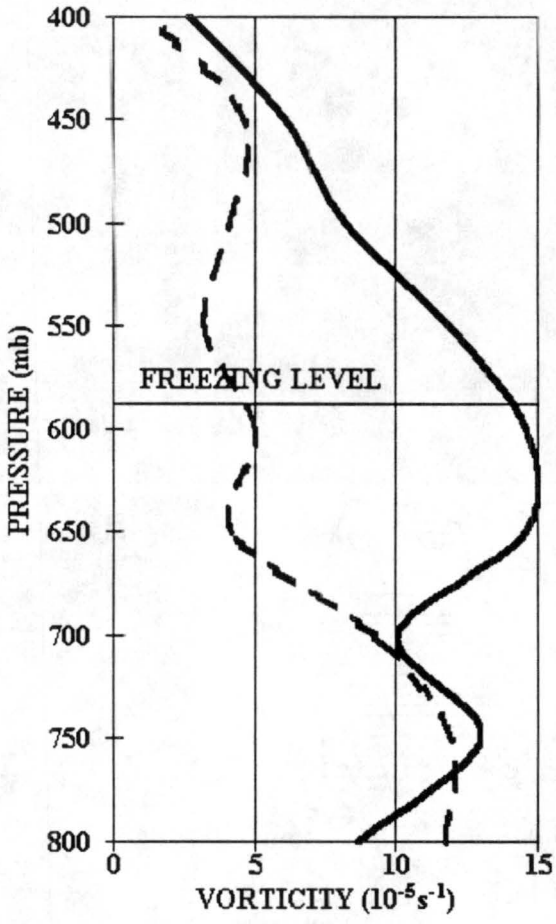

Figure 4.38: Average vertical profiles of relative vorticity for the 5 August 1993 MCS. The dashed line is for the beginning stage of the MCS and the solid line is for the maximum stage.

4.8 CASE #8

Case #8 occurred on August 13, 1993 and is an MCC that formed as an area of thunderstorms along the front range of Colorado (Figures 4.40 through 4.42). This system is associated with low-level warm air advection and convergence caused by a surface low and warm front plus upslope flow along the front range (Figure 4.39). The system has an upper-level trough upstream with an upper-level ridge downstream (Figure 4.39). The system begins in the early afternoon and by 0200 UTC becomes organized and begins to move. The MCC moves to the east - northeast at approximately 14 m s^{-1} and does not indicate a circulation in the satellite loop. It grows to cover a maximum area of approximately 280,000 km^2 by 0600 UTC.

The system grows and develops a stratiform region on the west side. The stratiform region is suggested in the 0635 UTC radar summary (Figure 4.40). The most intense convection occurs on the east side. The vorticity maximum starts on the west side of the MCC and appears to move to the stratiform region by 0600 UTC.

Figure 4.43 shows the beginning (0200 to 0400 UTC) and maximum (1000 to 1200 UTC) stage vertical profiles of relative vorticity between 800 mb and 400 mb. The mid-level relative vorticity starts with a maximum of $0.8 \times 10^{-5} s^{-1}$ at 600 mb and increases up to $13.4 \times 10^{-5} s^{-1}$, 30 mb below the freezing level (Figure 4.43). The time rate of change of the mid-level vorticity for the period from 0900 to 1100 UTC is $6.3 \times 10^{-9} s^{-2}$ while the stretching term is $6.0 \times 10^{-9} s^{-2}$. The ratio of the time rate of change of the vorticity to the stretching term is 1.05 or 105%, which suggests the tilting effects are small on this scale of computation for this system.

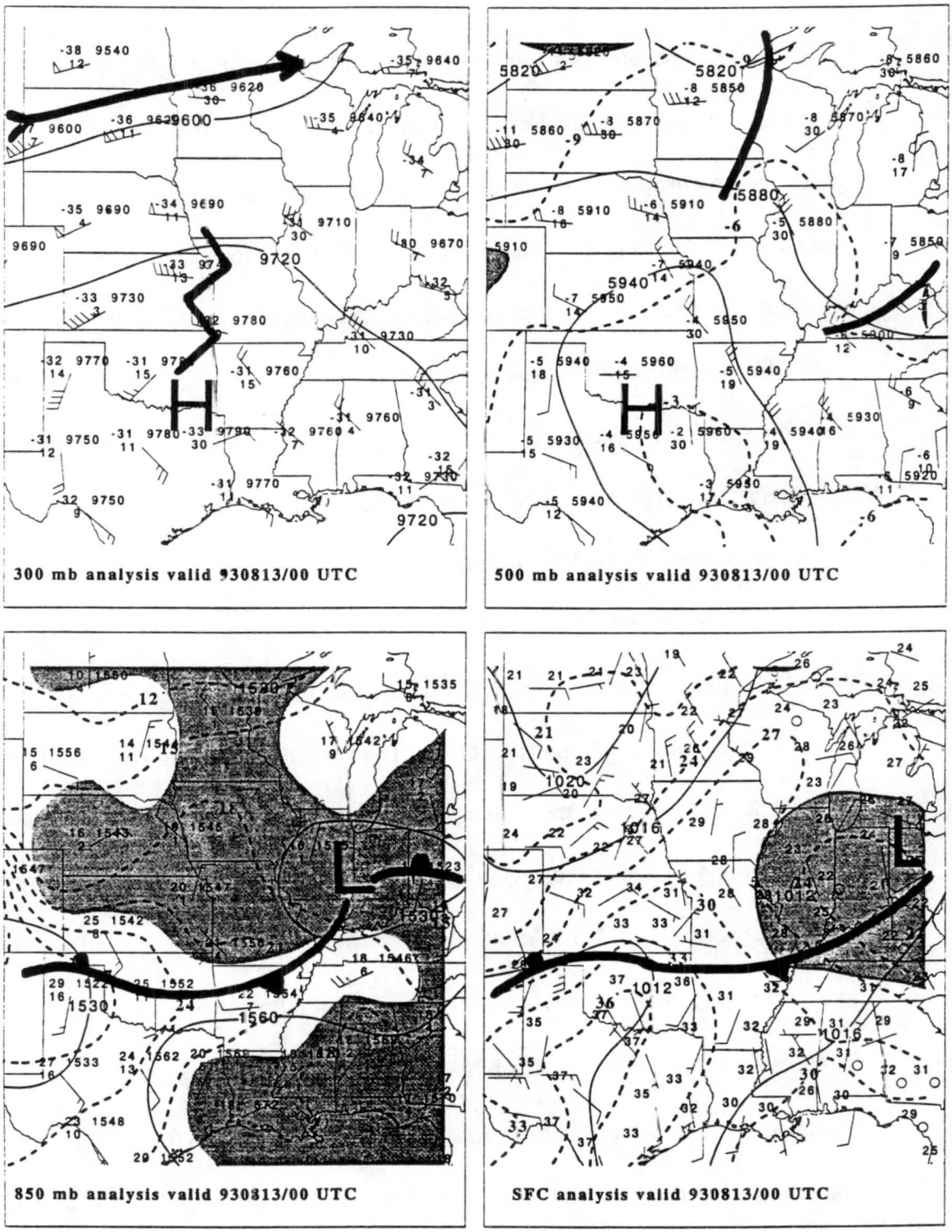

Figure 4.39: Analysis for 300 mb, 500 mb, 850 mb and surface levels at 0000 UTC 13 August 1993. The gray shaded regions are areas of dewpoint depressions of 5°C or less.

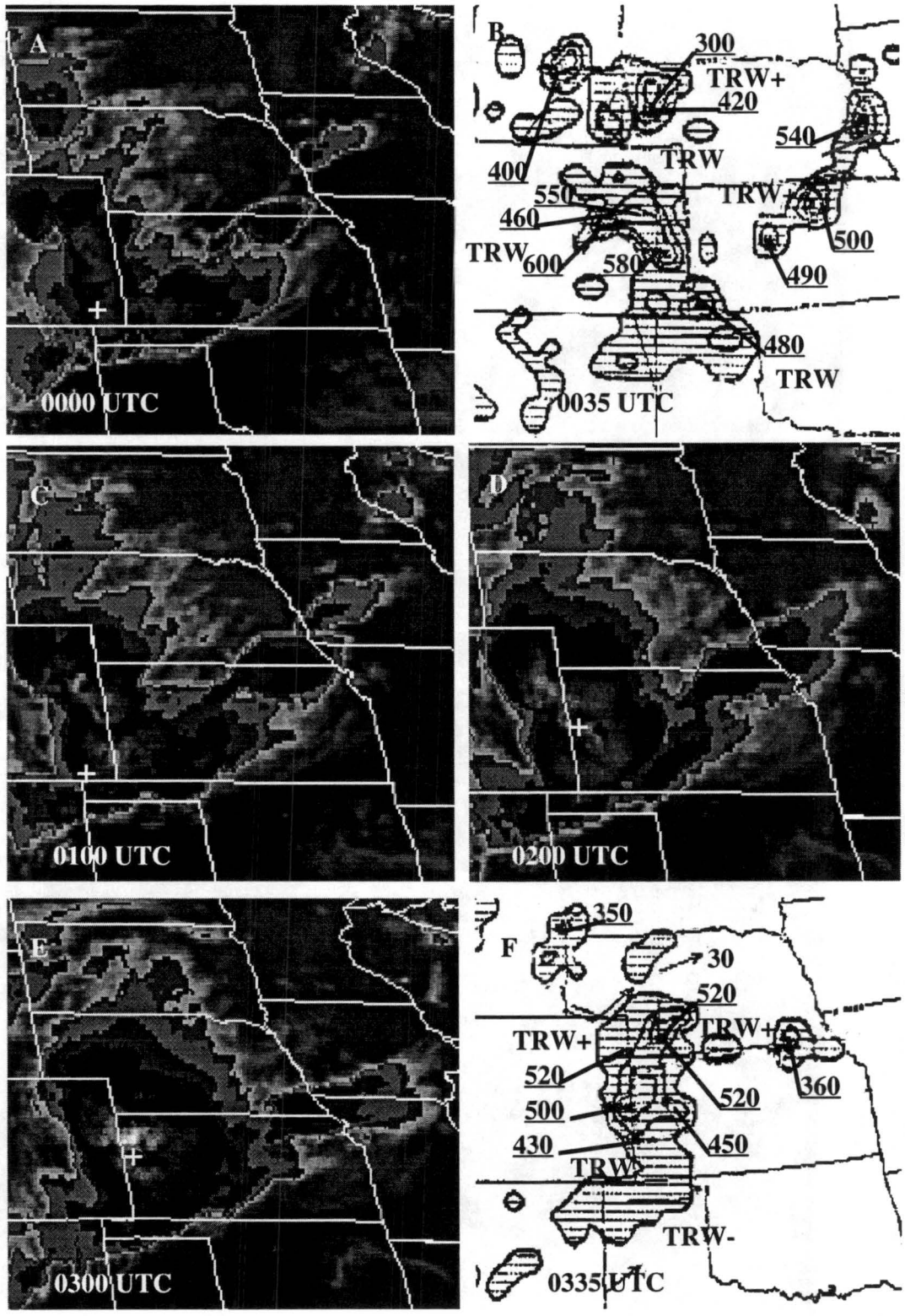

Figure 4.40: Infrared satellite images for (A) 0000 UTC, (C) 0100 UTC, (D) 0200 UTC, (E) 0300 UTC 13 August 1993; NWS radar summaries for (B) 0035 UTC and (F) 0335 UTC 13 August 1993.

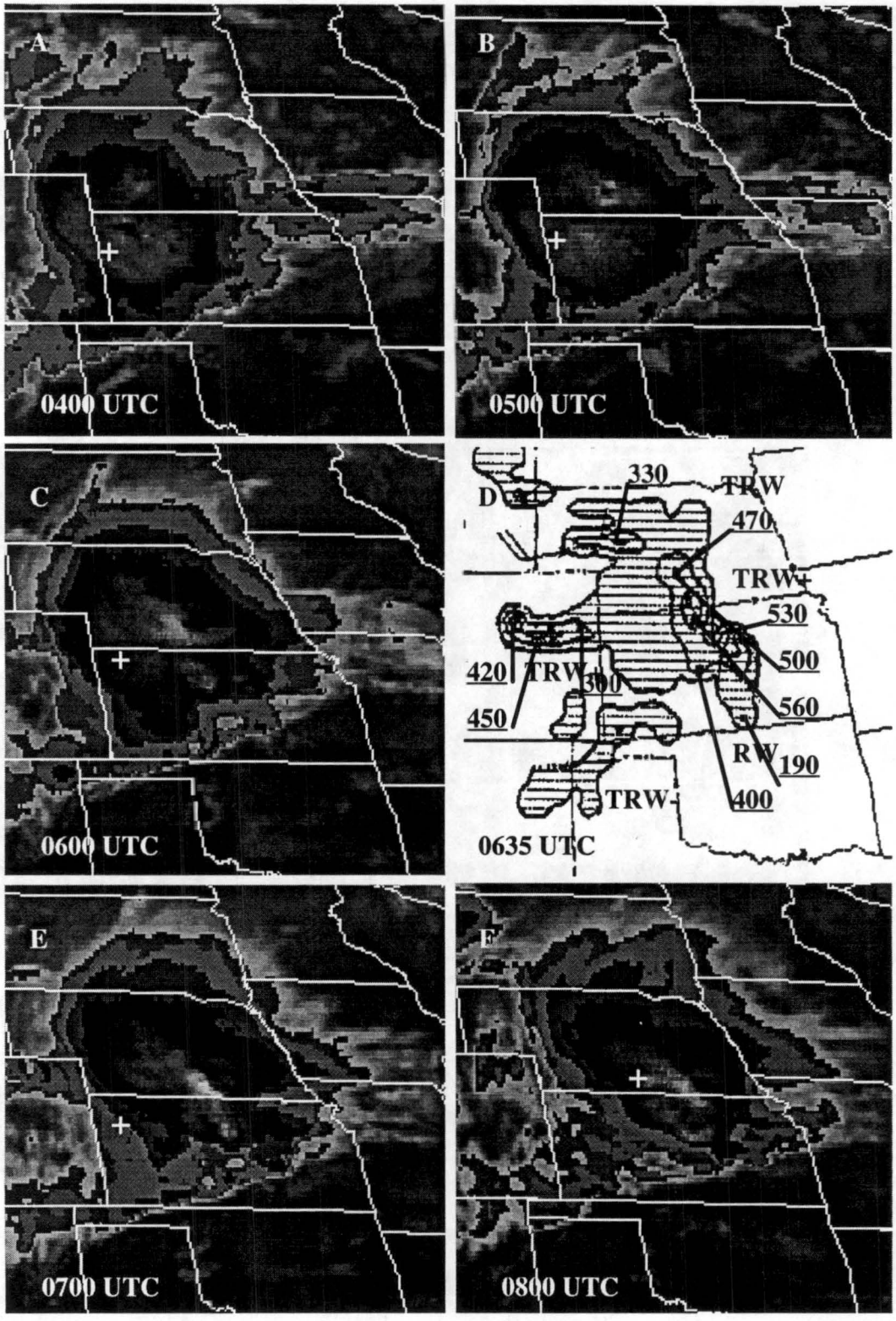

Figure 4.41: Infrared satellite images for (A) 0400 UTC, (B) 0500 UTC, (C) 0600 UTC, (E) 0700 UTC, (F) 0800 UTC 13 August 1993; NWS radar summary for (D) 0635 UTC 13 August 1993.

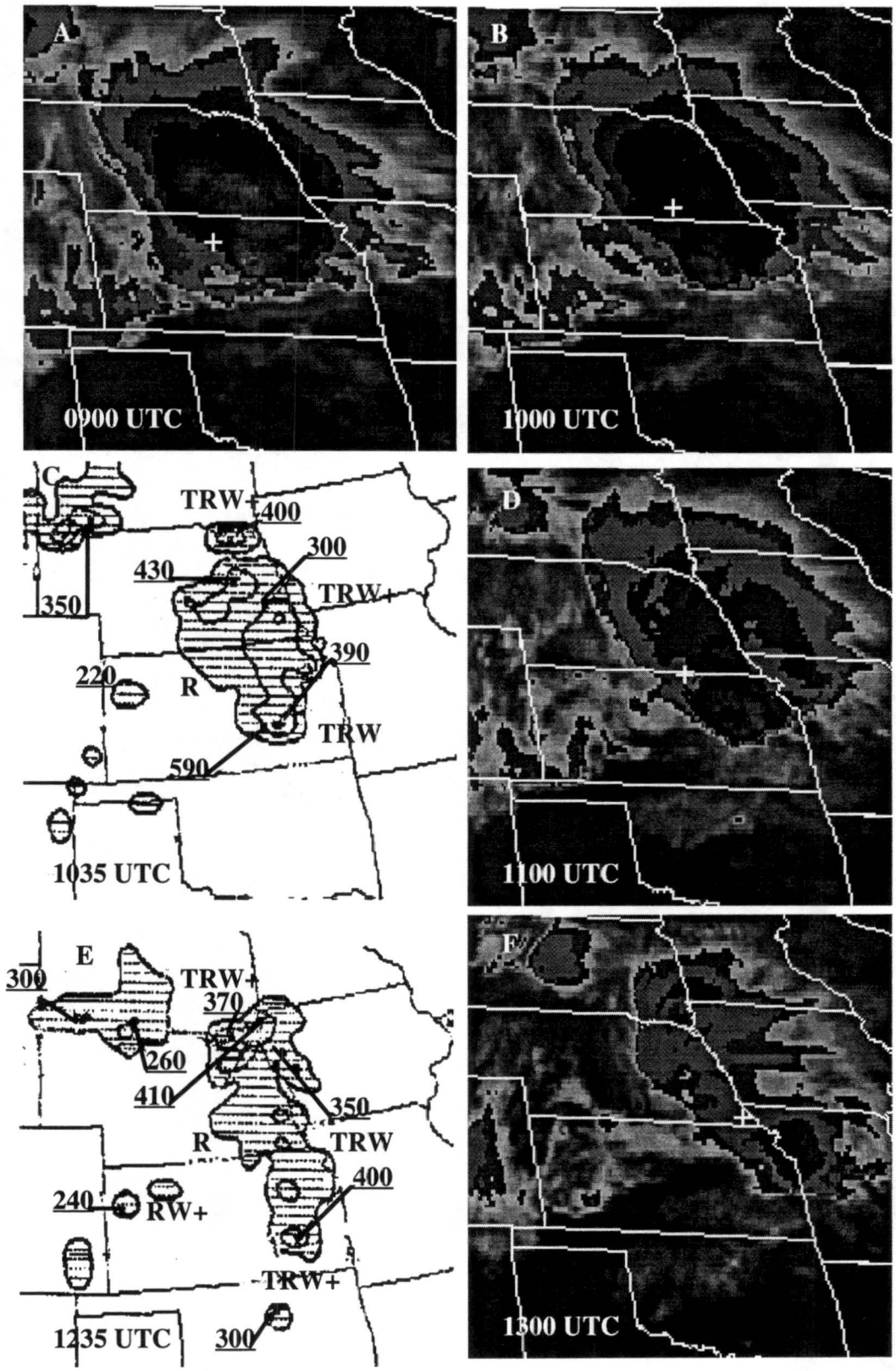

Figure 4.42: Infrared satellite images for (A) 0900 UTC, (B) 1000 UTC, (D) 1100 UTC, (F) 1300 UTC 13 August 1993; NWS radar summaries for (C) 1035 UTC and (E) 1235 UTC 13 August 1993.

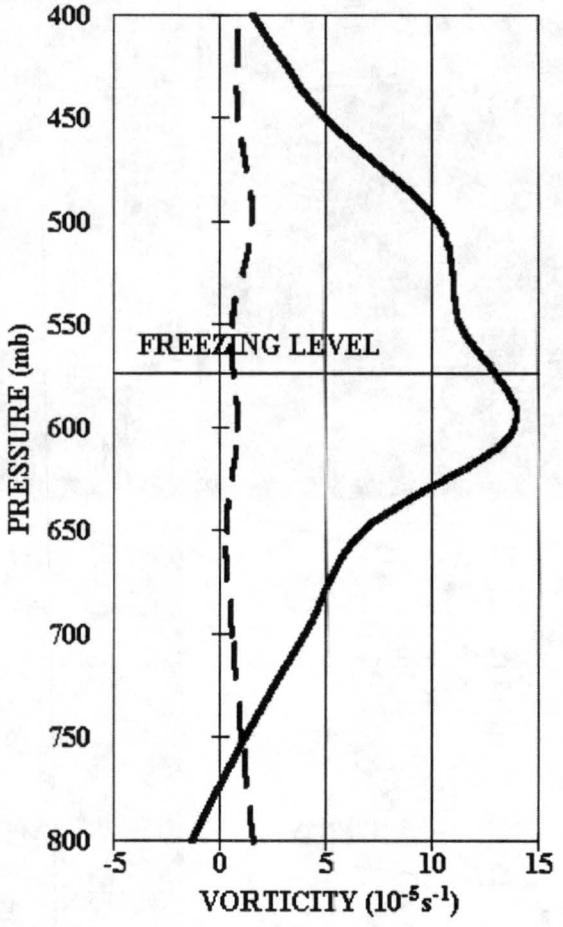

Figure 4.43: Average vertical profiles of relative vorticity for the 13 August 1993 MCC. The dashed line is for the beginning stage of the MCC and the solid line is for the maximum stage.

4.9 CASE #9

Case #9 occurred on August 22, 1993 and is an MCS (Figures 4.45 through 4.47) that formed in western Nebraska and moved to the east at approximately 18 m s^{-1} with a cyclonic circulation suggested in the satellite loop. This system is associated with a weak warm front enhanced by a 25 knot low-level jet (Figure 4.44). The system forms on the upstream edge of an upper-level ridge with a 500 mb trough to the west (Figure 4.44). The system becomes organized between 0100 UTC and 0200 UTC and grows to cover a maximum area of approximately 175,000 km^2 by 0600 UTC. This is not classified as an MCC because it does not meet the cold cloud top time requirements (Maddox, 1980).

The system grows and develops a stratiform region on the west side. The stratiform region is weakly suggested in the 0335 UTC radar summary (Figure 4.45) and strongly suggested in the 0635 UTC radar summary (Figure 4.46). The most intense convection occurs on the east and southeast side where it is probably being fed by the low level jet. The vorticity maximum starts on the south side of the MCS and appears to move to the stratiform region by 0400 UTC.

Figure 4.48 shows the beginning (0200 to 0400 UTC) and maximum (0700 to 0900 UTC) stage vertical profiles of relative vorticity. The mid-level relative vorticity starts with a maximum of $8.8 \times 10^{-5} s^{-1}$ at 650 mb and increases to $12.0 \times 10^{-5} s^{-1}$ at 600 mb, 30 mb below the freezing level (Figure 4.48) . This is the smallest increase of the nine systems studied. The time rate of change of the mid-level vorticity for the period from 0600 to 0800 UTC is $1.1 \times 10^{-8} s^{-2}$ while the stretching term is $8.2 \times 10^{-9} s^{-2}$. The ratio of the time rate of change of the vorticity to the stretching term is 1.34 or 134%, which suggests the tilting term is also contributing in this case.

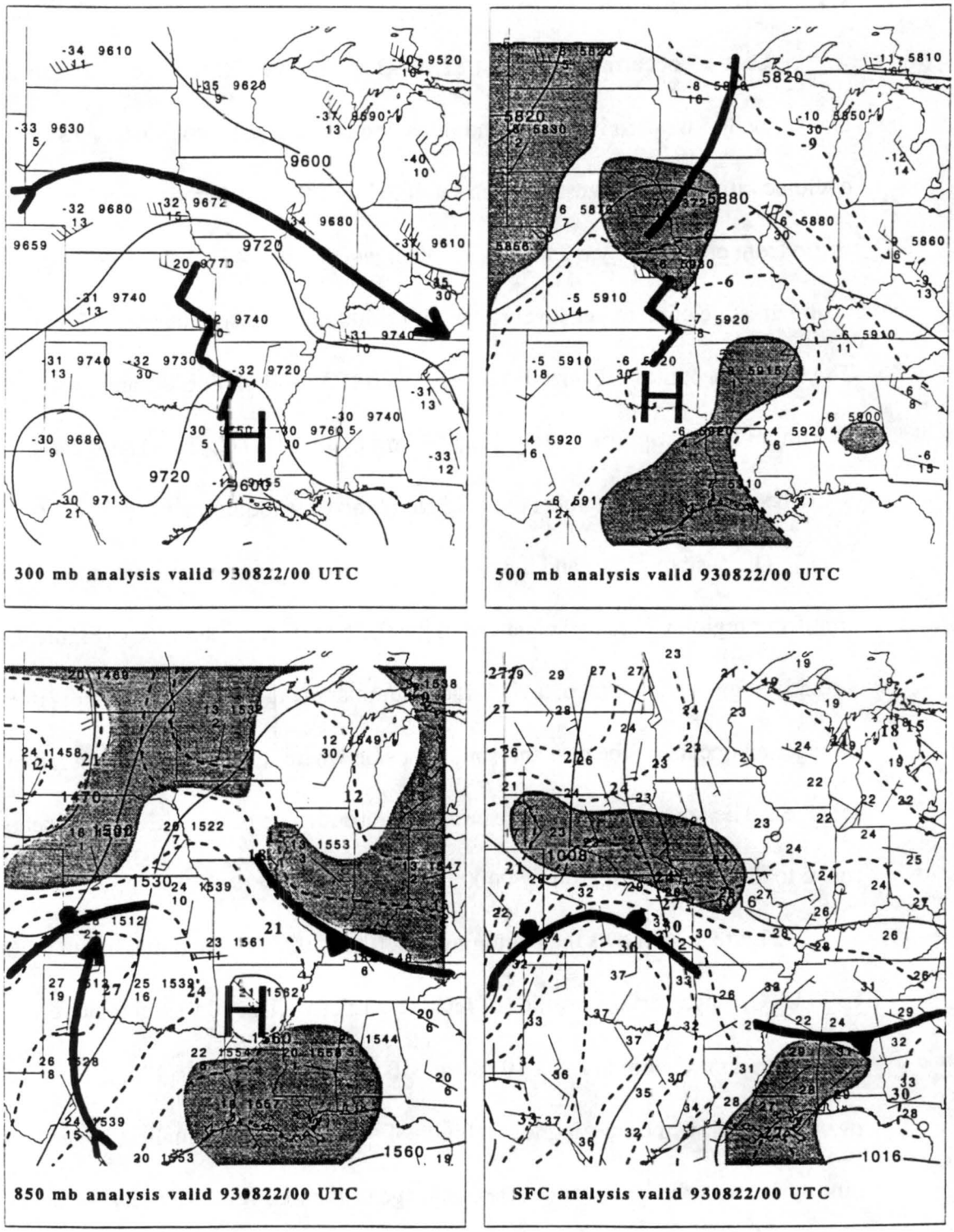

Figure 4.44: Analysis for 300 mb, 500 mb, 850 mb and surface levels at 0000 UTC 22 August 1993. The gray shaded regions are areas of dewpoint depressions of 5°C or less.

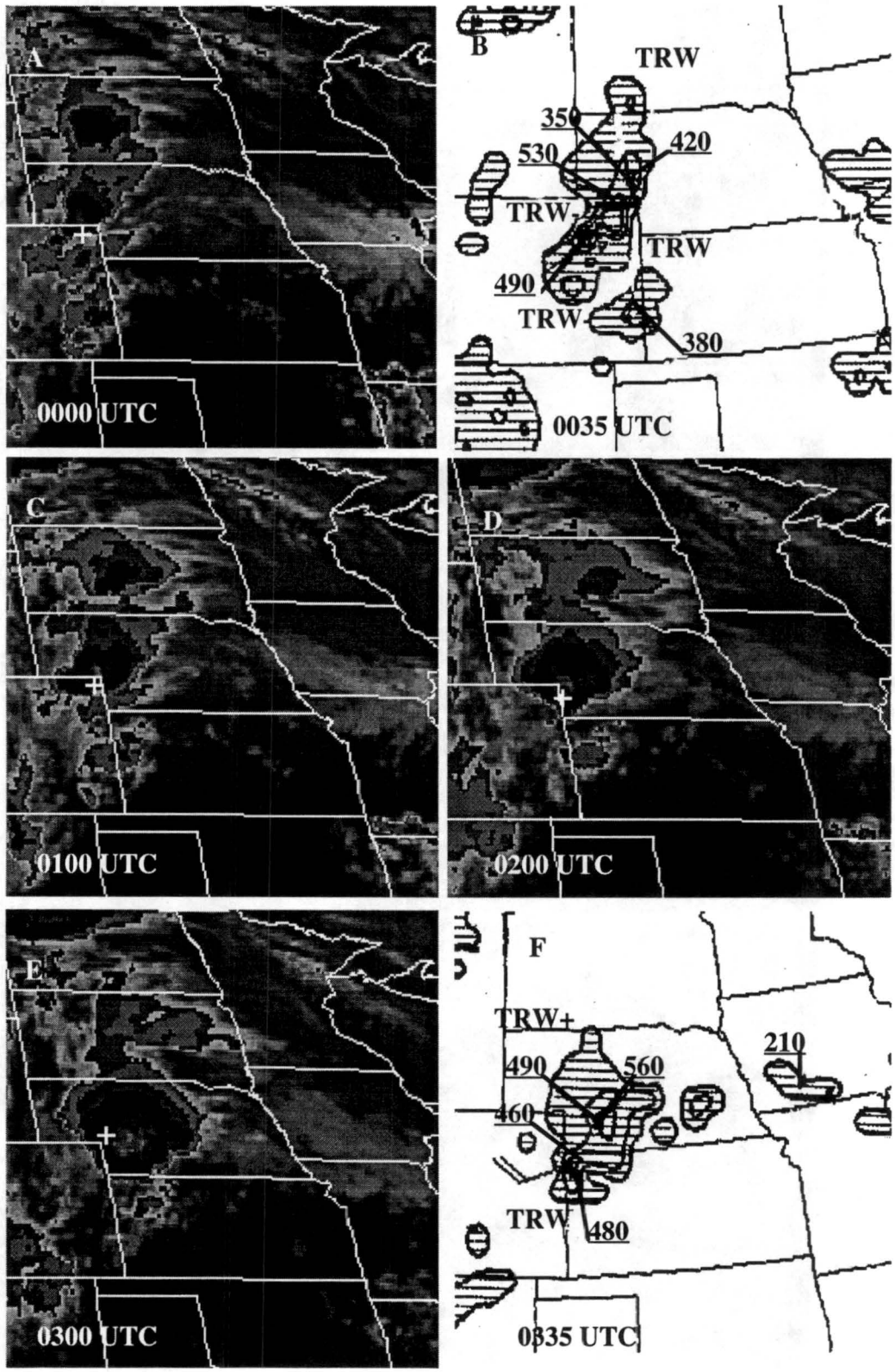

Figure 4.45: Infrared satellite images for (A) 0000 UTC, (C) 0100 UTC, (D) 0200 UTC, (E) 0300 UTC 22 August 1993; NWS radar summaries for (B) 0035 UTC and (F) 0335 UTC 22 August 1993.

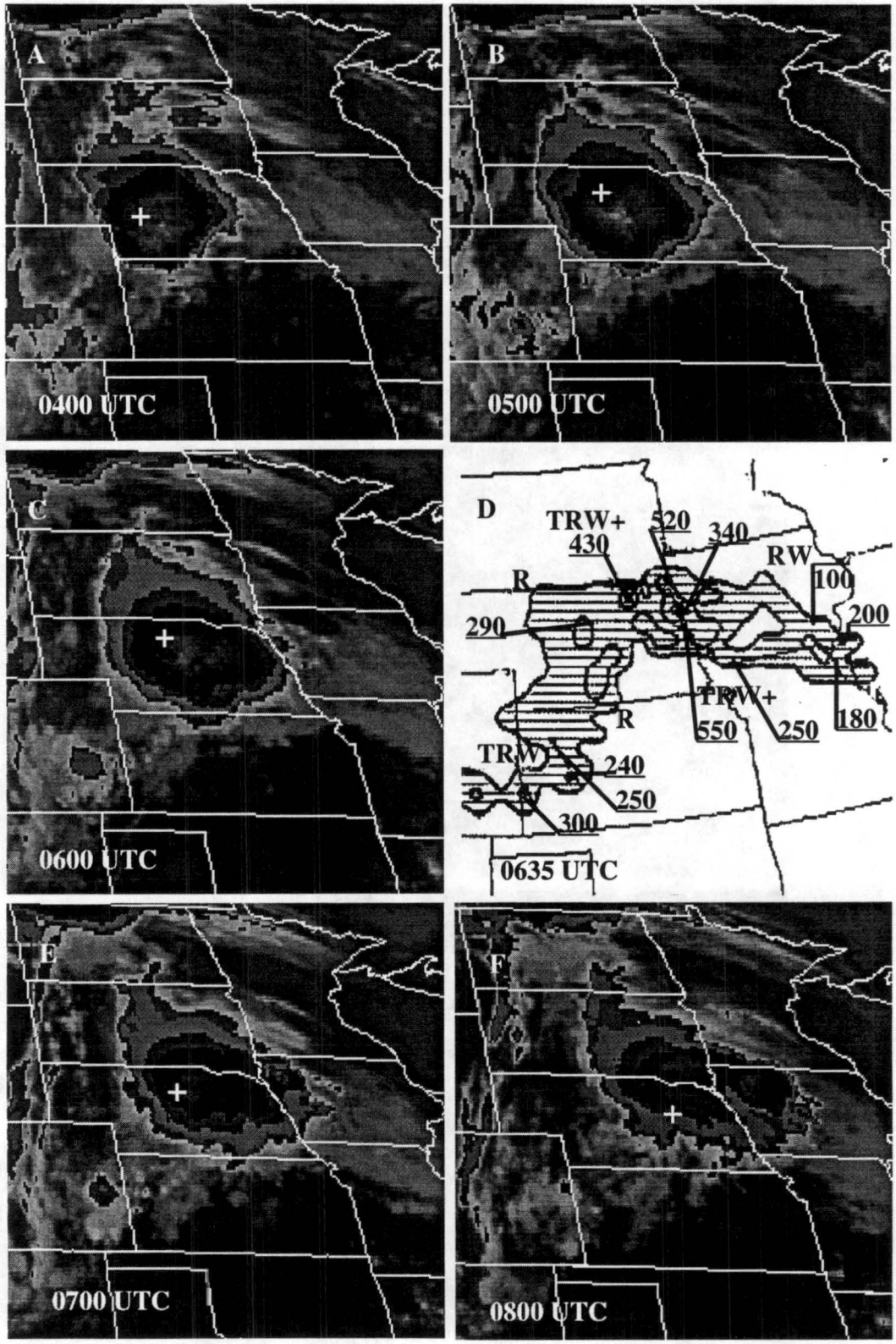

Figure 4.46: Infrared satellite images for (A) 0400 UTC, (B) 0500 UTC, (C) 0600 UTC, (E) 0700 UTC, (F) 0800 UTC 22 August 1993; NWS radar summary for (D) 0635 UTC 22 August 1993.

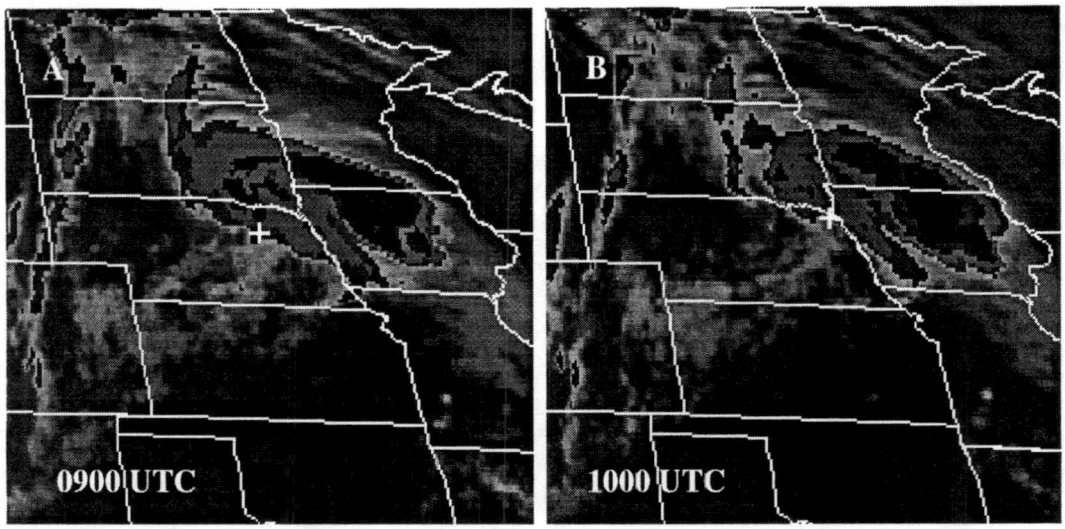

Figure 4.47: Infrared satellite images for (A) 0900 UTC and (B) 1000 UTC 22 August 1993.

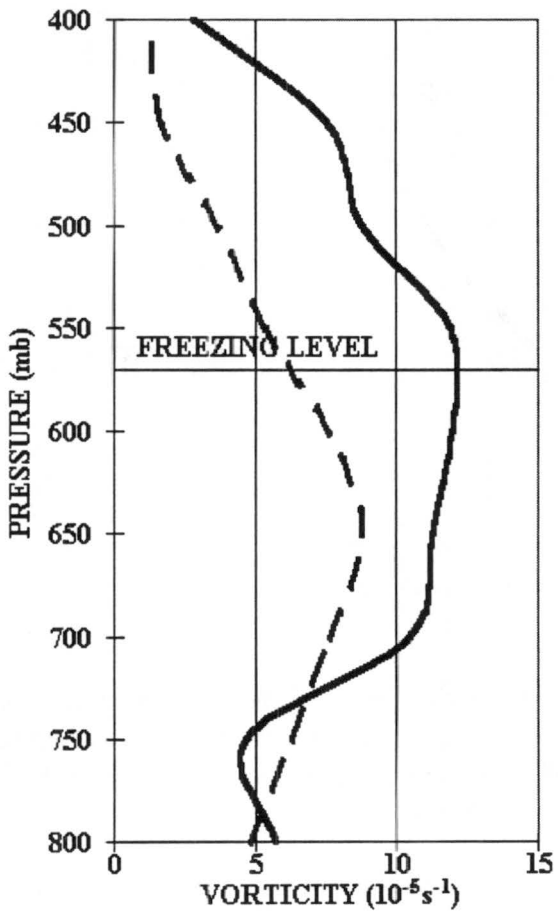

Figure 4.48: Average vertical profiles of relative vorticity for the 22 August 1993 MCS. The dashed line is for the beginning stage of the MCS and the solid line is for the maximum stage.

4.10 AVERAGE CASE

Figure 4.49 shows the average vertical profiles of the relative vorticity from 800 mb up to 400 mb for the beginning stage (dashed line) of the nine MCSs and the average maximum stage relative vorticity reached in the nine MCSs studied plus the standard deviation.

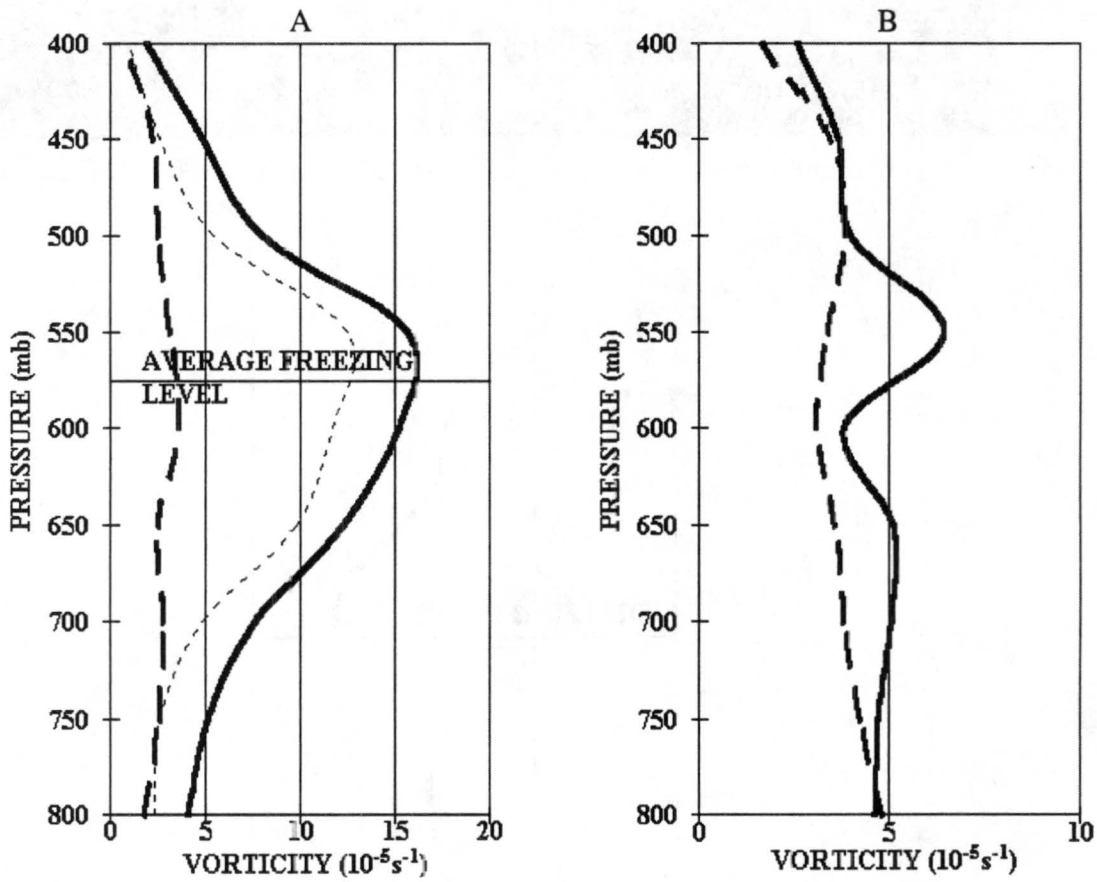

Figure 4.49: (A) Average vertical profiles of relative vorticity for the nine MCSs studied and (B) standard deviation. The long dashed line is for the beginning stage of the MCS and the solid line is for the maximum stage while the thin dashed line in A is the average increase of the relative vorticity.

It can be seen from these profiles that the mid-level relative vorticity of a MCS starts out with a relatively uniform vertical profile but increases on the average by 1.3 x $10^{-4}s^{-1}$ near the freezing level as the systems develop. This is consistent with

observational studies showing enhanced inflow into the MCSs near the melting level (e.g., Johnson *et al.*, 1995) and the idea that on the meso-α scale convergence production is the primary term contributing to vortex spin-up. Figure 4.50 shows the average hourly relative vorticity leading up to the maximum vorticity where the nine systems have been normalized to seven hours which is the average time it took the systems to reach the maximum stage.

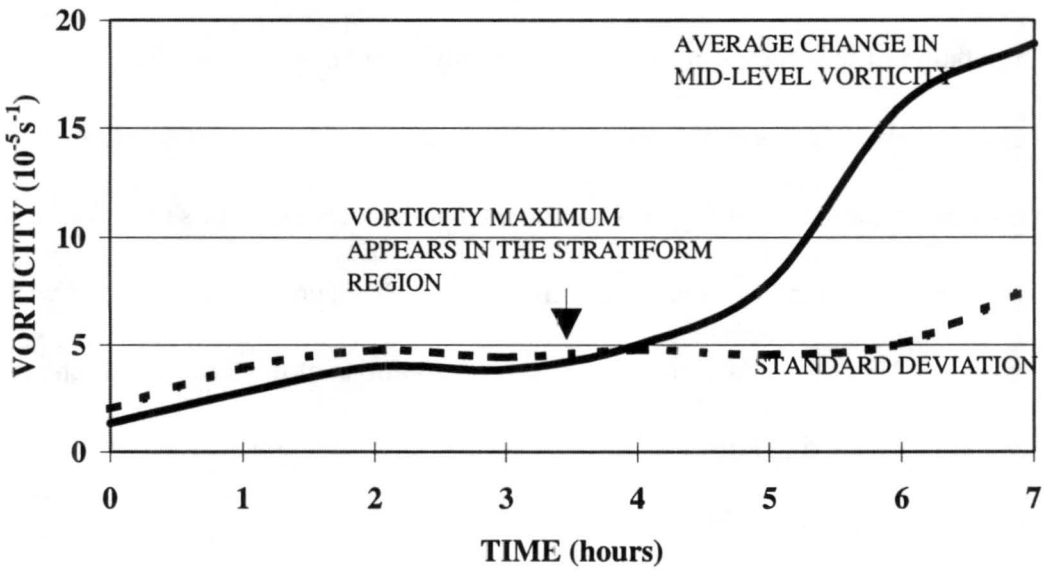

Figure 4.50: Average 600 mb relative vorticity (solid line) for the nine MCSs and the standard deviation (dashed line). The arrow indicates the average time where the vorticity maximum appears to move into the stratiform region.

The average mid-level vorticity starts out at approximately half or less of the Coriolis parameter in an MCS ($\cong 10^{-4}s^{-1}$) and shows only a slight increase for the first four hours. This trend changes shortly after the vorticity maximum appears to move away from the deep convection and into the stratiform region. The relative vorticity then begins to sharply increase over the next two to three hours leading to over an order of magnitude increase. One suggested cause for this sharp increase is the mid-level

convergence in the stratiform region. Comparing the average time rate of change of relative vorticity during the period of maximum increase to the average stretching term gives a ratio of 1.16 or 116%. This suggests the stretching term may be playing the most significant role in the formation of the MCV while the tilting term is contributing to a smaller order. This result is consistent with other observational studies (Bartels and Maddox, 1991; Johnson and Bartels, 1992) that have found the mid-level convergence production (stretching term) to be the primary producer of mid-level vorticity. Of course this computation of the change in the vorticity is only a rough approximation. One obvious error is that $\delta\zeta/\delta t$ was computed over the time period from hour 5 to hour 7 assuming a linear increase but Figure 4.50 shows that the increase in this time frame is not linear and would lead to an under estimate of $\delta\zeta/\delta t$. This possible error along with the coarse resolution of the data means that the computations of the time rate of change in vorticity and the stretching term are only approximate and firm conclusions cannot be drawn from this part of the study.

One last figure (Figure 4.51) shows the approximate position of the vorticity maximum at its maximum stage in relation to the satellite cloud shield normalized to the direction of movement of the MCSs. This shows the MCV will most often be found approximately half way between the leading edge of the cloud shield and the trailing edge of the cloud shield with respect to the system's movement. This is consistent with other studies that have found the MCV forms in the trailing stratiform precipitation region (Smull and Houze, 1985; Leary and Rappaport, 1987; Zhang and Fritsch, 1989; Johnson and Bartels, 1992; Fritsch *et al.*, 1994). Here again this is only suggestive because the

spacing of the wind profilers is approximately the same as the average radius of the cloud shield and the exact locations of the stratiform and convective regions are not known.

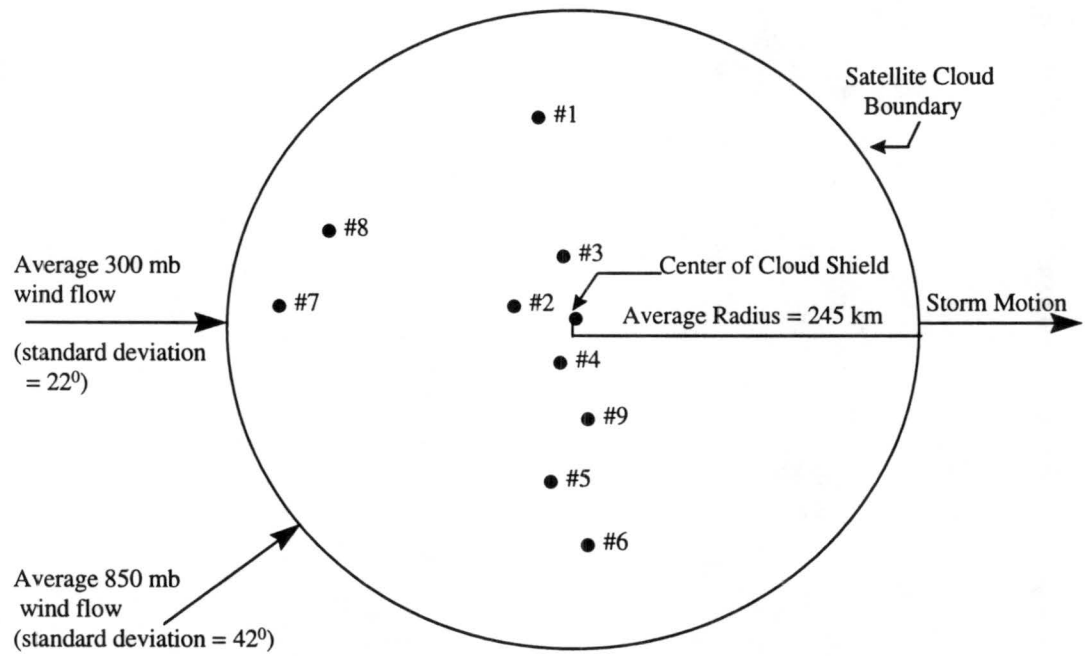

Figure 4.51: Approximate location of the vorticity center during the maximum stage for each case in relation to the satellite cloud shield and the storm motion.

Still a generalization of the precipitation patterns associated with the mature MCS (Houze *et al.*, 1990; Loehrer and Johnson, 1995) suggests that a convective region would be found in approximately the leading one third of the system while approximately two thirds of the system (trailing region) would have predominately stratiform precipitation. This would indicate the vorticity centers in Figure 4.51 most likely developed in the heavier stratiform precipitation area of the MCSs which is consistent with other observational studies of MCVs (Zhang and Fritsch, 1988; Johnson and Bartels, 1992). This finding is also consistent with the Houze *et al.*, (1989) conceptual model of a MCS (Figure 2.2) based on radar studies. Finally note that the motion of the systems is

strongly driven by the upper-level (300 mb) flow. Merritt and Fritsch (1984) found similar results in that MCSs tend to propagate with the thermal wind vector (wind shear) in the cloud layer.

Chapter 5

SUMMARY AND CONCLUSIONS

The objective of this study has been to examine and document the development of mid-level Mesoscale Convective Vortices (MCVs) within Mesoscale Convective Systems (MCSs) and Mesoscale Convective Complexes (MCCs) using the Central Plains Wind Profiler Demonstration Network (WPDN). Nine MCSs from the summer of 1993, the year of widespread flooding in the Midwest, were picked for this study based on their formation and lifetime spent over the WPDN.

The purpose of studying the development of mid-level vorticity was to gain more knowledge and understanding in the formation of the MCV that was first discovered using visible satellite imagery (Johnston, 1982). Since then, observational studies (Smull and Houze, 1985; Leary and Rappaport, 1987; Zhang and Fritsch, 1989; Johnson and Bartels, 1992; Fritsch *et al.*, 1994) have shown that the cyclonic circulation develops within the stratiform precipitation region of the MCS and Fritsch *et al.* (1994) tracked a MCV that was instrumental in initializing and organizing a series of five MCSs. The unique aspect of this research is that it represents the first attempt to use the WPDN to document the development and evolution of MCVs.

Bartels and Maddox's (1991) climatological study of MCVs for 1981 - 1988 estimated that less than 5% of MCSs exhibit a vortex whose clouds persist long enough

after the dissipation of the MCSs' high-level obscuring cirrus cloud to become apparent in visible satellite imagery. This estimate of MCVs in MCSs is most likely low because factors favorable for visual identification may not exist, i.e., a lack of persisting mid-level clouds after the dissipation of the upper-level cirrus clouds. In fact some researchers state that the MCV is an inherent part of the MCC circulation. For example, Velasco and Fritsch (1987) hypothesize: "The development (to varying degrees) of a latent-heat-driven, mesoscale warm-core vortex may very well be the feature which makes an MCC an MCC." Menard and Fritsch (1989) state that "Growing evidence suggests that MCCs exhibit three principal forms of meso-α scale circulations: 1) an upper tropospheric cold core anticyclone; 2) a mid-level warm core tropospheric vortex and; 3) a lower tropospheric outflow occasionally with a trailing mesolow." These features can be clearly seen in the Houze *et al.* (1989) conceptual model of a MCS with a trailing stratiform region (Figure 2.2).

The nine MCSs studied here do support the theory that the MCV forms in all large MCSs. Each of the nine cases developed to varying degrees a maximum of relative vorticity in the mid tropospheric levels with an average maximum of $17.3 \times 10^{-5} s^{-1}$ at 583 mb with a range in the maximum vorticity from $10.5 \times 10^{-5} s^{-1}$ to $3.0 \times 10^{-4} s^{-1}$ and with an average freezing level of 574 mb (Figure 4.42). This suggests the importance of latent heat processes enhancing the inflow and horizontal convergence which in turn produces vorticity through the stretching term of the vorticity equation (Eqn. 4.1). This result is consistent with other observational studies showing enhanced inflow into MCSs near the melting level (e.g., Johnson *et al.*, 1995). All nine of the MCSs developed mid-level relative vorticity on the order of $10^{-4} s^{-1}$ or greater once the vorticity moved into the

stratiform region (Figure 4.43) suggesting that the latent heat release in the stratiform region is the primary contributor to the circulation spin-up. This finding is consistent with modeling results (Zhang and Fritsch, 1988) as well as theoretical studies of Hertenstein and Schubert (1991) where they find that the diabatic heating distribution in the stratiform region is important for developing strong mid-tropospheric positive potential-vorticity anomalies. This is also somewhat supported by the results of comparing the average time rate of change of relative vorticity during the period of maximum increase in the mid-levels to the average stretching term which gives a ratio of 1.16 or 116%. This suggests the stretching term is playing a significant role in the production of vorticity but since the ratio is greater than one the tilting term must be contributing also. This result is consistent with other observational studies (Bartels and Maddox, 1991; Johnson and Bartels, 1992) that have found the mid-level convergence production (stretching term) to be the primary producer of mid-level vorticity.

Whatever the cause of MCVs, this study has shown that relative vorticity increases significantly in the mid-levels of MCSs on the meso-α scale. This work has been on a rather coarse scale but future work in this area could include combining wind profiler data with NEXRAD Doppler radar data to show the development of the MCV on a smaller (meso-β) scale. Incorporating radar data would improve the resolution and result in a more accurate knowledge of the vertical motions which would allow computing all the terms in the vorticity budget to gain further understanding of the processes leading to the formation of a MCV. Lastly, this study has concentrated on only one summer with a small sample size. Future studies should concentrate on different time periods and larger sample sizes to determine if the same results can be found.

REFERENCES

Atlas, D., R. Tatehira, R.C. Srivastava, W. Marker and R.E. Carbone, 1969: Precipitation-induced mesoscale wind perturbations in the melting layer. *Quart. J. Roy. Meteor. Soc.*, **95**, 544-560.

Augustine, J.A., and K.W. Howard, 1988: Mesoscale convective complexes over the United States during 1985. *Mon. Wea. Rev.*, **116**, 685-701.

Barnes, S.L., 1964: A technique for maximizing details in numerical weather map analysis. *J. Appl. Meteor.*, **3**, 396-409.

Bartels, D.L. and R.A. Maddox, 1991: Mid-level cyclonic vortices generated by mesoscale convective systems. *Mon. Wea. Rev.*, **119**, 104-118.

Biggerstaff, M.I., and R.A. Houze, Jr., 1991: Midlevel vorticity structure of the 10-11 June 1985 squall line. *Mon. Wea. Rev.*, **119**, 3066-3079.

Bluestein, H.B., 1993: *Synoptic-Dynamic Meteorology in Midlatitudes. Volume II: Observations and Theory of Weather Systems.* Oxford University Press, New York, 584 pp.

Carlson, D.L., 1981: Weather satellite interpretation. *National Oceanic and Atmospheric Administration, National Weather Service Technical Memorandum,* **NOAA TM NWS SR-103**.

Cotton, W.R., M.S. Lin, R.L. McAnelly, and C.J. Tremback, 1989: A composite model of mesoscale convective complexes. *Mon. Wea. Rev.*, **117**, 756-783.

Dobson, E.B., 1970: Doppler radar measurements of mean wind variations in the clear atmosphere, *14th Conf. Radar Meteor.* Tucson, Amer. Meteor. Soc., 69-72.

Doviak, R.J., and D.S. Zrnic, 1984: *Doppler Radar and Weather Observations,* Academic Press. New York, 458 pp.

Fritsch, J.M., R.J. Kane, and C.R. Chelius, 1986: The contribution of mesoscale convective weather systems to the warm-season precipitation in the United States. *J. Clim. Appl. Meteor.*, **25**, 1333-1345.

Fritsch, J.M., J.D. Murphy and J.S. Kain, 1994: Warm core vortex amplification over land. *J. Atmos. Sci.*, **51**, 1780-1807.

Frisch, A.S. and B.L. Weber, 1992: The distribution of C_n^2 as measured by 50, 405 and 915 MHz wind profilers. *J. Atmos. Oceanic Tech.*, **9**, 318-322.

Fujita, T.T., 1955: Results of detailed synoptic studies of squall lines. *Tellus*, **7**, 405-436.

Hertenstein, R.F.A., and W.H. Schubert, 1991: Potential vorticity anomalies associated with squall lines. *Mon. Wea. Rev.*, **119**, 1663-1672.

Houze, R.A., Jr., S.A. Rutledge, M.I. Biggerstaff and B.F. Smull, 1989: Interpretation of Doppler weather radar displays of midlatitude mesoscale convective systems. *Bull. Amer. Meteor. Soc.*, **70**, 608-619.

Houze, R.A., Jr., B.F. Smull and P. Dodge, 1990: Mesoscale organization of springtime rainstorms in Oklahoma. *Mon. Wea. Rev.*, **118**, 613-654.

Johnson, R.H. and D.L. Bartels, 1992: Circulations associated with a mature-to-decaying midlatitude mesoscale convective system. Part II: Upper-level features. *Mon. Wea. Rev.*, **120**, 1301-1320.

Johnson, R.H., B.D. Miner and P.E. Ciesielski, 1995: Circulations between mesoscale convective systems along a cold front. *Mon. Wea. Rev.*, **123**, 585-599.

Johnston, E.C., 1982: Mesoscale vorticity centers induced by mesoscale convective complexes. *9th Conf. on Wea. Forecasting and Analysis,* Seattle, Amer. Meteor. Soc., 196-200.

Kuo, Y.H., and Y.R. Guo, 1989: Dynamic initialization using observations from a hypothetical network of profilers. *Mon. Wea. Rev.*, **117**, 1975-1998.

Lang, A.G. and J.M. Fritsch, 1993: Mesoscale convective complexes in Africa. *Bull. Amer. Meteor. Soc.*, **121**, 2254-2263.

Leary, C.A., and E.N. Rappaport, 1987: The life cycle and internal structure of a mesoscale convective complex. *Mon. Wea. Rev.*, **115**, 1503-1527.

Lin, C.A. and R.E. Stewart, 1986: Mesoscale circulations initiated by melting snow. *J. Geophys. Res.*, **91**, 13299-13302.

Loehrer, S.M., and R.H. Johnson, 1995: Surface pressure and precipitation life cycle characteristics of PRE-STORM mesoscale convective systems. *Mon. Wea. Rev.*, **123**, 600-621.

Maddox , R.A., 1980: Mesoscale convective complexes. *Bull. Amer. Meteor. Soc.*, **61**, 1374-1400.

Maddox, R.A., 1983: Large-scale meteorological conditions associated with midlatitude mesoscale convective complexes. *Mon. Wea. Rev.*, **111**, 1475-1493.

Menard, R.D. and J.M. Fritsch, 1989: An MCC generated inertially stable warm core vortex. *Mon. Wea. Rev.*, **117**, 1237-1261

Merritt, J.H., and J.M. Fritsch, 1984: On the movement of the heavy precipitation areas of midlatitude mesoscale convective complexes. *Preprints, 10th Conf. On Wea. Forecasting and Anal.*, Tampa, AMS, 529-536.

Monna, W.A.A., 1994: On the use of wind profilers in meteorology. *Ann. Geophys.*, **12**, 482-486.

Newton, C.W., 1950: Structure and mechanisms of the prefrontal squall line. *J. Meteor.* **7**, 210-223.

Nichols, M.E., R.A. Pielke and W.R. Cotton, 1991: Thermally forced gravity waves in an atmosphere at rest. *J. Atmos. Sci.*, **48**, 1869-1884.

Ogura, Y. and M.T. Liou, 1980: The structure of a midlatitude squall line: a case study. *J. Atmos. Sci.*, **37**, 553-567.

Olsson, P.Q., 1994: Evolution of balanced flow in a simulated mesoscale convective complex. Colo. State Univ. Res. Paper No. 570, 177 pp.

Orlanski, I., 1975: A rational subdivision of scales for atmospheric processes. *Bull. Amer. Meteor. Soc.*, **56**, 527-530.

Petterssen, S., 1956: *Weather Analysis and Forecasting. Volume I: Motion and Motion Systems,* McGraw-Hill Book Co., New York, 442 pp.

Riehl, H. and J.S. Malkus, 1958: On heat balance in the equatorial trough zone. *Geophysica,* **6**, 503-538.

Schlatter, T.W., and F.S. Zbar, 1994: *Wind Profiler Assessment Report and Recommendations for Future Use.*, U.S. Department of Commerce, NOAA, Silver Spring, Maryland, 141 pp.

Schreiber, P., 1886: Bestimmung der Bewegung eines Luft-ballons durch trigonometrische Messungen von zwei Standpunkten, *Meteorol. Z.*, **3**, 341-345.

Schubert, W.H., J.J. Hack, P.L. Silva-Dias, and S.R. Fulton, 1980: Geostrophic adjustment in an axisymmetric vortex. *J. Atmos. Sci.*, **37**, 1464-1484.

Serafin, R.J., and W.F. Dabberdt, 1990: Profiling networks and developments in the United States. *Meteorologische Rundschau*, **42**, 70-83.

Smull, B.F, and R.A. Houze, Jr., 1985: A midlatitude squall line with a trailing region of stratiform rain: Radar and satellite observations. *Mon. Wea. Rev.*, **113**, 117-133.

Smull, B.F. and J.A. Augustine, 1993: Multiscale analysis of a mature mesoscale convective complex. *Mon. Wea. Rev.*, **121**, 103-123.

Southard, R., 1995: Flood volumes in the upper Mississippi River Basin. U.S. Geological Survey. Circulars 1120-H, 32 pp.

Szeto, K.K., C.A. Lin and R.E. Stewart, 1988: Mesoscale circulations forced by melting snow. Part I: Basic simulations and dynamics. *J. Atmos. Sci.*, **45**, 1629-1641.

Tollerud, E.I. and R.S. Collander, 1993: Mesoscale convective systems and extreme rainfall in the central United States. *Inter. Assoc. Hydro. Sci.*, **213**, 11-19.

Velasco, I., and J.M, Fritsch, 1987: Mesoscale convective complexes in the Americas. *J. Geophys. Res.*, **92**, 9591-9613.

Verlinde, J. and W.R. Cotton, 1990: A mesoscale vortex couplet observed in the trailing anvil of a multicellular convective complex. *Mon. Wea. Rev.*, **118**, 993-1010.

Wetzel, P.J., W.R. Cotton and R.L. McAnelly, 1983: A long-lived mesoscale convective complex. Part II. Evolution and structure of the mature complex. *Mon. Wea. Rev.*, **111**, 1919-1937.

Williams, J., 1994: The great flood. *Weatherwise*, **47**, 17-22.

Zhang, D.L. and J.M. Fritsch, 1988: A numerical investigation of a convectively generated, inertially stable, extratropical warm-core mesovortex over land. Part I: Structure and evolution. *Mon. Wea. Rev.*, **116**, 2660-2687.

Zhang, D.L., 1992: Formation of a cooling-induced mesovortex in the trailing stratiform region of a midlatitude squall line. *Mon. Wea. Rev.*, **120**, 2763-2785.